RICE UNIVERSITY

A low-cost platform for cervical cancer detection

by

Benjamin David Grant

A THESIS SUBMITTED
IN PARTIAL FULFILLMENT OF THE
REQUIREMENTS FOR THE DEGREE

Doctor of Philosophy

APPROVED, THESIS COMMITTEE

Rebecca Richards-Kortum, Chair
Malcom Gillis University Professor
Department of Bioengineering
Rice University

Tomasz S. Tkaczyk
Associate Professor
Department of Bioengineering
Rice University

Kathleen M. Schmeler
Associate Professor
Department of Gynecologic Oncology and Reproductive Medicine
UT MD Anderson Cancer Center

Richard G. Baraniuk
Cameron Professor of Engineering
Electrical and Computer Engineering
Rice University

Andrew Ellington
Wilson and Kathryn Fraser Research Professor in Biochemistry
Department of Chemistry
University of Texas at Austin

HOUSTON, TEXAS
May 2016

ABSTRACT

A low-cost platform for cervical cancer detection

by

Benjamin D. Grant

Cervical cancer causes an estimated 265,000 deaths annually, 90% of which occur in developing countries. To reduce the global burden of cervical cancer, screening programs and HPV vaccination are needed worldwide. Screening techniques that have had significant success in high resource settings have failed in low-to middle-income countries due to a variety of factors, including lack of highly trained personnel and lack of laboratory infrastructure.

Two alternative methods have been employed for cervical cancer screening in low resource settings: visual inspection with acetic acid and human papillomavirus (HPV) DNA testing. While both methods are promising, they both suffer from low specificity. In this thesis, I explored the ability of the high-resolution microendoscope (HRME) to discriminate between neoplastic cervical precancerous lesions and benign conditions in vivo in a pilot study of 59 patients in Barretos, Brazil. By calculating mean nuclear eccentricity and area, neoplastic lesions were discriminated from benign conditions with 92% and specificity of 77%. Further, I designed a new mobile-phone based HRME which reduced the size of the HRME by a factor of four and the prototype cost from $5,000 to $1,700.

In addition to imaging techniques, I explored low-cost immunoassays to aid both in cervical cancer screening and HPV vaccination efforts. Detection of the HPV oncoprotein E7 in cervical swabs may offer more specificity than HPV DNA testing, but current testing is both time and equipment intensive. I have developed a paper-based platform for running highly sensitive immunoassays without the need for sophisticated laboratory equipment. In a proof-of-principle malaria antigen assay, this device achieved equivalent limit-of-detection to a standard ELISA. Additionally, I present a modified version of this device for a serological HPV antibody test. In a pilot study of 24 volunteers, the test correctly identified those who had received two or more HPV vaccines with 100% accuracy. Such a test is needed to reduce unnecessary revaccination and to promote efficient vaccination in settings with poor medical records.

This work provides an improvement upon the HRME imaging technique and a highly sensitive point-of-care molecular diagnostic platform to aid in cervical cancer screening, detection and prevention in low-resource settings. The preliminary results from clinical pilot studies provide the foundation for further work to help reduce the global cervical cancer burden.

Acknowledgments

I would first like to thank my family for their unwavering support throughout my pursuit of my doctoral degree. My sisters and parents have been there every step of the way and without them I would not have been able to complete this work. My family, from my sisters and parents to my aunts, uncles and grandparents have always supported, encouraged and inspired me to work hard to achieve my goals.

I would like to thank all of my mentors and advisors I had in graduate school. My advisor, Dr. Rebecca Richards-Kortum, gave me the opportunity to join her lab and pursue research I was passionate about. Her guidance has allowed me to pursue a career in research for low-resource settings for which I am very grateful. Dr. Kendra Woods at The University of Texas MD Anderson Cancer Center wouldn't let me quit when things were hard and provided much needed support, advice and encouragement throughout my graduate school career. Dr. Schmeler, also at MD Anderson, was instrumental in collaborating for clinical studies. She also offered an invaluable clinical perspective. Dr. Karen Stortz provided critical technical advice and perspectives for HPV related work.

Finally, I'd like to thank all my friends both in the lab and outside of it. Kelly Aylsworth is a wonderful friend who has picked me back up when I have fallen more times than I can count. Dr. Anne Hellebust, Dr. Nadhi Thekkek, Tim Quang, Chelsey Smith and Jennifer Burnett are all great friends who also taught me many skills and

helped with much of the work presented here. Rachna Khare has been a great friend throughout nearly all of graduate school and provided invaluable support and guidance. Lastly, my dog Nike has been my loyal friend every step of the way and never fails to make me smile.

Contents

List of Figures

List of Tables

Nomenclature

HRME	High-resolution microendoscope
mHRME	Mobile high-resolution microendoscope
CIN	Cervical intraepithelial neoplasia
HPV	Human papillomavirus
POC	Point-of-care
LFA	Lateral flow assay
RDT	Rapid diagnostic test
SBR	Signal-to-background ratio
FBS	Fetal bovine serum
PBS	Phosphate buffered saline
PBST	Phosphate buffered saline with Tween 20
LMIC	Low and middle income countries
ROI	Region of interest

Chapter 1: Introduction

1.1. Overview

Cervical cancer is a major global health concern that disproportionally affects women in low resource settings. Of the estimated 265,000 cervical cancer deaths in 2012, 90% occurred in developing countries[1]. The primary reason for the discrepancy is lack of access to screening programs. The Papanicolaou test allows for early detection and subsequent treatment of precancerous lesions. However, developing countries typically lack the required laboratory infrastructure and human and economic resources necessary to implement screening programs. As virtually all cervical cancer is caused by the human papillomavirus (HPV), the development of HPV vaccines offers the opportunity to significantly reduce the burden of this disease. However, the full benefits of the HPV vaccine will not be realized for decades. Alternative screening technologies have been shown to be effective in low-resource settings including visual inspection with acetic acid (VIA)

and HPV DNA screening. Unfortunately, both of these techniques have a low positive-predictive value, leading to substantial overtreatment when used as part of a screen-and-treat program. To reduce the burden of cervical cancer in developing countries, low-cost, point-of-care tests to improve the specificity of screening and diagnosis of cervical precancer are needed.

This work explores two categories of devices to address this need. The first is a high-resolution microendoscope (HRME), a device that allows imaging of epithelial cell nuclei *in vivo*. In this thesis, the performance of this device is evaluated in pilot study in Brazil. Additionally, a new version of this device utilizing a mobile phone is described and characterized. The second is a device for molecular testing for HPV oncoproteins. While the complete development of such a test is beyond the scope of this thesis, a proof-of-principle paper-based immunoassay is developed with sensitivity equivalent to gold standard laboratory based tests.

The final goal of this work is to aid in improving the efficiency of HPV vaccination programs. HPV vaccination rates remain low in many countries. One challenge faced in extending vaccine coverage is identifying patients who have not yet received vaccination. This can be difficult in regions with poor medical records as self-reporting on HPV vaccination is highly inaccurate[2]. A rapid, low-cost test to assess HPV immune response is presented in this work to help identify those that have yet to receive three doses of the vaccine.

1.2. Objective and Specific Aims

The objective of my research is to improve upon and develop new tools for screening and diagnosing cervical cancer at the point-of-care. To achieve this objective, I carried out the following specific aims:

(1) *Evaluate the high-resolution microendoscope's ability to discriminate cervical precancer from benign conditions in a pilot study in Barretos, Brazil.*

Previous studies diagnosing cervical pre-cancer with the high-resolution microendoscope have utilized nuclear-to-cytoplasmic ratio to separate high grade dysplasia from less severe abnormalities. In this aim I seek to evaluate other nuclear morphological parameters in order to optimize diagnostic performance.

(2) *Develop a more economical, portable mobile high-resolution microendoscope (mHRME).*

The previously reported high-resolution microendoscope relies upon a research-grade camera and laptop computer. In this aim, I seek to develop a more economical and more portable high-resolution microendoscope by utilizing recent advances in mobile phone technology.

(3) *Develop a platform for a highly sensitive immunoassay amenable to the point-of-care*

A highly sensitive point-of-care immunoassay platform is necessary in order to develop a human papillomavirus oncoprotein based screening

test appropriate for the point-of-care. In this aim I develop a highly sensitive, equipment-free two-dimensional paper network for the detection of specific proteins in a plasma sample. I demonstrated the proof-of-concept of this approach with the malarial antigen histidine rich protein 2.

(4) Develop a rapid diagnostic test to determine if an individual has developed an immune response consistent with receiving two or more HPV vaccinations.

My final aim is to develop a paper based immunoassay for the detection of serum antibodies to the human papillomavirus. This test is needed to improve the efficiency of vaccination programs.

1.3. **Chapter Overview**

This thesis details the assessment of the HRME as a tool to diagnose cervical precancer *in vivo*, the design of a mobile high-resolution microendoscope and the development of two paper based lateral flow assays.

Chapter 2 provides the background and motivation for this project. The background covers cervical cancer etiology, prevention, screening and the role of human papillomavirus in the context of cervical cancer. Chapter two also provides a brief overview of novel methods for rapid immunoassays designed for the point-of-care.

Chapter 3 presents a pilot study designed to evaluate the performance of the HRME in discriminating between precancerous and benign conditions in 59 patients in Barretos, Brazil. Chapter 4 discusses data from an additional 228 patients enrolled in this study. Chapter 5 details the design and characterization of a mobile-phone based mHRME to reduce the cost and size of the HRME system.

Chapter 6 describes a novel two-dimensional paper network to perform a highly sensitive immunoassay on paper. Chapter 7 introduces a rapid diagnostic test for determining an individual's HPV status. Finally, chapter 8 summarizes the work provided here and examines future directions for the research.

Chapter 2: Background and Motivation

2.1. Cervical cancer overview

Cervical cancer is a major global health concern that disproportionally affects low-income countries. In 2012, there were an estimated 527,600 new cases and 265,700 deaths attributed to cervical cancer[1]. Over 90% of all deaths occurred in developing countries[1]. **Figure 2-1** depicts the incidence of cervical cancer globally[3]. The highest rates are seen in sub-Saharan Africa, Central and South America and South-Eastern Asia[1,3]. While cervical cancer is not one of the top five most common types of cancer in countries with a high or very high human development index (HDI), it is the most commonly diagnosed cancer in countries with the lowest HDI[4]. The discrepancy in both incidence and mortality between highly developed and less developed countries can be attributed to the effectiveness of national screening programs[5]. Cervical cancer screening focuses on detecting precancerous lesions

that can be removed before cervical cancer develops, thereby lowering both the associated incidence and mortality.[5] The rates of cervical cancer in North America and Europe prior to the implementation of national Pap screening programs were similar to those seen in developing countries today[5].

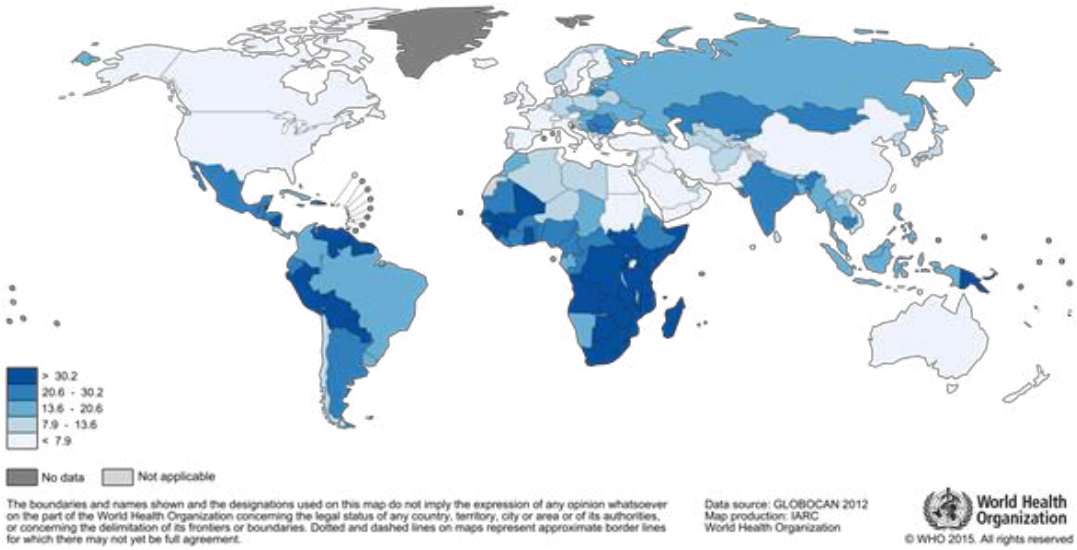

Figure 2-1: Estimated cervical cancer indicence worldwide in 2012.
Incidence reported in age-standardised rates per 100,000[3]

2.2. Etiology of Cervical Cancer

Human papillomavirus (HPV) causes virtually all cases of cervical cancer[6–8]. Approximately 200 strains of HPV have been identified[9]. Research has shown that persistent infection with 15 of these strains causes nearly all cases of cervical cancer[8]. Strains 16 and 18 cause approximately 70% of all cervical cancers and 50% of grade 3 cervical intraepithelial neoplasia (CIN3)[8]. The eight most common HPV infections found in cervical cancer specimens, in descending order, are HPV16, HPV18, HPV45, HPV31, HPV33, HPV52, HPV58, HPV35 and they are responsible for approximately 90% of all cervical cancers worldwide[10].

The human papillomavirus is contained in a protein shell comprised of two molecules: L1 and L2. In addition to these two proteins, the HPV genome has the capability to code for six other early proteins: E1, E2, and E4-E7[10]. Of these proteins, the two most critical for oncogenesis are proteins E6 and E7[11]. In fact, the presence of E6 and E7 alone are sufficient for keratinocyte immortalization[12]. These proteins both code for low molecular weight proteins of ~100 amino acids (E6) and ~150 amino acids (E7)[11]. Understanding the molecular oncogenic process of HPV infection can help shed light on the critical nature of these two proteins.

Unlike most viruses, HPV cannot simply infect a cell and create a progeny virus from the same cell. Instead, the synthesis of new HPV virions occurs due to the host cell undergoing mitosis[13]. HPV infects only the cells located in the basal cell layer of the squamous epithelium via small microwounds. After infection, the small

HPV genomes are established as extrachromosomal elements. They do not encode any enzymes necessary for viral replication and rely on the host cell replication proteins[13]. After a persistent HPV infection, i.e. those associated with high-grade lesions, HPV DNA becomes integrated into the host chromosome. The proliferation of these infected cells is dependent primarily on the retinoblastoma family of proteins, specifically p105(RB), p107 and p130. Thus, a primary target of high-risk E7 is the retinoblastoma (Rb) protein[13–15]. While E7 proteins from all HPV strains bind Rb, those from high-risk HPV strains do so with much higher affinity[11,13,16]. E7 targets Rb for degradation, leading to the release of transcription factor E2f that produces an increase in S phase genes and therefore increased cellular proliferation[13]. However, this high binding affinity of Rb by E7 triggers a response from tumor suppressor gene p53. The activation of p53 leads to reduce cell-growth and apoptosis. To combat this regulatory pathway, the HPV E6 protein targets p53 for degradation[11,13,17]. E5 works in concert with E6 and E7 to facilitate malignant proliferataion[13]. If the immune system is unable to clear the infection, cervical cancer can develop after several decades[13]. The molecular pathways described above are illustrated in **Figure 2-2**[13].

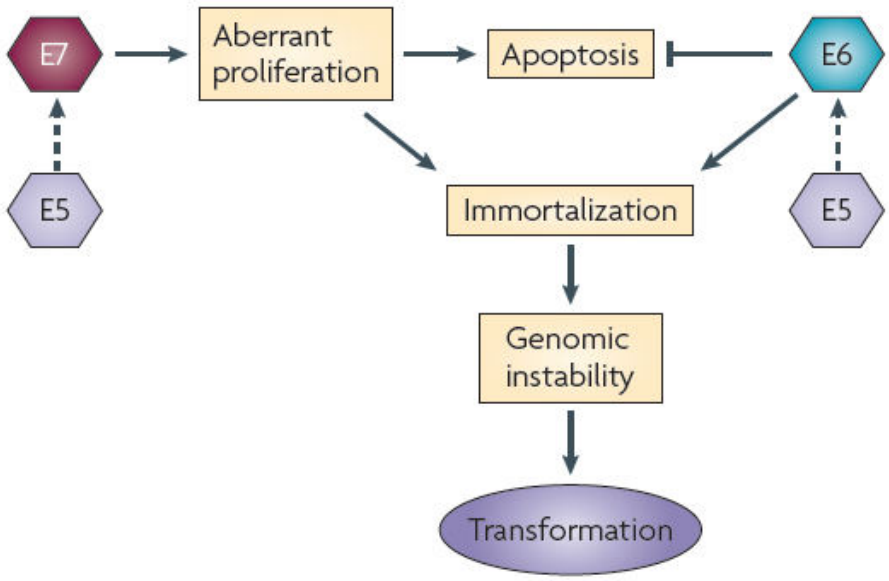

Figure 2-2: Molecular mechanism of HPV infection. Hyperproliferation is caused by E7 induced degradation of Rb protein. This hyperproliferation leads to p53-induced apoptosis. However, E6 leads to the degradation of p53 allowing aberrant proliferation to continue. These events lead to a cascade of disruption of cellular checkpoints resulting in the immortalization of the infected cell line[13]. Reprinted by permission from Macmillan Publishers Ltd: Nature Reviews Cancer, copyright 2010.

There are a variety of abnormalities that may affect the squamous epithelium of the cervix. These abnormalities can be divided into two subgroups. The first group consists of benign conditions that do not pose an increased risk of progression into invasive cervical cancer. This group includes basal cell hyperplasia, immature and mature squamous metaplasia and reserve cell hyperplasia.[18] Abnormalities that pose a significant risk of developing into an invasive neoplasm are generally referred to as dysplasia or carcinoma in situ. Previously, dysplasia was simply classified as mild, moderate or severe. However, current nomenclature refers to all degrees of squamous epithelium dysplasia of the cervix as cervical intraepithelial neoplasia (CIN). CIN is further broken down into CIN 1,

corresponding to mild dysplasia, CIN 2, moderate dysplasia, and finally CIN 3 which includes high grade dysplasia and carcinoma in situ[18].

Grading CIN is based primarily on the proportion of the epithelium thickness that is occupied by undifferentiated neoplastic cells. In CIN 1 the upper two thirds of the epithelium still undergo cytoplasmic differentiation[18]. All cells will show prominent nucleoli and will be irregular in shape. However, only cells in the bottom third of the epithelium will feature high nuclear-to-cytoplasmic ratio and exhibit nuclear crowding. Surface cells may appear largely normal in appearance aside from abnormal nuclei. Mitotic features are sometimes seen in CIN 1 but typically only in the bottom third of the epithelium. These mitotic features are usually still normal in appearance.[18] CIN 1 often presents with koilocytes, a change brought on by HPV, in the top layers of the epithelium[19,20]. CIN 2 is similar to CIN 1 except crowded nuclei and high nuclear to cytoplasmic ratio extend beyond the lower third of the epithelium.[18] Abnormal mitotic features are seen in the bottom two-thirds of

the epithelium. CIN 3 features undifferentiated basaloid cells with nuclear crowding to a greater degree than CIN 1 or CIN 2. Abnormal mitotic features are common and often in the upper-third of the epithelium. This type of CIN 3 is referred to as "small cell undifferentiated type" although other types exist[18]. In other types of CIN 3, the degree of the epithelium that is undifferentiated does not exceed two-thirds and

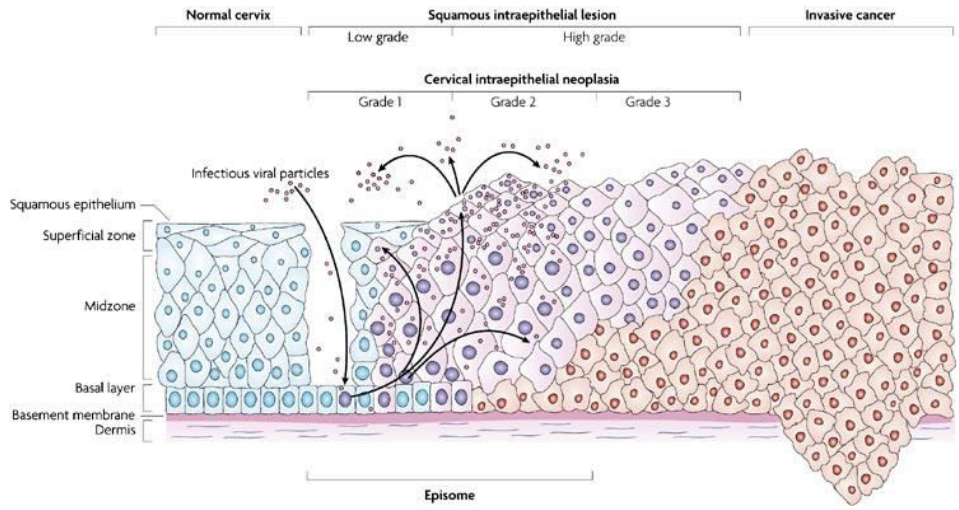

Figure 2-3: Progression from normal squamous epithelium to cervical cancer[21]. Reprinted by permission from Macmillan Publishers Ltd: Nature Reviews Cancer[21], copyright 2007.

other metrics must be used. Relevant features include lack of stratification and the site and abnormality of mitotic features. These types of CIN 3 that do not have undifferentiated cells throughout the entire epithelium still show a lack of stratification and abnormal mitotic features at all levels of the epithelium[18]. The underlying cellular changes that occur in the progression from normal squamous epithelium to CIN3 are depicted in **Figure 2-3**[21].

2.3. Cervical Cancer Prevention

The incidence and mortality of cervical cancer can be reduced through screening methods and HPV vaccination. Screening methods focus on the detection and treatment of cervical intraepithelial neoplasia to prevent the development of cancer. HPV vaccination works by preventing infection of HPV types that cause the most cases of cervical cancer. Both techniques face unique challenges in developing countries.

2.3.1. The Effect of Screening

In the United States, cervical cancer caused the most cancer deaths in women prior to the implementation of cytology based screening programs[22]. Since 1930 and the implementation of Pap testing, mortality due to cervical cancer has dropped by 80%[23]. This is due primarily to the detection and treatment of cervical pre-cancer[23]. Additionally, screening led to early detection of cervical cancer where five-year survival rates are significantly higher[22,23].

The best data for comparing incidence and mortality before and after screening program implementation is available for Nordic countries[5]. While controlled prospective studies do not exist to evaluate the efficacy of Pap smear testing, the trends in mortality provide strong evidence that Pap testing has helped to substantially reduce the mortality of cervical cancer[5,24]. Läärä et al., evaluated the

trends in mortality of cervical cancer in Denmark, Finland, Iceland, Norway and Sweden during the time period over which cervical screening programs were introduced[24]. In each country, the mortality rate of cervical cancer fell between 1965 and 1982. In Iceland, where coverage was greatest and screening intervals were shortest, mortality rates dropped by over 80%. In Finland the mortality rates dropped by 50% and in Sweden by 34%. In Norway, with only 5% of the country covered by organized screening, the mortality dropped by only 5%[24]. In addition to lowering mortality, screening has also substantially reduced the incidence of cervical cancer[5]. Hakama et al., reported a significant decrease in incidence of cervical cancer in Iceland, Finland and Sweden after the implementation of national screening programs[25]. Lynge et al., reported a 30% reduction in incidence after five years of national screening in Iceland[26]. While less data is available for comparing incidence before and after screening in the United States, cervical cancer incidence and mortality have dropped sharply since the introduction of screening in the 1970s[27].

2.3.2. Screening and intervention in high income countries

The 2012 guidelines from the American Cancer Society (ACS), American Society for Colposcopy and Cervical Pathology (ASCCP) and the American Society for clinical Pathology (ASCP) recommend no screening for women under the age of 21. From ages 21 to 29 women are encouraged to get a Pap smear every 3 years. HPV testing is not recommended in this age group. The incidence of HPV is too high in females under the age of 30 in the United States for HPV DNA testing to be an

effective screening modality[22,28]. Many of these cases are only transient infections and do not lead to cervical cancer. These screening guidelines are very effective. Modeling predicts a lifetime risk of cervical cancer in the United States to be between 31 and 33 cases per 1000 women[22]. However, screening every 3 years reduces the incidence to 5 to 8 cases per 1000 women. Moreover, early stage cervical cancer has an exceptionally high 5-year survival rate of 92%. Because screening catches many cases early, the lifetime risk of dying due to cervical cancer when screening is performed every 3 years is only .05 per 1000 women[22].

For women between the ages of 30 and 65, the ACS, ASCCP and ASCP all agree that HPV-based and cytology-based testing should be performed every 5 years. If it is not feasible to follow this recommendation, they recommend cytology screening every 3 years[22]. Although Pap testing has been used successfully for decades, HPV DNA testing offers a unique ability to improve screening.

Four large, randomized trials have compared cytology-based cervical screening with HPV DNA based screening in Sweden, the Netherlands, England and Italy[29]. A total of 176, 464 women were randomly assigned to either HPV-based or cytology-based screening arms. The women were followed for a median of 6.5 years. The results showed that HPV-based screening was superior to cytology based screening. Specifically, HPV-based screening offered 60-70% greater protection against cervical cancer when compared to Pap testing[29]. The study also compared direct referral to colposcopy based on HPV DNA screening versus HPV DNA screening followed by cytological triage. In cytological triage, patients positive for

high-risk HPV DNA testing but negative for cytological testing are referred for repeat DNA testing after a rest period. If the HPV DNA test is still positive, indicating a persistent infection, they are then referred to colposcopy. The results showed similar efficacy between both methods[29]. However, cytological triage offered a significant reduction in cost by reducing the number of colposcopies and biopsies.

Colposcopically-directed biopsies are the next step in the diagnostic process. During this procedure, dilute acetic acid (3-5%) is applied to the cervix[30]. Abnormal areas of the cervix turn white in the presence of acetic acid, a process known as acetowhitening. While the complete mechanisms of acetowhitening are unknown, nuclear protein precipitation plays a major role[31]. Acetic acid causes the temporary precipitation of nuclear proteins with which it comes in contact. Due to the increased nuclear protein in regions of precancer and metaplasia, this precipitation causes a noticeable difference in white light scattering in these regions[31]. Clinicians identify acetowhite areas using a colposcope, a low-power white light microscope[30]. Suspicious regions are then biopsied and sent to a pathologist for diagnosis[30,32]. Biopsies with histopathological diagnosis of CIN2 or CIN3 are generally then referred for treatment by a loop-electrosurgicial excision procedure (LEEP) to remove the precancerous lesions[30] or a cold-knife cone if a larger section of tissue must be removed[8].

2.3.3. Screening in low-to-middle income countries

This significant reduction in cervical cancer incidence and mortality has yet to be realized in developing countries due to the lack of nationwide screening programs[33]. There are many barriers to screening programs in low-resource settings. These include competing health needs, lack of financial and human resources, poor healthcare and laboratory infrastructure and widespread poverty[33,34]. Screening and diagnosis in high-income countries relies heavily on cytotechnologists and pathologists. While there are approximately 20,000 people for every one pathologist in the United States, there are between 200,000 and 5,000,000 people per pathologist in countries throughout sub-Saharan Africa, as shown in **Figure 2-4**[35]. This makes implementation of identical screening and

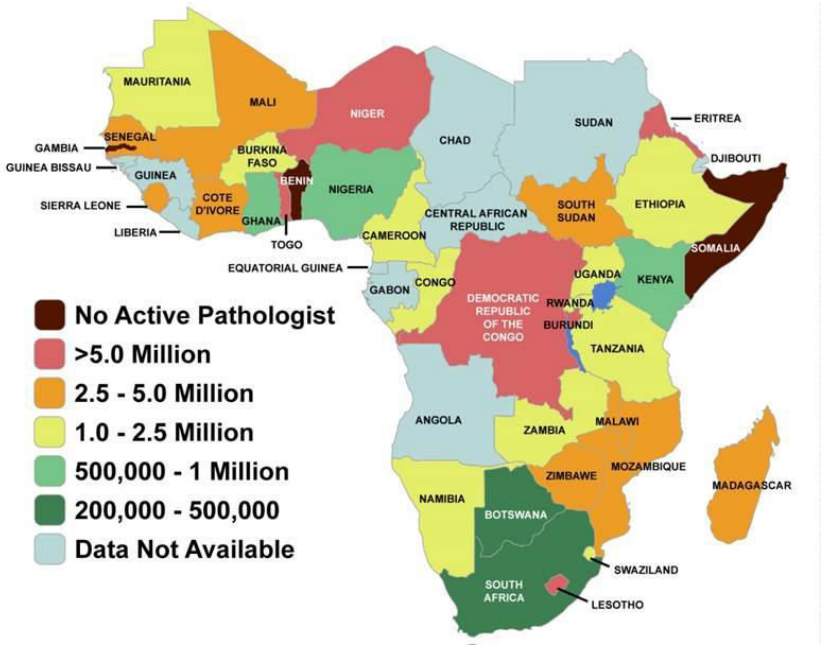

Figure 2-4: Number of people per pathologist in sub-Saharan Africa[35]. Reprinted with minimal adaptations from The Lancet, vol. 14, Adekunkle et al., "Improvement of pathology in sub-Saharan Africa" , e153, Copyright 2013, with permission from Elsevier.

diagnostic programs in low-resource settings very difficult.

In high-income settings, between 40% and 50% of women have undergone routine screening for cervical dysplasia in the last five years, compared to only 5% in developing countries[34]. Establishing high quality cytologic services is particularly challenging. Lazcano-Ponce et al., reported that false negative rates of cytology readings across 16 cytologic screening sites in Mexico were as high as 54%[36]. In addition to the challenges in establishing screening programs, patient follow-up after detected abnormalities is poor[37]. Gage et al., found that only 25% of 183 women with abnormal cytology findings in San Martín, Perú, received appropriate follow-up care[37].

Alternative screening techniques have been developed for low-resource settings to eliminate the need for extensive laboratory infrastructure and highly trained medical personnel. These techniques focus on immediate diagnosis, eliminating the necessity of patient follow-up for treatment[38]. Due to the fact that detection and treatment are performed in the same visit, these techniques are referred to as see "screen-and-treat" programs. The most widely studied and recommended technique for use in low resource settings is visual-inspection with acetic acid[38–43]. The test consists of applying dilute acetic acid directly to the cervix and examining the cervix for areas of acetowhitening, which constitutes a positive VIA test[39]. Alternatively, both acetic acid and Lugol's iodine can be applied in a technique called visual-inspection with Lugol's Iodine (VILI)[44,45]. Lugol's iodine, which stains glycogen-rich epithelium, provides additional contrast to aid in

identifying lesions[44]. Normal, mature squamous epithelium contains an abundance of glycogen, while CIN, metaplasia and columnar epithelium does not[44]. An example of lesions identified by VIA and VILI is provided in **Figure 2-5**. Identified lesions are typically removed immediately with cryotherapy[39,46,47], which effectively eliminates

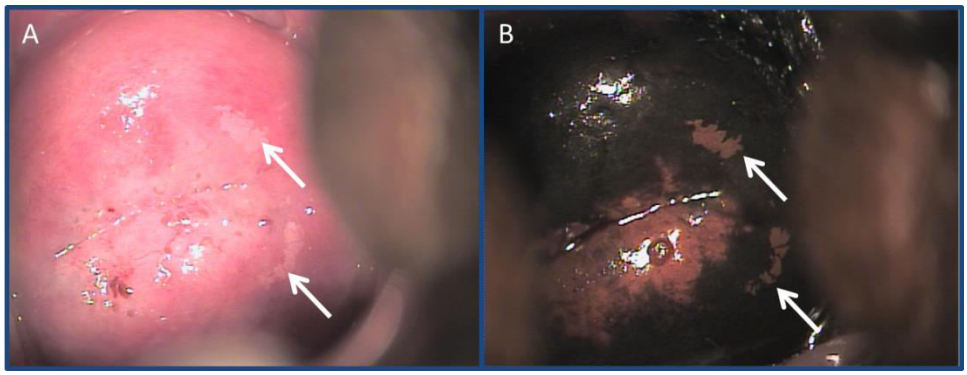

Figure 2-5: Visual inspection with acetic acid and Lugol's Iodine. (A) Colposcopic image of the cervix after the application of 3% acetic acid. Acetowhite lesions are indicated with white arrows. **(B)** Colposcopic image of the cervix after application of 5% Lugol's Iodine. The same lesions seen in **(A)** are visible in **(B)** as light areas that do not stain with Lugol's Iodine. These lesions are indicated with white arrows. Images courtesy of Dr. Jose Humberto, Barretos Cancer Hospital and Dr. Kathleen Schmeler, University of Texas MD Anderson Cancer Center

the progression of the disease in 88% of cases[47]. More recently, human papilloma virus (HPV) DNA testing has been explored for cervical cancer screening in low-resource settings[48].

The World Health Organization recommends alternative screening strategies, HPV DNA testing, VIA or VILI, where traditional programs based on Pap testing and

diagnosis have failed to be implemented[43]. However, HPV testing, VIA and VILI all have limited specificity leading to significant overtreatment. In a study of 31,343 women screened with VIA in rural India, VIA significantly reduced both the incidence and mortality of cervical cancer compared to the control group who received only education regarding cervical cancer signs, symptoms and screening[49]. However, VIA had a positive predictive value (PPV) of only 9.2% for high-grade cervical precancer or cancer[49]. In 2009 Sankaranarayanan et al, reported a cluster-randomized study of 131,746 women in rural India assigned to received HPV testing, cytologic testing, VIA or standard of care (cervical cancer education)[50]. While both HPV testing and VIA significantly decreased incidence and mortality of cervical cancer, the PPV were 11.3% and 7.4%, respectively[50]. These low positive predictive values translate to significant overtreatment in a screen-and-treat program.

VIA and VILI bother suffer from low specificity because they are subject to false positives from benign conditions which do not necessitate treatment; these conditions include inflammation and low grade dysplasia (CIN1). HPV DNA testing lacks specificity because it cannot differentiate between a transient and persistent HPV infection.[51] The detection of the oncoprotein E7 in liquid-based cytology may help discriminate persistent HPV infections from transient infections[52]. However, the current method for detecting E7 requires a time- and equipment-intensive enzyme-linked immunosorbent assay (ELISA)[52]. Before an E7 test can be designed

for use in resource constrained settings, a rapid instrument free ELISA platform is needed.

2.3.4. High-Resolution Microendoscopy for the Detection of Cervical Precancer

In an attempt to improve the specificity and positive predictive value of biopsy-free cervical precancer diagnosis, flexible fiber optic microscopes have been developed to provide real time images of the morphologic features of neoplasia *in vivo*. High-resolution optical techniques can image tissue with sub-cellular resolution to evaluate changes in epithelial morphology[53–56]. The Richards-Kortum group has developed a high-resolution microendoscope (HRME) capable of imaging epithelial cells *in vivo*[57–59].

The HRME, shown in **Figure 2-6**, is a fiber-optic fluorescence microscope. An LED provides excitation light that is collimated and directed into the fiber bundle.

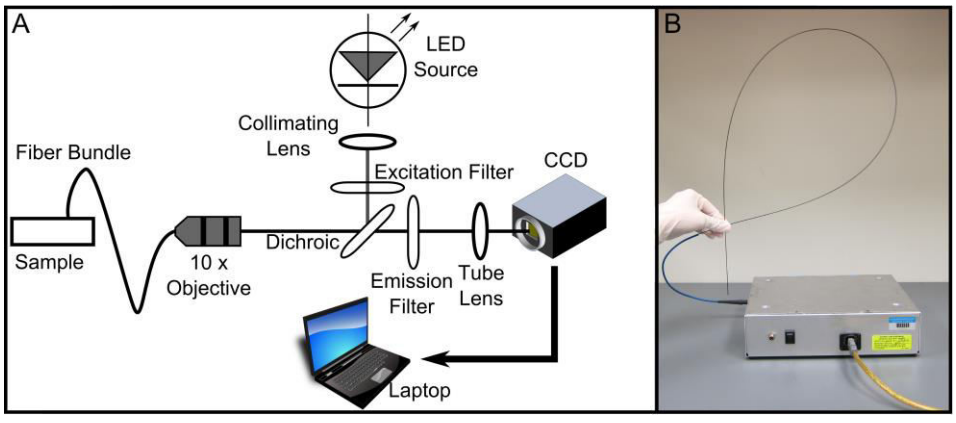

Figure 2-6: The high-resolution microendoscope[59]. (A) Schematic of the HRME. (B) Photograph of the HRME.

The fiber bundle is placed is placed directly in contact with the epithelial tissue of interest. Emitted light is collected through the same fiber bundle, filtered and focused onto a charge-coupled device (CCD). Utilizing the exogenous contrast agent proflavine, nuclear features including area, shape and spacing can be observed in real time without the need for biopsy. Proflavine is a fluorescent topical antiseptic with a peak excitation wavelength of 445 nm and peak emission wavelength of 515 nm that selectively stains cell nuclei.[60].

Pilot studies of this technology have demonstrated the potential to discriminate between neoplastic and non-neoplastic tissue in a variety of organ sites, including the esophagus[61–63], the oral cavity[64,65], and uterine cervix[60,66]. Using image analysis software, the nuclear-to-cytoplasmic ratio and other morphological parameters can be computed for each HRME image. This ratio increases as cells undergo precancerous changes, providing an objective metric to discriminate between benign and precancerous images. This strategy has been used to evaluate the HRME as a method to increase the specificity of VIA in two pilot studies in China and Botswana[60,66].

Pierce et al. utilized the HRME to examine 173 patients in Shanxi, China. Each patient underwent VIA examination followed by colposcopic examination. All acetowhite lesions were imaged with the HRME and biopsied. Additionally, one colposcopically normal site was imaged per patient. In total, 195 sites were imaged, of which 79 were colposcopically abnormal[60]. The median nuclear-to-cytoplasmic ratio for sites with a high grade dysplasia histopathologic diagnosis (CIN2, CIN3,

squamous cell carcinoma) was consistently higher than sites with non-neoplastic or low-grade dysplasia diagnosis (normal, inflammation, metaplasia, CIN1)[60]. The median nuclear-to-cytoplasmic ratio for the high grade group was .251 versus .164 for the combined CIN1 and benign group. Using a nuclear-to-cytoplasmic ratio threshold of .185, colposcopically abnormal sites with high grade histopathologic diagnosis were separated from all other colposcopically abnormal sites with 100% sensitivity and 65% specificity[60]. Additionally, only 8.4% of colposcopically normal sites exceeded this threshold. However, these sites had no corresponding biopsies so no definitive diagnosis is known. Quinn et al., reported a similar study at the Princess Marina Hospital in Botswana[66]. In this study, HRME images from 44 sites were obtained. These sites consisted of both colposcopically normal and colposcopically abnormal locations. Again, the nuclear-to-cytoplasmic ratio was computed and compared to histopathologic diagnosis. A nuclear-to-cyoptlasmic ratio threshold of .163 to discriminate between high-grade and not high-grade sites, resulted in a sensitivity of 86% and a specificity of 87%.[66] It is important to note that the specificity and sensitivity reported for the China study were for only colposcopically abnormal sites while the Botswana study included colposcopically abnormal and normal sites.

Despite these encouraging primary results, more research is needed to validate and improve the system. Pierce et al., noted that inflammation also leads to an increase in nuclear-to-cytoplasmic ratio[60]. In populations with higher rates of inflammation, alternative morphological parameters may be necessary to maintain

acceptable specificity. Furthermore, the current HRME system requires a research grade camera, a laptop with firewire support, and is not easily transported from one location to another[59]. Shin et al., reported the ability to use a consumer-grade digital single-lens reflex (DSLR) camera in lieu of a computer and research grade camera[67]. However, this eliminates the computer and thus the ability to perform image processing to compute objective measurements such as nuclear-to-cytoplasmic ratio. Additional methods to reduce the cost and size of the HRME while maintain the ability to perform image analysis are needed.

2.3.5. Human Papillomavirus Vaccination

There are currently three prophylactic vaccines available for use in the protection against HPV strands 16 and 18. These strands cause an estimated 70% of cervical cancers in women[1]. One, Cervarix is a bivalent vaccine that offers protection from only HPV types 16 and 18[68]. The second, Gardasil, is a quadravalent vaccine that provides protection from oncogenic types 16 and 18 and non-oncogenic HPV types 16 and 11, which are responsible for 90% of cases of genital warts[69]. Both vaccines have been shown to significantly reduce the risk of high-grade CIN related to HPV 16 or HPV 18 in large randomized trials[70,71]. The Center for Disease Control recommends HPV vaccination with one of these two vaccines for all females and males at age 11 or 12. Additionally, vaccination is recommended for all females ages 13 to 26 and males ages 13 to 21 who have not yet received the vaccines[72].

More recently, a nonavalent vaccine has been introduced. This vaccine includes protection against HPV types 31, 33, 45,52 and 58 in addition to the four subtypes of the quadravalent vaccine[73]. The addition of these five HPV types increases protection from cervical cancer from an estimated 70% to an estimated 90%[73]. All three vaccines require three doses of the vaccine given over a six-month period[70,71,73]. While HPV vaccines offer tremendous promise to reduce the global burden of cervical cancer, effective screening programs remain important for the foreseeable future[1]. Currently available HPV vaccines are for the prevention of infection with HPV and have not shown any benefit to those already infected[74].

The largest obstacle to vaccine coverage in developing countries is the price of the vaccine[75]. The three-dose series costs approximately $360 in the United States[75]. Many developing countries are seeking to implement national vaccination programs subsidized by the government or with commercial partners[76]. In order to optimize cost-effectiveness, it is critical that vaccines are provided only to those who have yet already received the vaccine. A study evaluating the accuracy of self-reporting of HPV vaccination history among adolescents revealed major inaccuracies[2]. Of the 66 adolescents who had received at least one HPV vaccine, only 36 (54%) reported having received the vaccine. Of the 48 who had received all three vaccines, only 17(35%) correctly reported having all three doses[2]. Due to the under-reporting of HPV vaccine status and the lack of reliable medical records in many developing countries, there is a significant possibility of unnecessary revaccination. Currently, an enzyme-linked immunosorbent assay (ELISA) or a

neutralization assay are necessary to test if someone has mounted an immune response following the administration of the HPV vaccine[77]. However, these tests require sophisticated laboratory instrumentation and highly trained personnel. Low-cost alternatives to these tests are needed to help facilitate efficient vaccination programs.

2.4. Paper based diagnostics

Paper-based rapid diagnostics tests (RDTs) offer a unique ability to bring immunoassay testing to the point-of-care[78]. This category of device arose specifically in order to develop tests for developing countries meeting the ASSURED criteria: affordable, sensitive, specific, user-friendly, rapid and robust, equipment-free and deliverable to end-users[78,79]. Paper-based devices offer several desirable properties for meeting these criteria. Paper is ubiquitous, inexpensive and it naturally wicks fluids, providing pump-free flow[78]. Lateral flow assays utilize nitrocellulose paper to create equipment-free immunoassays[80].

Lateral flow assays were first established in order to provide an at-home

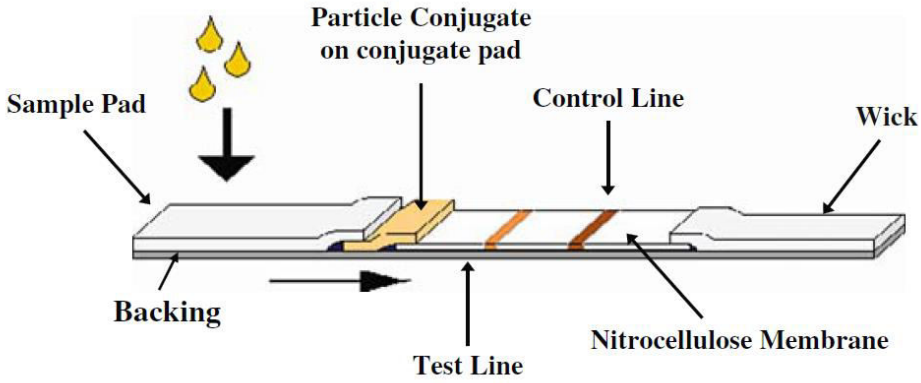

Figure 2-7: Typical layout of a lateral flow assay. A capture antibody is adsorbed to the nitrocellulose at the test line. A dried detection antibody, conjuated to a colorimetric particle such as a gold or latex, is located on the conjugate pad. When the sample is placed on the sample pad, it rehydrates the detection antibody. If the analyte of interest is found in the sample, it binds to the detection antibody and continues to flow down the nitrocellulose strip, towards the wicking pad. It is then capture by the immobilzed antibody at the test line. Unbound detection antibody continues to flow and is captured at the control line to indicate a successful test[80]. Figure reproduced from Wong RC, Tse HY, editors. Lateral Flow Immunoassay[80]. New York: Humana Press; 2009. Reproduced with permission of Springer in the format Thesis/Dissertation via Copyright Clearance Center.

pregnancy test[80]. These assays, regardless of the application, generally resemble a configuration similar to that shown in **Figure 2-7**[80]. A direct immunoassay consists of a capture antibody immobilized at a test location on the nitrocellulose. Downstream, a capture antibody targeted against the species of the detection antibody is immobilized on the control line. Upstream of both test lines is a conjugate pad that contains immobilized detection antibody. The detection

antibody is conjugated to a particle that provides a colorimetric readout, e.g. colloidal gold or colored latex[80]. In contact with the conjugate pad is a sample pad. When the sample, e.g. plasma, is placed on the sample pad it begins to wick onto the conjugate pad. There, it rehydrates the detection antibody. The detection antibody binds to any antigen present and the bound and unbound detection antibody continue to wick down the nitrocellulose strip. Any antigen is captured at the test line, and unbound detection antibody continues to flow until the control line. The captured labeled antigen and detection antibody provide visual colorimetric readout to the end user[80].

While lateral flow assays offer an excellent solution to performing immunoassays at the point-of-care, they often are less sensitive than their traditional laboratory ELISA counterparts[81]. One reason for this is that lateral flow assays cannot incorporate an enzyme-linked component due to the direct contact between the sample and conjugate particle. In order to overcome this obstacle, the Yager group has produced two-dimensional paper networks (2DPNs)[81–84]. Instead of only containing a single linear nitrocellulose channel, 2DPNs incorporate nitrocellulose legs perpendicular to the primary nitrocellulose test strip. These legs allow for the sequential delivery of reagents, as illustrated in **Figure 2-8**. Sequential delivery of reagents at the test zone enables more sophisticated assays, including gold enhancement and enzymatic amplification[82,85]. Using these methods, Fu et al., have developed a 2DPN for the detection of the malarial antigen histidine-rich protein 2. They report a limit of detection of 2.9 ng/mL, a four-fold improvement

over non-amplified techniques[82]. While a significant improvement, the test still falls short of the best reported limit of detection of 0.1ng/mL for a standard ELISA for this target[86]. These results are promising, but sensitivity equivalent to standard ELISAs will be needed for an effective HPV E7 screening test.

2.5. Summary

New techniques are needed for the screening and diagnosis of cervical cancer in developing countries. The HRME offers a novel technique for *in vivo* imaging and analysis of nuclear morphology. Initial results suggest that the HRME may offer the ability to improve specificity in screen-and-treat programs; however, additional data is needed to identify optimal parameters to discriminate between inflammation and CIN2 or CIN3. Furthermore, the HRME design needs to be optimized to reduce size and cost. Complementary molecular diagnostic testing is needed as an initial highly sensitive screening test. Point-of-care immunoassays offer the possibility of performing HPV oncoprotein based screening and to monitor immune response to HPV vaccines. However, in order for such tests to be developed, a platform to improve the sensitivity of currently available lateral flow tests is needed.

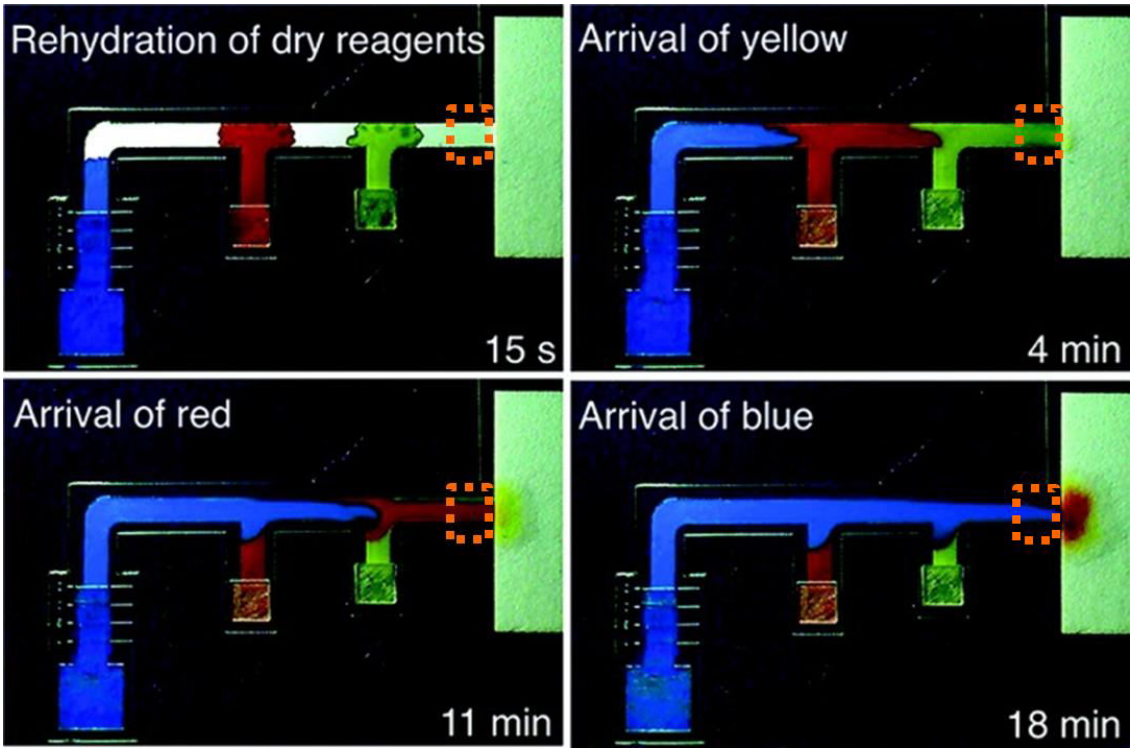

Figure 2-8: Reagent delivery in two-dimesional paper networks[82]**.** Each color of food coloring represents a different reagent. The dotted orange square is the location of the theoretical test location. Reprinted with permission from Fu E, Liang T, Spicar-Mihalic P, Houghtaling J, Ramachandran S, Yager P. Two-dimensional paper network format that enables simple multistep assays for use in low-resource settings in the context of malaria antigen detection. *Anal Chem* 2012;84(10):4574–9. Copyright 2012 American Chemical Society.

Chapter 3: High-resolution microendoscopy: A point-of-care diagnostic for cervical dysplasia in low-resource settings[+]

3.1. Introduction

There are more than 520,000 new cases of cervical cancer and 265,000 related deaths annually [1]. More than 85% of cases of and deaths due to cervical cancer occur in low- and middle-income countries (LMICs), where cervical cancer is the third leading cause of cancer death among women[1]. Cervical cancer incidence and mortality rates are much lower in high-resource settings due to the

[+] This paper has been published in Grant B, Guerreiro-Fregnani J, Possati-Resende J, Scapulatempo-Neto C, Matsushita G, Mauad E, Quang T, Stoler M, Castle P, Schmeler K and Richards-Kortum R. High-resolution microendoscopy: A point-of-care diagnostic for cervical dysplasia in low-resource settings. Eur J Cancer Prev 2015. [100]

implementation of organized screening programs based on Pap and/or HPV testing, diagnosis by colposcopy and biopsy, and timely treatment of cervical precancer and early-stage cancer. However, many LMICs have been unable to implement such screening programs due to the high cost of necessary infrastructure and lack of qualified personnel[87,88]. Screening programs are also hampered by loss to follow-up of screen-positive women who do not receive accurate diagnosis and timely treatment. As a result, many women still die needlessly due to cervical cancer.

The World Health Organization recently recommended alternative screening strategies of HPV DNA testing or visual inspection with acetic acid (VIA) and screen-and-treat (S&T) protocols where traditional programs based on Pap testing and diagnosis have not been implemented [43]. However, like Pap testing, both VIA and HPV testing have limited specificity, i.e., the vast majority of screen-positive women do not have cervical precancer or cancer. HPV detection cannot distinguish between benign high-risk HPV infections destined to resolve and those associated with the development of preinvasive and invasive cancer. In a study of 31,343 women screened with VIA in India, VIA had a positive predictive value (PPV) of only 9.2% for high-grade cervical precancer or cancer[49]. In a subsequent study, Sankaranarayanan *et al.* (2009) randomized 131,746 women in rural India to receive either a single lifetime screening test using cytology, VIA, HPV testing or standard care (cervical cancer health education). Both VIA and HPV testing were associated with low PPV: 7.4% for VIA and 11.3% for HPV testing[89]. Therefore, using only HPV or VIA screening would lead to substantial overtreatment.

Thus, there is an important need for affordable tools to enable accurate, real-time diagnosis of cervical precancer and early invasive cancer in screen-positive women in low-resource settings. In an attempt to better detect early cervical neoplasia at the point-of-care in screen-positive women, flexible fiber optic microscopes have been developed to provide real-time images of the morphologic features of neoplasia *in vivo*. High-resolution optical techniques can image tissue with sub-cellular resolution to evaluate changes in epithelial morphology [53]. We developed a high-resolution microendoscope (HRME) capable of imaging epithelial cells *in vivo* [57,58]. The HRME utilizes a small (1 mm) fiber optic probe placed in direct contact with the cervical epithelium, allowing real-time imaging of the underlying tissue. Utilizing the exogenous contrast agent proflavine, nuclear features including area, shape and spacing can be observed in real-time without the need for biopsy.

Pilot studies of this technology have demonstrated the potential to discriminate between neoplastic and non-neoplastic tissue in a variety of organ sites, including the esophagus [61,62,90], the oral cavity [64,65,91], the colon[92] and the cervix [60,66]. In this study, we evaluate the diagnostic accuracy of the HRME imaging system to identify precancerous lesions of the cervix *in vivo* in a pilot study in Barretos, Brazil.

3.2. Methods

3.2.1. Study Overview

The National Committee for Ethics in Research (CONEP) of Brazil and the Institutional Review Boards from Hospital de Câncer de Barretos (Barretos, Brazil), MD Anderson Cancer Center, and Rice University (Houston, USA) reviewed and approved this study. Female patients residing in the state of São Paulo, Brazil were eligible to participate if they had been referred to Hospital de Câncer de Barretos for colposcopy due to a subset of abnormal Pap tests. Eligible referral Pap tests included low-grade squamous intraepithelial lesion (LSIL), high-grade squamous intraepithelial lesion (HSIL), atypical squamous cells – cannot exclude HSIL (ASC-H) and atypical glandular cells (AGC). A Pap diagnosis of atypical squamous cells of undetermined significance (ASC-US) was generally insufficient for inclusion unless the patient had a previous, more severe Pap diagnosis. Exclusion criteria included women who were pregnant, have had a hysterectomy, or were nursing.

3.2.2. High-resolution Microendoscope

The high-resolution microendoscope (HRME) is a battery-powered, fiber-optic fluorescence microscope. The design of the system has been described in detail previously [57,58]. The device is approved only for investigational use. An image of the system is provided in **Figure 3-1**. The system is designed to image cervical epithelium following topical application of proflavine, a fluorescent contrast agent that stains cell nuclei. Proflavine has a history of safe clinical use as a topical

antiseptic [93], although its use as a contrast agent is investigational. Proflavine has a peak excitation wavelength of 445 nm and a peak emission wavelength of 510 nm. The HRME system provides excitation light to the tissue via a blue LED with a center wavelength of 455 nm. The light is collimated, filtered and directed into a 1.0 mm diameter flexible fiber optic bundle containing 30,000 individual fibers. Proflavine dye is applied topically to stain epithelial cell nuclei and the fiber bundle is placed in gentle contact with the tissue site to be imaged. Proflavine fluorescence is then captured by the same fiber optic bundle, filtered, and focused onto a battery-powered charge-coupled device (CCD) sensor. The image is displayed in real-time on a laptop computer which also controls image acquisition. The CCD captures video at 10 frames per

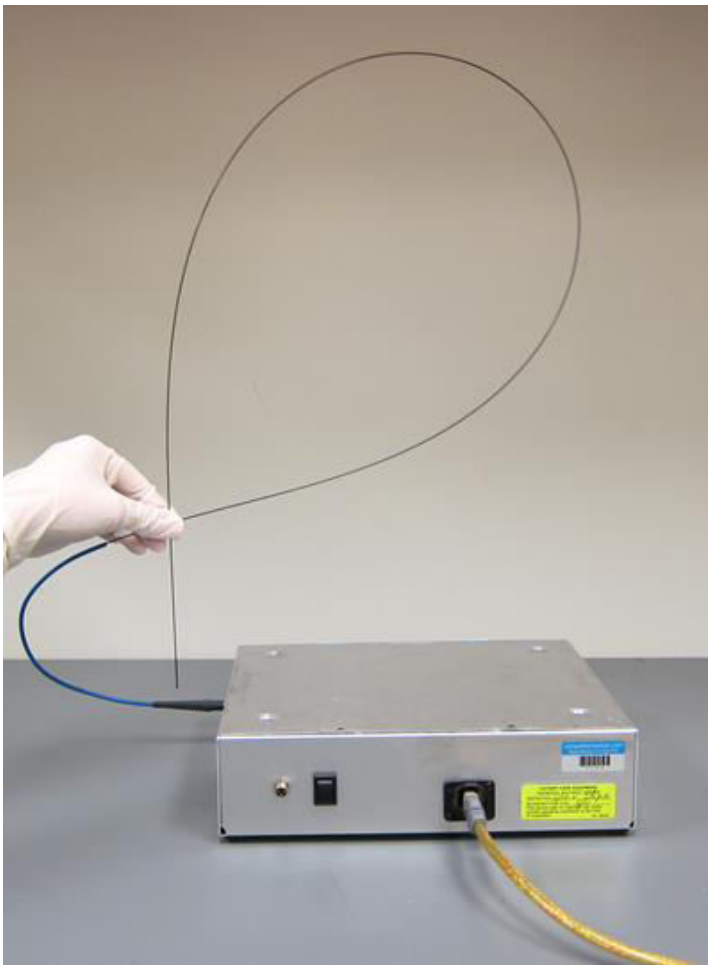

Figure 3-1: Picture of the high-resolution microendsocope (HRME) system[66]

second.

3.2.3. Study Procedure

After consenting to participate in the study, each woman was first interviewed by a trained healthcare professional to obtain basic demographic information. All women received a urine based pregnancy test before proceeding with the study. Next, routine colposcopy with 5% acetic acid was performed to identify acetowhite lesions on the cervix. If acetowhite lesions were identified, 0.01% proflavine in sterile water was applied to the cervix using a spray bottle. The cervix was wiped with a cotton swab to ensure even distribution of proflavine. The clinician then applied 5% Lugol's Iodine to the cervix, and any lesions that excluded iodine staining were noted. Finally, 0.01% proflavine was re-applied to ensure a strong fluorescence signal. The clinician then placed the distal tip of the fiber probe in gentle contact with each suspicious region identified during colposcopy and acquired a two second video from each site. The clinician also placed the HRME probe and acquired videos from a site which appeared by colposcopy to be normal squamous epithelium. The entire imaging procedure lasted less than ten minutes. After HRME imaging was performed, a biopsy was obtained from each suspicious site and submitted for histopathological diagnosis.

Each biopsy was examined by two pathologists at Hospital de Câncer de Barretos, referred to in this manuscript as the clinical pathologists. All biopsies

were also independently reviewed by a study pathologist at the University of Virginia. Samples were classified as normal, inflammation, cervical intraepithelial neoplasia (CIN) grade 1 (CIN1), CIN grade 2 (CIN2), CIN grade 3 (CIN3) or cancer using standard criteria [94]. All pathologists were blinded to the HRME images and to the other pathologists' diagnoses. The two clinical pathologists came to a consensus diagnosis in any cases where their initial diagnoses disagreed. In cases where the clinical pathologists' and study pathologist's diagnoses did not agree, samples were classified as the more severely neoplastic diagnosis.

3.2.4. Data Analysis

A researcher blinded to the histopathologic diagnosis selected the highest quality frame from each video with respect to clarity of focus. Sites were excluded from further analysis if more than 50% of the HRME image in the highest quality frame was out of focus or obscured by debris at the probe tip. The remaining images were analyzed using a custom Matlab 2012b script, designed to segment individual nuclei in each image and to quantify nuclear area and eccentricity. Briefly, the program first finds the outline of the fiber bundle and removes signal outside its boundary. Next, the image is Gaussian filtered to remove image artifacts due to the outline of individual fiber cores in the image. After the Gaussian filter is applied, a top-hat filter is used to reduce background and increase contrast between nuclei and the background. This new image is used to automatically select a region-of-interest (ROI). The ROI is calculated automatically by first selecting the entire area inside the fiber boundary. Next, areas of the image that are too dimly lit,

saturated, or homogenous are removed from the ROI. After the final ROI is determined, a binary threshold is applied to segment individual nuclei from the background. The threshold value is chosen automatically by Otsu's method[95]. The nuclear-to-cytoplasmic ratio, mean and median nuclear area, standard deviation of the nuclear area, median perimeter and median eccentricity are calculated and recorded for each image.

A test of trend [96] was used to examine the relationship between HRME categorizing the lesion as positive (CIN2+) and severity of histopathologic diagnosis by the study pathologists. A Fisher's exact test was used to test for differences in HRME positivity for CIN2 or more severe diagnoses (CIN2+) vs. <CIN2 diagnoses. Sensitivity, specificity, and odds ratio (OR) with 95% confidence intervals (95%CI) were calculated for HRME detection of CIN2+ and CIN3 or more severe diagnoses (CIN3+). P values of <0.05 were considered statistically significant.

3.3. Results

A total of 59 patients were enrolled in the study between June 17, 2013 and June 21, 2013. All patients successfully underwent HRME imaging without any

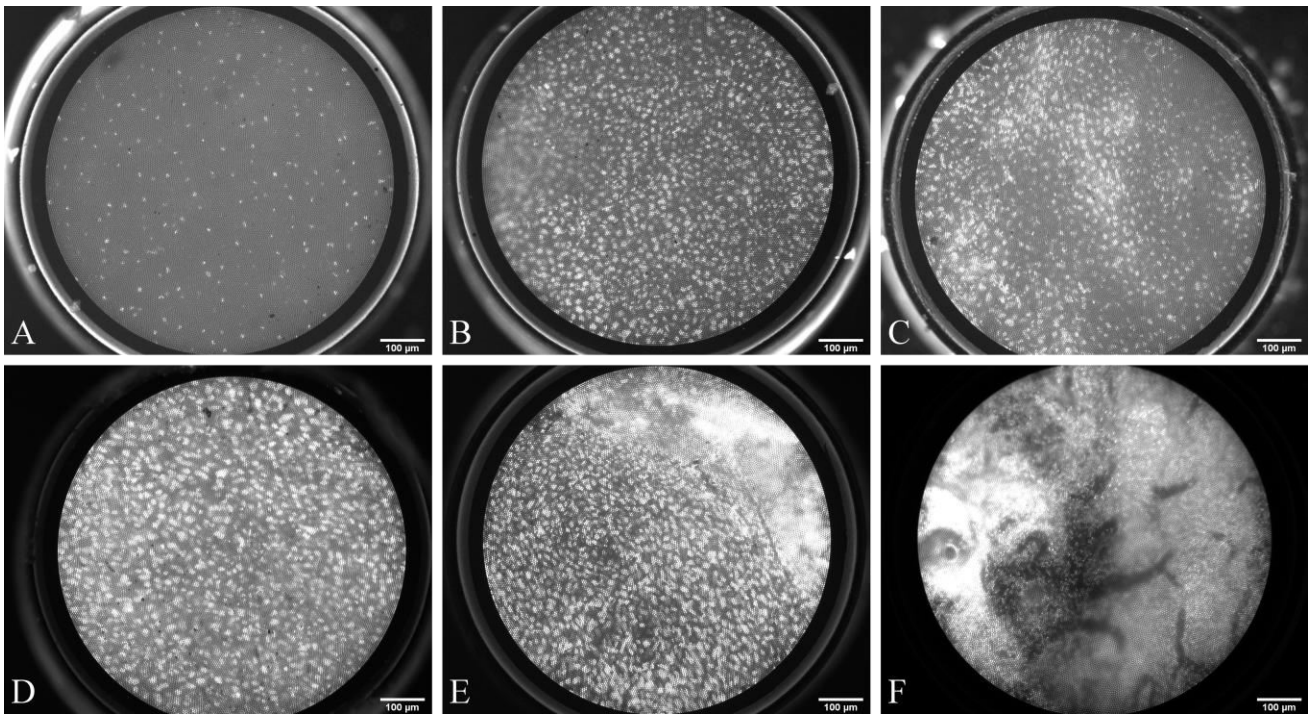

Figure 3-2 Representative HRME images of cervical epithelium stained with proflavine and Lugol's iodine. (A) HRME image of colposcopically normal site shows round, small, evenly spaced nuclei. **(B-F)** HRME images of colposcopically abnormal sites. **(B)** HRME image of a site with histologic diagnosis of inflammation, characterized by evenly spaced, small, crowded nuclei. **(C)** HRME image of a site with histologic diagnosis of CIN1, with slightly enlarged, evenly spaced nuclei. **(D)** HRME image of a site with histologic diagnosis of CIN2 with enlarged, crowded, pleomorphic nuclei. **(E)** HRME image with a histologic diagnosis of CIN3 showing similar features to CIN2, with more pronounced nuclear crowding and pleomorphism. **(F)** HRME image of a second site diagnosed as CIN3 with very prominent vessels visible.

adverse events. The median age was 34 (range: 18-67). Referral Pap tests ASC-US (n =1, 1.7%), LSIL (n=7, 11.9%), HSIL (n = 20, 33.9%), ASC-H (n=29, 49.2%) and AGC (n=2, 3.4%). HRME images were obtained from 84 colposcopically abnormal sites and 59 colposcopically normal sites. Fifty-nine of the 84 colposcopically

abnormal sites imaged and biopsied were adequate for evaluation. Forty-nine of the 59 colposcopically normal sites imaged passed quality control review. **Table 3-1** summarizes the colposcopic impression and consensus histologic diagnosis for the sites imaged with the HRME that passed quality control review.

Table 3-2 summarizes the agreement between the clinical and study pathologists for the sites with images passing quality control (QC) review. For 75% of these sites, the diagnoses provided by the clinical and study pathologists were identical. In cases where the diagnosis differed, they did not disagree by more than one degree, e.g. CIN2 versus CIN3.

Colposcopic Impression	Histologic Diagnosis	Number of Sites Measured Passing QC Review	Number of sites HRME Positive	% HRME positive
Normal	NA	49	3	6%
Abnormal	Normal/ Inflammation	8	2	25%
Abnormal	CIN1	14	3	21%
Abnormal	CIN2	13	11	85%
Abnormal	CIN3	21	20	95%
Abnormal	Cancer	3	3	100%

Table 3-1 Fraction of sites classified as positive by HRME image analysis versus colposcopic impression and histologic diagnosis. The HRME system was used to collect images from 108 sites in 59 patients referred to Hospital de Câncer de Barretos between June 17, 2013 and June 21 on the basis of an abnormal Pap test. The colposcopic impression, histopathologic diagnosis and HRME diagnosis are reported for each site passing quality control.

Figure 3-2 shows representative HRME images for each histologic diagnosis, progressing from normal squamous epithelium in **Figure 3-2A** to CIN3 in **Figure 3-2F.** The figure illustrates the changes seen in underlying nuclear size, shape and crowding. While normal tissue shows small, well-spaced uniform nuclei, high grade dysplasia features large, crowded, irregularly shaped nuclei. In some cases, HRME images of CIN3 and cancer show prominent vessels (**Figure 3-2F**). In this study, vessels were present in three of the 24 cases of CIN3 or cancer and were not present in any other histological classification.

		Study Pathologist					
		Negative	CIN1	CIN2	CIN3	Cancer	Total
Clinical Pathologists	Negative	**8 25% HRME+**	1 0% HRME+	0	0	0	9
	CIN1	6 17 % HRME+	**7 29% HRME+**	3 67% HRME+	0	0	16
	CIN2	0	0	**10 90% HRME+**	2 100% HRME+	0	12
	CIN3	0	0	2 100% HRME+	**17 94% HRME+**	0	19
	Cancer	0	0	0	1 100% HRME+	**2 100% HRME+**	3
	Total	14	8	15	20	2	59

Table 3-2 Comparison of the histologic diagnosis between the clinical pathologists and study pathologist for all 59 colposcopically abnormal sites. The clinic pathologist designates the two pathologists working at Hospital de Câncer de Barretos and the study pathologist refers to a blinded third pathologist at the University of Virginia. The bold text in the boxes along the diagonal indicates cases where the clinical and study pathologists agreed exactly on the histologic diagnosis. In each category, the fraction of sites which were classified as neoplastic based on features of the HRME image is indicated.

We evaluated the ability of each quantitative nuclear feature to discriminate between <CIN2 and CIN2+. Two parameters – mean nuclear area and median nuclear eccentricity – provided the clearest delineation between neoplastic and non-neoplastic sites. Eccentricity is a measure of the circularity of an object; the higher the eccentricity the less circular the object is. As cells progress from low-

grade to high-grade disease, their eccentricity and mean nuclear area both increase [97]. **Figure 3-3** shows a scatter plot graph of median nuclear eccentricity vs mean nuclear area for the 108 sites passing QC. Using these two parameters, we were able to separate the 59 biopsied sites into <CIN2 and CIN2+ populations with a sensitivity of 92% (34/37, 95% CI = 78.1% - 98.2%) and a specificity of 77% (17/22, 95% CI = 54.6% to 92.1%). The OR, as a measure of association and accuracy of HRME with CIN2+, was 38.5 (95% CI = 8.2-181). There was a significant trend of increasing HRME positivity with increasing severity of diagnosis ($p_{trend} < 0.001$), and HRME positivity was strongly associated with a CIN2+ diagnosis ($p < 0.001$). Using the same cutoff to separate biopsied sites into < CIN3 and CIN3+ results in a sensitivity of 96% (23/24, 95% CI = 78.8% to 99.3%) and a specificity of 54% (19/35, 95% CI = 36.7% to 71.2%). The OR for CIN3+ was 27.3 (95% CI = 3.3 – 225).

Figure 3-3 also shows the value of these parameters for the 49 colposcopically normal sites. All but three colposcopically normal sites were classified as non-neoplastic. **Table 3-1** lists the fraction of sites which were classified as neoplastic according to these HRME parameters by colposcopic impression and histologic diagnosis, where available. All of the sites diagnosed as cancer and 95% of sites diagnosed as CIN3 were correctly classified as neoplastic based on the HRME image. Only 6% of colposcopically normal sites were classified as HRME positive.

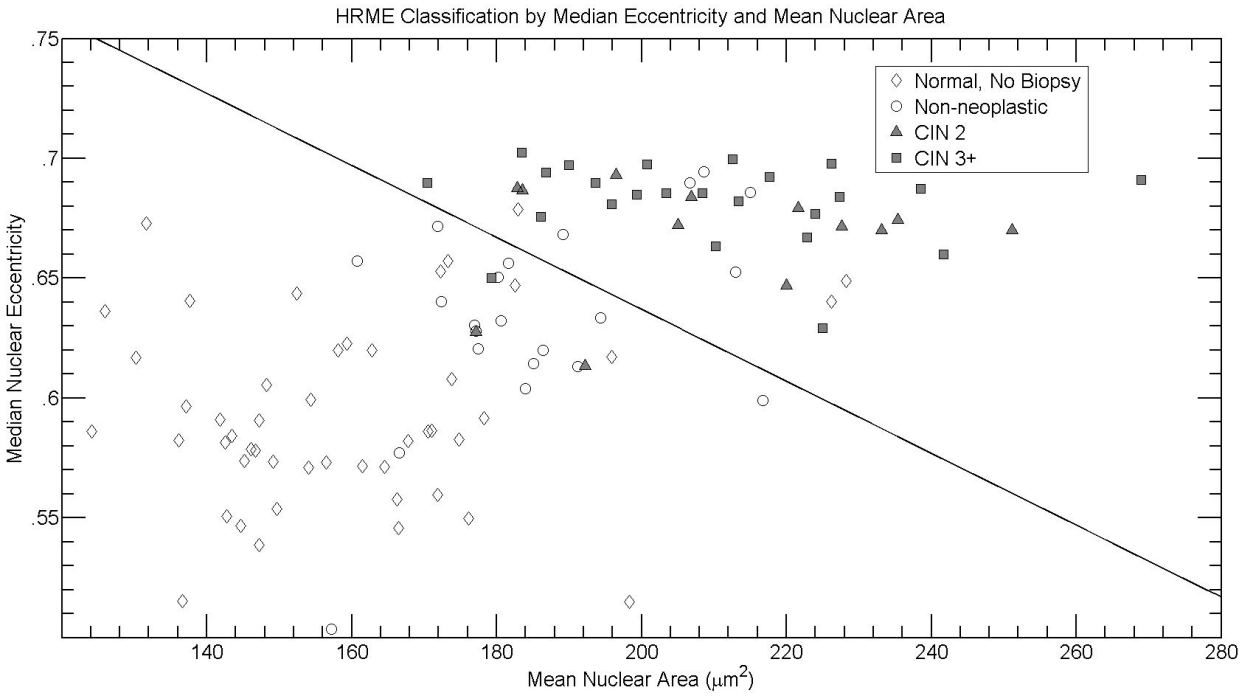

Figure 3-3 Scatter plot of mean nuclear area versus median nuclear eccentricity calculated from HRME images for each site. The gold standard histologic diagnosis for colposcopically abnormal sites that were biopsied is indicated by the marker shown in the legend. The gold standard histologic diagnosis is defined as the more severe diagnosis between the clinical pathologists' consensus diagnosis and the study pathologist's diagnosis. The black line was selected to maximize accuracy for separation of neoplastic (CIN2+) and non-neoplastic (<CIN2 i.e., normal, inflammation, CIN1) sites.

We also explored whether the fraction of sites classified as neoplastic was related to inter-observer agreement between the clinical and study pathologists. **Figure 3-4** shows a bar graph of the fraction of sites classified as neoplastic by the HRME versus the histologic diagnosis of the pathologists. In cases where the clinical and study pathologists both provided a diagnosis of CIN1, only 29% of samples were classified as neoplastic based on the HRME image. In contrast, in cases where the pathologists provided differing diagnoses of CIN1 or CIN2, 67% of samples were classified as neoplastic by HRME imaging. Similarly, in cases where the clinical and study pathologists both provided a diagnosis of CIN2, 90% of samples were classified as neoplastic based on the HRME image. In contrast, in cases where the

pathologists provided differing diagnoses of CIN2 or CIN3, 100% of samples were classified as neoplastic by HRME imaging. Thus, if either the clinical or study

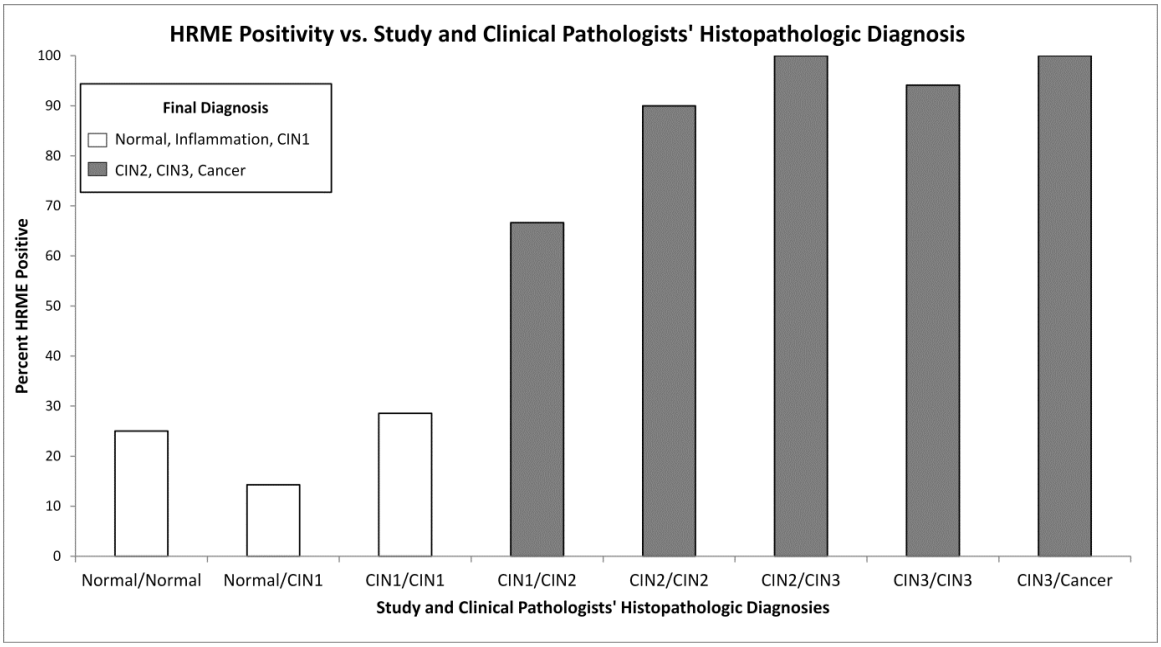

Figure 3-4 Bar graph depicting the percent of sites classified as neoplastic based on features of the HRME image versus clinical and study pathologists' histologic diagnosis.

pathologist classified the biopsy as high grade, the HRME diagnosis was more likely to be positive.

3.4. Discussion

This pilot study demonstrates the ability to use parameters derived from HRME images to objectively discriminate between non-neoplastic and neoplastic cervical tissue with a low false negative and false positive rate. Two of the three

sites that were falsely classified as negative using HRME image parameters had a histologic diagnosis of CIN2, a less reproducible and reliable diagnosis than CIN3 [98]. One additional possible cause for the false negatives in this study is imperfect correlation between the imaged location and the biopsy location. In the future, mosaicking could be implemented to acquire HRME images from a larger field of view in the region-of-interest, reducing the chance of missing focal lesions [99]. All four of the sites (100%) classified as CIN2 by one pathologist and CIN3 by another pathologist were classified neoplastic by the HRME algorithm. However, when the clinical and study pathologists agreed on a CIN2 diagnosis, the HRME-based algorithm was falsely negative for one of ten sites (10%); when they disagreed between a diagnosis of CIN1 and CIN2, one of three (33%) of samples was falsely classified as negative. These results suggest that the HRME-based algorithm may identify nuclear changes present in more advanced CIN2 cases; however, a larger study is necessary to validate this finding.

The sensitivity and specificity reported here are for the 59 sites that were colposcopically abnormal, i.e., the subset of sites exhibiting acetowhitening. In a VIA screen-and-treat program, all 59 of these sites would be treated, including the 22 sites that were histologically non-neoplastic. Only five of these 22 (23%) sites were falsely classified as positive by HRME image analysis. Thus, in this study, the HRME would reduce overtreatment compared to using VIA by 77%. It is not possible to determine whether the three HRME images acquired from colposcopically normal sites are truly falsely positive because they were not biopsied. These results

support the concept that HRME image parameters could be used to improve the specificity of screen-and-treat programs by quantitatively identifying nuclear features associated with neoplasia, without requiring a biopsy and pathology services.

The 92% sensitivity and 77% specificity of the algorithm based on HRME image parameters reported here compares favorably to a previous study our group performed in China (sensitivity = 100% and specificity = 67%) [60]. In the previous study, the authors used nuclear-to-cytoplasmic ratio to discriminate between neoplastic and non-neoplastic sites. The majority of the false-positive sites (17/19, 89%) in the China study were sites with underlying chronic inflammation. One concern was that in low-resource settings, the higher rates of inflammation would lead to lower HRME-based specificity. Indeed, using only nuclear-to-cytoplasmic ratio to classify the images acquired in the current study resulted in a sensitivity of 76% and a specificity of 45%. We found that utilizing the mean nuclear area and median eccentricity helped to reduce the number of false positives. We hypothesize these parameters are less susceptible to change due to inflammation than the nuclear-to-cytoplasmic ratio as inflammation can lead to an increase in nuclear-to-cytoplasmic ratio due to nuclear crowding. Conversely, nuclear area remains small and nuclei do not exhibit significant pleomorphism. The addition and utilization of these parameters helped to improve both sensitivity and specificity in this study population; however, more data are needed to validate including this parameter in HRME image classification.

While the results of this study are encouraging, there are limitations. Only 59 women were included in this pilot study. A larger prospective study is necessary to validate the algorithm. In addition, lesions that are not visible by VIA will be missed by this modality. Furthermore, the HRME images from 30% of sites that were biopsied did not pass quality control. This would result in an unacceptably high number proportion of patients not receiving a diagnosis by HRME. To eliminate this problem, the software in future iterations of the device will provide feedback to the user to indicate whether an in-focus image was acquired. If the image is out of focus, the user will be prompted to acquire another image until an image of sufficient quality is obtained. After an image of sufficient quality is obtained, it will be analyzed immediately to provide an objective classification of the underlying tissue as low-grade or high-grade. The end user will not be required to interpret the mean nuclear area and median eccentricity but will instead receive a direct diagnosis of "high grade" or "not high grade" from the software. This automated software has been developed and will be validated in a future study. The HRME system costs approximately $5,000 and the cost of reagents is negligible. We are currently testing versions of the device that cost under $2,000 to better facilitate their use in low-resource settings.

Further evaluation of the HRME modality in a large prospective study is ongoing. Our results suggest that HRME imaging may provide a low-cost, accurate, point-of-care alternative to colposcopy and directed cervical biopsies for the diagnosis of cervical dysplasia in lower-resource settings, where there is often a lack

of colposcopy and pathology services. Some settings may not accept a screen-and-treat strategy due to concerns of overtreatment and yet lack the diagnostic capacities to provide a biopsy-proven diagnosis. In these settings, we envision the technology being used in conjunction with VIA or HPV DNA screening. Women who screen positive would then be evaluated with the HRME for immediate treatment if indicated, thereby reducing losses to follow-up.

Chapter 4: High-resolution microendoscopy: A point-of-care diagnostic for cervical dysplasia in low-resource settings, continued

4.1. Overview

An additional 228 patients were enrolled in the study to evaluate the diagnostic performance of the HRME. The motivation and aims are as described in the preceding chapter.

4.2. Methods

4.2.1. Study Overview

The National Committee for Ethics in Research (CONEP) of Brazil and the Institutional Review Boards from Hospital de Câncer de Barretos (Barretos, Brazil), MD Anderson Cancer Center, and Rice University (Houston, USA) reviewed and approved this study. The inclusion and exclusion criteria and study procedure are identical to those outlined in Chapter 3. The high-resolution microendoscope (HRME) used is the same device described in Chapter 3. The study procedure is identical to that in chapter 3, with one exception; in this study, two pathologists at Hospital de Câncer de Barretos independently provided histopathological diagnosis for each biopsy. Biopsies were classified as metaplasia, inflammation, cervical intraepithelial neoplasia (CIN) grade 1 (CIN1), CIN grade 2 (CIN2), CIN grade 3 (CIN3) or cancer using standard criteria [94]. In cases where the two pathologists disagreed, they reviewed the cases together and came to a consensus diagnosis. In the event that the pathologists were unable to determine if a biopsy was CIN2 vs CIN3, the final diagnosis used in this analysis is designated as CIN2/3.

4.2.2. Image Analysis

One movie frame was selected from each biopsy location. A researcher blinded to histopathological diagnosis selected a frame they deemed to be of the highest quality and most dysplastic appearing image from each imaging site. Images in which greater than half of the field-of-view was not in focus or in which greater

than half of the field-of-view was occluded by large debris were manually identified and excluded from further analysis. The remaining images were analyzed using a custom Matlab 2012b script. First, the user manually selected the outline of the fiber bundle. Signal outside of this boundary was disregarded. A Gaussian filter was applied to remove artifacts from individual fiber cores. Next, a top-hat filter was applied to reduce background variance and increase contrast. From this image, a region-of-interest (ROI) for further analysis was automatically determined. The ROI was calculated by taking the area inside of the fiber and removing any saturated, dimly lit, or homogenous areas[90]. Inside the ROI, a binary threshold was applied to separate nuclei from the background. The threshold was determined automatically using Otsu's method [95]. The nuclear-to-cytoplasmic ratio, mean nuclear area, median nuclear eccentricity and number of nuclei were calculated for each ROI. To quantify image quality in order to facilitate automatic image quality control, the Michelson contrast and average intensity of each ROI was calculated. Additionally, abnormal nuclei were identified in each image. A nuclei was classified as abnormal if its area was greater than 195 μm^2 and its eccentricity was greater than 0.65. These thresholds were selected based on comparing the mean nuclear area and nuclear eccentricity of non-neoplastic and neoplastic sites imaged in Chapter 3. Based on this information, the percent of nuclei which were classified as abnormal was calculated for each image. Finally, the number of abnormal nuclei per unit area of the ROI was also calculated. Images with a Michelson contrast of less than 0.15

and an average intensity of less than 40 were automatically excluded from further analysis. Images with less than 100 nuclei in the field-of-view were also excluded.

Four methods were compared for classifying images as non-neoplastic (inflammation, metaplasia, and CIN1) vs neoplastic (CIN2, CIN2/3, CIN3, cancer). The first method used the parameter of mean nuclear area and median eccentricity for classification; as described in Chapter 3. The same cutoff line using data from the previous 59 patients was used. The second method used nuclear-to-cytoplasmic ratio to classify images as non-neoplastic or neoplastic. The third method used the percent of nuclei that were abnormal in the ROI and the final method used the number of abnormal nuclei per unit area of the ROI as classification parameters. For the second, third and fourth methods the cutoff was chosen as the highest cutoff-value that achieved 90% sensitivity. For each method, a test of trend[96] was used to examine the relationship between a neoplastic HRME diagnosis and the severity of the histopathological diagnosis. Sensitivity, specificity, and odds ratio (OR) with 95% confidence intervals (95% C.I.) were calculated for HRME detection of CIN2 or more severe diagnosis (CIN2+) + and CIN3 or more severe diagnoses (CIN3+). P values of <0.05 were considered statistically significant.

4.3. Results

A total of 228 patients were enrolled in the study between September 8, 2014 and January 26, 2015. All patients successfully underwent HRME imaging without any adverse events. HRME images were obtained from 253 colposcopically

abnormal sites. Images from twenty three of these sites were removed by the automatic quality control algorithm. Twenty two of these images were removed because they were below the Michelson contrast and average intensity metrics. One was removed due to an insufficient number of nuclei found in the image. An additional eleven images were removed through the manual QC process. The distribution of the consensus histopathologic diagnosis for the remaining 219 sites is as follows: eleven inflammation (5%), four metaplasia (2%), one-hundred and one CIN 1 (46%), forty CIN 2 (18%), seven CIN 2/3 (3%), forty six CIN 3(21%), eight squamous cell carcinoma (4%) and two adenocarcinoma (1%).

The result of the four methods for classifying images as neoplastic or non-

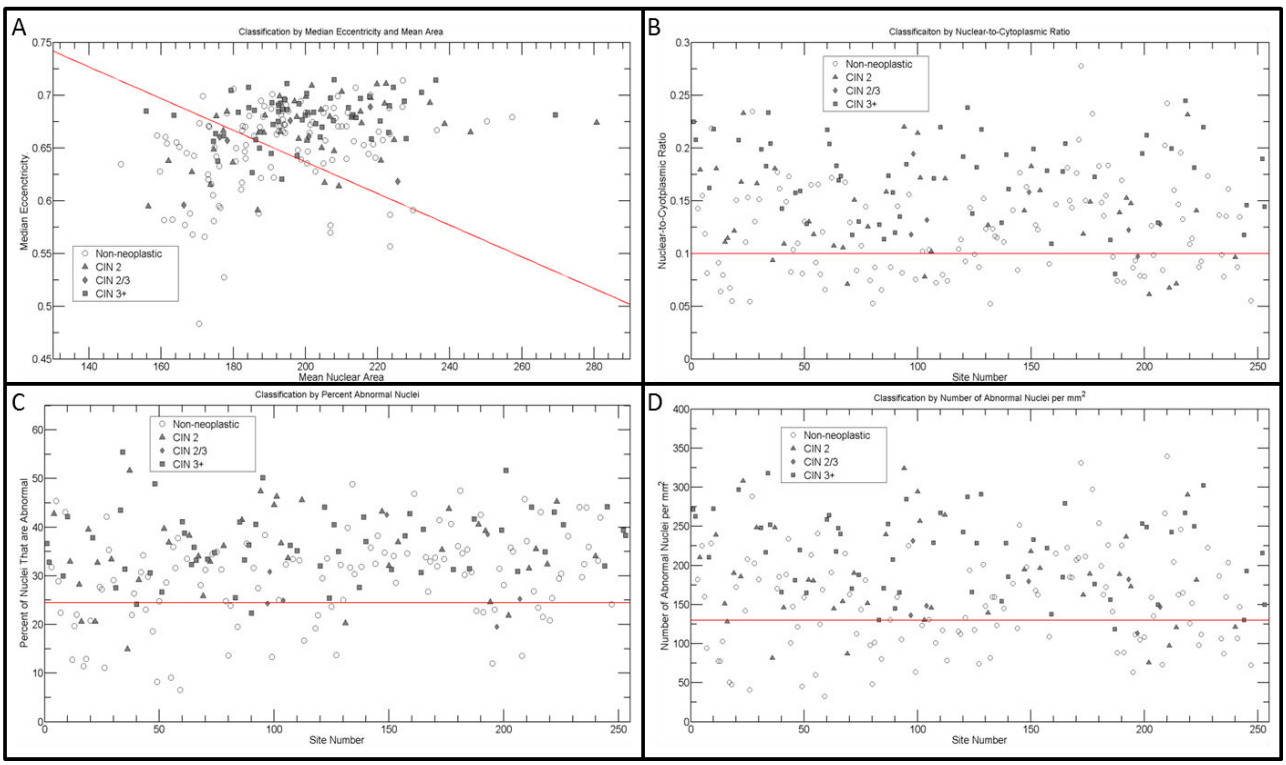

Figure 4-1: Classification of sites as neoplastic or non-neoplastic by four different methods. (A) Classification by median eccentricity and mean nuclear area. **(B)** Classification by nuclear-to-cytoplasmic ratio **(C)** Classification by percent of nuclei that are abnormal **(D)** Classification by number of abnormal nuclei per unit area

neoplastic is shown in **Figure 4-1.** The corresponding sensitivities, specificities, test of trend and odds ratio are provided in **Table 4-1.** All methods showed a significant trend ($p<0.05$) between increasing severity of histopathologic diagnosis and HRME positivity. Of the three methods achieving a minimum sensitivity of 90%, the specificity was greatest using the number of abnormal nuclei per unit area (38.9%), followed by NC ratio (37.1%) and percent of total nuclei that were abnormal (26.7%). If the cutoff is adjusted to achieve greater than 90% sensitivity using mean area and median eccentricity, the specificity for this method drops to 30.2%.

	HRME positive by number abnormal per unit area	HRME positive by fraction of nuclei that are abnormal	HRME positive by mean area and median eccentricity	HRME positive by NC ratio
Inflammation	9/11 (81%)	9/11 (81%)	6/11 (54%)	8/11 (72%)
Metaplasia	1/4 (25%)	3/4 (75%)	3/4 (75%)	1/4 (25%)
CIN1	61/101(59%)	73/101(71%)	60/101 (56%)	64/101 (62%)
CIN2	33/40 (83%)	35/40 (87.5%)	30/40 (75%)	33/40 (83%)
CIN2/3	6/7 (86%)	5/7 (71%)	4/7 (57%)	6/7 (86%)
CIN3	45/46 (98%)	45/46(98%)	38/46 (83%)	45/46 (98%)
Squamous Cell Carcinoma	8/8(100%)	7/8 (87.5%)	6/8 (75%)	8/8(100%)
Adenocarcinoma	2/2 (100%)	2/2 (100%)	2/2 (100%)	2/2 (100%)
Sensitivity CIN2+ (95% C.I.)	91.3% (84.1% – 95.9%)	91.3% (84.1% – 95.9%)	77.7% (68.4%– 85.3%)	91.3% (84.1 % to 95.9%)
Specificity CIN2+ (95% C.I.)	38.9% (29.9% - 48.2%)	26.7% (18.9% - 35.7%)	40.5% (31.5% - 50.0%)	37.1% (28.3% to 46.5%)
Sensitivity CIN3+ (95% C.I.)	98.2% (90.5 – 100%)	96.5% (87.9% - 99.6%)	82.1% (69.6%-91.1%)	98.2% (90.5 – 100%)
Specificity CIN3+ (95% C.I.)	32.5% (25.4% - 40.3%)	23.3% (17.1% - 30.6%)	36.8% (29.4% - 44.7%)	31.52 % (24.5% to 39.2%)
Odds Ratio CIN2+ (95% C.I.)	6.6 (3.0 to 14.4)	3.8 (1.7 to 8.5)	2.4 (1.3 to 4.3)	6.2 (2.8 to 13.4)
Odds Ratio CIN3+ (95% C.I)	26.5 (3.6 to 196.7)	8.2 (1.9 to 35.2)	2.7 (1.3 to 5.7)	25.0 (3.4 to 186)
Test of Trend	P < 0.001	P< 0.025	P<0.025	P<0.001

Table 4-1 Comparison of performance of four different methods for classifying HRME images

The association of HRME positivity with CIN2+ was evaluated using OR. The OR for CIN2+ was 6.6 (95% C.I. = 3.0 – 14.4) using the number of abnormal nuclei per unit area, 6.2 (95% C.I. = 2.8 to 13.4) using NC ratio, 3.8 (95% C.I. =1.7 to 8.5) using fraction of nuclei that were abnormal and 2.4 (95% C.I. = 1.3 to 4.3) using

median area and eccentricity. The odds ratio for HRME positivity with CIN3+ was 26.5 (95% C.I. = 3.6 to 196.7) for number abnormal nuclei per unit area, 25.0 (95% C.I. = 3.4 to 186.0) for NC ratio, 8.2 (95% C.I. = 1.9 to 35.2) for fraction of nuclei that were abnormal, and 2.7 (95% C.I. =1.3 to 5.7) for mean area and median eccentricity.

4.4. Discussion

The specificity was significantly lower using any method presented here compared to the reported specificity of 77% achieved for the first 59 patients[100]. Cut-off values for the three new classification algorithms were chosen to ensure a minimum of 90% sensitivity. This decision was made because it is critical that the HRME does not incorrectly classify high grade dysplasia as non-neoplastic. This choice, however, resulted in low specificity for all classification methods. One major difference between the population of the pilot study of the first 59 patients and the population reported in this study is the fraction of sites with a non-neoplastic histopathological diagnosis. In the first study, only 22 of 59 sites (37%) were classified as non-neoplastic. In this study, 116 of 219 sites analyzed were non-neoplastic (53%). There was a large degree of heterogeneity amongst these non-neoplastic sites. This is evident by the large variation seen across all parameters for non-neoplastic sites, as shown in **Figure 4-1.**

The challenges this heterogeneity presents are evident in the example images in **Figure 4-2**. **Figure 4-2A** shows an HRME image of a site with a

histopathologic diagnosis of CIN1. Every classification method correctly identified this site as non-neoplastic. **Figure 4-2B** is an HRME image from a site with a histopathological diagnosis of inflammation. The pathology report also noted the biopsy contained only endocervical tissue without any squamous cells. The densely packed columnar cells of endocervical tissue are difficult to distinguish from high grade dysplasia using HRME imaging. All four methods incorrectly identified this location as neoplastic. **Figure 4-2C** shows an HRME image from a site with a histopathological diagnosis of CIN1 with metaplasia. The high nuclear density seen in inflammatory conditions in conjunction with the densely packed columnar tissue found in metaplastic tissue also presents challenges for HRME imaging. All classification algorithms also incorrectly identified this site as neoplastic. Finally, **Figure 4-2D** shows an HRME image from a site with a histopathologic diagnosis of CIN3. This region was classified as neoplastic using the number of abnormal nuclei per unit area method and NC ratio method. It was incorrectly identified non-neoplastic by the other two algorithms. Because it is critical to not misclassify high-grade cases, it is difficult to achieve high specificity with the wide array of cases seen in non-neoplastic cervical tissue.

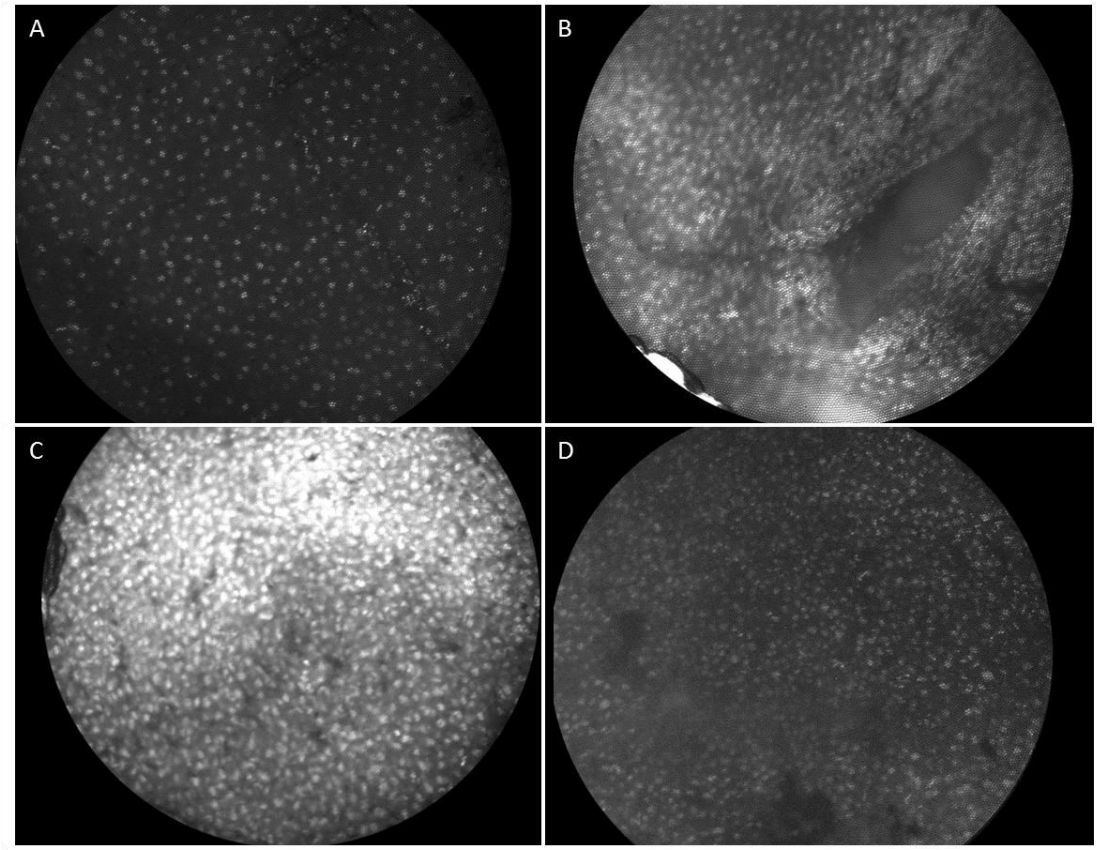

Figure 4-2: Challenges in separating HRME images from non-neoplastic sites (A-C) from HRME images from neoplastic sites(D). (A) HRME image from a site diagnosed as CIN1. This site was correctly identified as non-neoplastic by all HRME classification algorithms. **(B)** HRME image from a site with a histopathologic diagnosis of inflammation. The biopsy showed endocervical tissue without any squamous tissue. All HRME algorithms incorrectly diagnosed this as site as neoplastic. **(C)** HRME image from a site with a histopathologic diagnosis of CIN1 with metaplasia. All algorithms incorrectly classified this site as neoplastic **(D)** HRME image from a site with a histopathologic diagnosis of CIN3. It was correctly identified as high grade using the number of abnormal nuclei per unit area method and NC ratio method. It was incorrectly identified as non-neoplastic sby the fraction of nuclei that are abnormal method and by using median eccentricity and mean area.

In future studies, HRME analysis should be streamlined. First, the outline of the fiber should be determined automatically. This proved to be difficult for this study because of the presence of debris on the fiber boundaries. In future studies, a calibration image of a fluorescent target should be taken in order to define the fiber boundaries prior to *in vivo* imaging. Additionally, a single image should be taken from each site of interest. Taking movies at each location is not conducive to near real-time HRME analysis and diagnosis. Furthermore, selection by an individual introduces a degree of unwanted variability to the analysis process. After an image is acquired, Michelson contrast and mean intensity should be calculated to determine if the image acquired is of sufficient quality to be analyzed. If not, the user should be prompted to take another image until an image of sufficient quality is obtained. Increasing specificity may require more advanced image processing algorithms or an additional contrast agent.

In the immediate future, either NC ratio or the number of abnormal nuclei per unit area should be used. These algorithms both correctly identified 45 out of 46 CIN3 sites as neoplastic. Additionally, they both classified all ten cases of cancer as neoplastic. These algorithms both depend directly on the automatically determined ROI. It is important to continue to refine the ROI selection process to avoid selecting large areas where the fiber is not in contact with tissue or is occluded by debris.

Chapter 5: A mobile-phone based high-resolution microendoscope

5.1. Introduction

Cervical cancer remains a major global health concern with an estimated 527,600 new cases and 265,700 deaths attributed to cervical cancer in 2012. Nearly 90% of all cervical cancer deaths occurred in developing countries[1]. In countries with the financial and human resources to support national screening programs, the incidence and mortality of cervical cancer has dropped drastically [5]. Screening prevents cervical cancer by allowing for the detection and treatment of cervical precancer [5]. An effective vaccine has been developed against HPV 16 and 18 which together are responsible for an estimated 70% of cervical cancer cases[68,71]. More recently, a 9-valent HPV vaccine has been developed which offers protection against oncogenic HPV strands responsible for approximately 90% of all cervical cancers[73].

However, implementation in low resource settings is limited largely due to the high cost of the vaccine[75]. Furthermore, the vaccine is not effective for women who are already infected with HPV. Screening will continue to remain important for decades for those that did not receive the vaccine prior to infection and for those infected with oncogenic HPV types the vaccine does not protect against [74]. Unfortunately, in low- to middle-income countries (LMICs) screening programs are difficult to implement due to a lack of human and financial resources and inadequate infrastructure[33].

Alternative, low-cost screening techniques appropriate for LMICs have been developed to decrease the global burden of cervical cancer. Visual inspection with acetic acid (VIA) and visual inspection with Lugol's iodine (VILI) are two alternative screening techniques [33]. In VIA, a clinician applies dilute acetic acid directly to the cervix and examines the cervix for signs of acetowhitening, a localized whitening of the epithelium associated with abnormal underlying tissue [39]. In VILI, dilute Lugol's iodine is applied topically to the cervical epithelium, staining normal glycogen-rich squamous epithelium preferentially, leaving glycogen-depleted proliferative cancerous and precancerous lesions unstained[45]. More recently, human papillomavirus (HPV) DNA screening has been explored for cervical cancer screening. HPV DNA testing is highly sensitive [101] because virtually every case of cervical cancer is caused by a persistent high-risk HPV infection [7]. However, VIA, VILI and HPV DNA testing are all limited by high false-positive rates and low

positive-predictive values [45,49,89,102], leading to substantial overtreatment when used as part of a see-and-treat strategy.

Various optical imaging techniques have also been explored to allow for identification of cervical precancer *in vivo* [53]. One such technique is the high-resolution microendoscopy [57,58,67]. The high-resolution microendoscope (HRME) is a fiber bundle-based fluorescence microscope capable of imaging cell nuclei *in vivo*. The HRME system is used following topical application of the fluorescent topical contrast agent proflavine, which selectively stains cell nuclei. HRME images obtained with the device can be used to quantify nuclear features associated with neoplastic progression, such as nuclear-to-cytoplasmic ratio and nuclear eccentricity [60,66]. In pilot studies in China [60] and Botswana [66], the HRME identified cervical pre-cancer with high sensitivity and specificity. However, the high cost ($5,000) and size (28cm x 23cm x 6.5cm) of the device preclude its use in some low-resource settings. The cost and size of the standard HRME are driven by three main components: a scientific-grade camera, a laptop and off-the-shelf optomechanics [57,58]. Recent advances in mobile phone technology, including high processor speeds and compact digital cameras, provide a unique opportunity to simultaneously reduce both the size and cost of the HRME. Due to the ubiquity of mobile phones and their increasingly sophisticated cameras, other research groups have designed mobile phone-based microscopes [103,104]. Here, we report a low-cost, highly portable mobile HRME (mHRME) utilizing a mobile phone and custom 3D-printed parts in lieu of a scientific-grade camera, laptop and commercial optomechanics.

5.2. Materials and Methods

5.2.1. Optical Design

The mHRME is a fiber-based fluorescence microscope, similar in operation to that described by Muldoon et al. [57]. The mHRME consists of four main components: optical lenses and filters, a mobile phone, a light emitting diode (LED) light source and a one millimeter outer-diameter coherent fiber bundle. The device was designed with a target magnification of 1.0 to ensure that the entire field-of-view (FOV) of the fiber fit within the dimension of the cell phone's complementary metal-oxide-semiconductor (CMOS) sensor. To minimize distortion, Steinheil lenses were selected for all of the imaging optics because they are optimized for 1:1 conjugate ratios. To create a compact, portable device, all lenses had a maximum diameter of no more than 12.5 mm. ZEMAX was used to aid in commercial lens selection and positioning.

An overview of the device's optical pathway is shown in **Figure 5-1A**. An LED (LED Engin, LZ1-10DB00) provides excitation light centered at 460 nm. The LED is powered in one of two ways. For cell phones that offer USB on-the-go support, the LED is powered through a USB cable connected to the phone. For phones lacking this capability, an external USB battery pack (e.g., Anker 10,000 mAh battery pack) may be used. The current is regulated by a 1000 mAh LED driver (LED Supply, 03023-D-E-1000P). The LED is collimated through an achromatic doublet (Edmund optics, 65-550) before passing through a 20 nm band-pass excitation filter centered

at 448 nm (Edmund Optics, 86-975). The excitation light is then reflected towards the fiber bundle via a dichroic mirror with a 482 nm cut-on wavelength (Edmund 86-317). After reflecting off the dichroic mirror, the light is coupled to a fiber bundle (Fujikura, FIGH-30-850N) by a pair of 18 mm effective focal length (EFL) triplet lenses (Edmund Optics, 45-399). The fiber bundle used here is composed of 30,000 fibers with 4 μm spacing between each fiber. The dimensions of the fiber bundle also directly determine the field-of-view of the system.

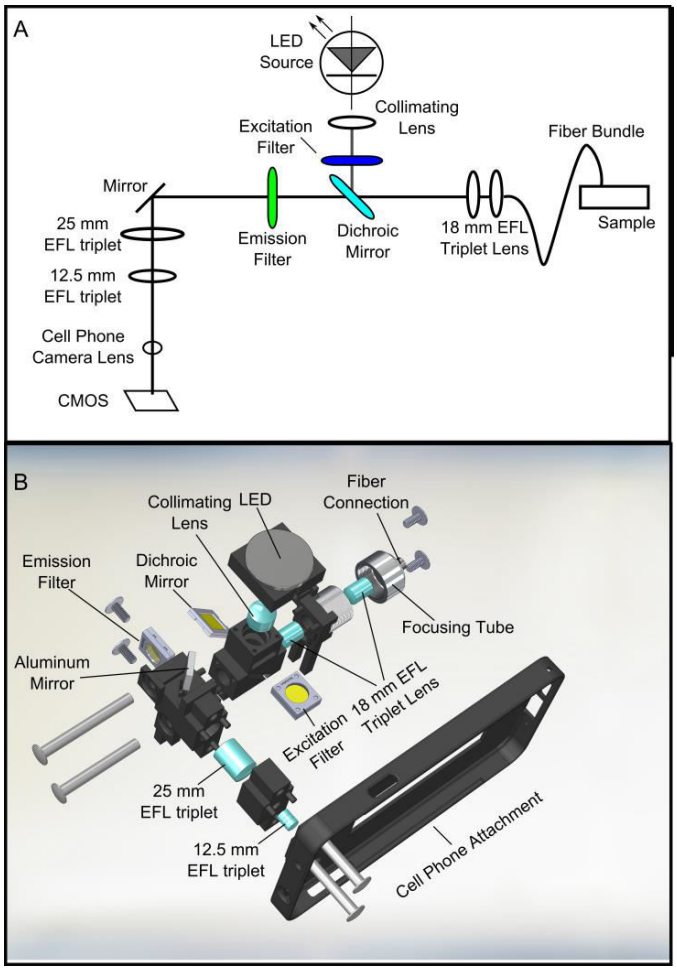

Figure 5-1: Schematic of mHRME. (A) Diagram of optical layout of the system. **(B)** Solidworks illustration depicting all components of the system.

The system is designed to be used with the fiber bundle placed in direct contact with proflavine-stained epithelial tissue. Light emitted from the tissue is

then collected through the same fiber. After passing through the fiber, emission light is collected through the pair of triplet lenses prior to transmitting through the dichroic mirror. Next, the emitted light is filtered by a 515 nm long-pass color glass emission filter (Schott OG-515). The remaining signal is redirected with an aluminum mirror (Thorlabs ME05S-G01) through a 25mm EFL triplet lens (47-675 Thorlabs) and it is coupled to the cell phone's lens through a 12.5 mm EFL triplet.

Based on the optimal lens positions identified in ZEMAX, the cell-phone attachment and optomechanic holder was printed with a 3D printer (3D systems, South Carolina). The 3D-printed structure consists of individual pieces that snap together as shown in **Figure 5-1B**. The pieces contain cutouts corresponding to the exact size of the lenses, ensuring that the lenses are positioned accurately and precisely. After assembly, four threaded aluminum rods are placed in through-holes to ensure stability during use. The optical system connects directly to the phone, thereby ensuring alignment of the optics with the mobile phone camera. We tested the mHRME using two phones: the Samsung Galaxy Note 3, which features 13 a megapixel camera and 2.3 GHz processor and an HTC One X+, an older, midlevel international smartphone with 8 megapixel resolution.

5.2.2. Imaging Testing

5.2.2.1. *In Vitro* Imaging

We first determined the resolution of the system using a standard Air Force Resolution Target. To validate the ability of the mHRME to image cell nuclei and to

assess the signal-to-background ratio (SBR) we evaluated its performance in cultured HeLa cells. HeLa cells were cultured in Dulbecco's Modified Eagle's Medium (DMEM) in a 150 mm Petri dish until approximately 50% confluent. The media was aspirated and the cells were washed once with phosphate buffered saline (PBS). After aspirating the PBS, 1 mL of 0.01% proflavine in PBS was applied to cover the cells. After one minute, the proflavine was removed and cells were washed twice with PBS. The cells remained in PBS solution and were imaged with the mHRME system directly in the Petri dish; the tip of the fiber was placed in direct contact with the cells.

5.2.2.2. *In Vivo* Imaging

After successfully imaging cultured cells, we proceeded to test the mHRME *in vivo*. Patients with abnormal Pap smears in the state of Sao Paulo, Brazil referred to Hospital de Câncer de Barretos for colposcopy were enrolled in a pilot study to evaluate the efficacy of the standard HRME in discriminating between non-neoplastic and neoplastic lesions[100]. The National Committee for Ethics in Research (CONEP) of Brazil and the Institutional Review Boards from Hospital de Câncer de Barretos, MD Anderson Cancer Center and Rice University approved this study. A subset of the patients in this study was also imaged with our mHRME to assess its *in vivo* imaging capabilities.

During routine colposcopy, the clinician first evaluated the cervix using 5% acetic acid under white-light conditions. If an abnormal region was observed, the

clinician then applied .01% (w/v) proflavine solution to the cervix using a spray bottle and cotton swab. After the application of proflavine, Lugols' iodine was applied as part of the standard of care for colposcopy at Hospital de Câncer de Barretos . Proflavine was then applied again to enhance signal strength. Next, the clinician placed the tip of the mHRME probe in gentle contact with an area of the cervix that appeared normal by colposcopy. Images were captured using the android app Camera FV-5 (FGAE studios, Stuttgart, Germany). The software contrast preset was set to a maximum value of 10 for all images. After acquiring images of normal squamous epithelium, mHRME images were collected from a colposcopically abnormal lesion.

5.3. Results

5.3.1. System Characterization

The key properties of the system are outlined in **Table 3-1**. The device,

	Standard HRME	mHRME – Galaxy Note 3	mHMRE – HTC One X+
Image Sensor Size (diagonal)	11 mm	5.87 mm	5.68 mm
Spatial Resolution	4.4 μm	4.9 μm	4.9 μm
Fiber Bundle Size	30,000 fiber cores	30,000 fiber cores	30,000 fiber cores
Pixels per fiber	27 pixels	20.7 pixels	9.8 pixels
Field-of-View	750 μm	750 μm	750 μm
Weight*	2500 g	170 g	170 g
Dimensions	28 cm x 23 cm x 6.5 cm	15 cm x 7 cm x 8 cm	13 cm x 7 cm x 8 cm
Prototype Cost	$5,500	$1,650	$1,350

Table 5-1 Key system parameters for the standard HRME and mHRME using the Galaxy Note 3 and HTC One X+. Both mHRMEs are significantly smaller, lighter and less expensive than the standard HRME system. *Weight excludes the weight of the laptop or mobile phone

excluding the mobile phone, weighs 170 g and is 15 cm x 7 cm x 8 cm using the Galaxy Note 3. The power output at the distal end of the fiber is 0.8 mW/cm^2 and the field-of-view is 750 μm. The system is capable of resolving element five of group six, as shown in **Figure 5-2** using both the Galaxy Note 3 and HTC One X+; this element corresponds to a line-width of 4.9 μm.

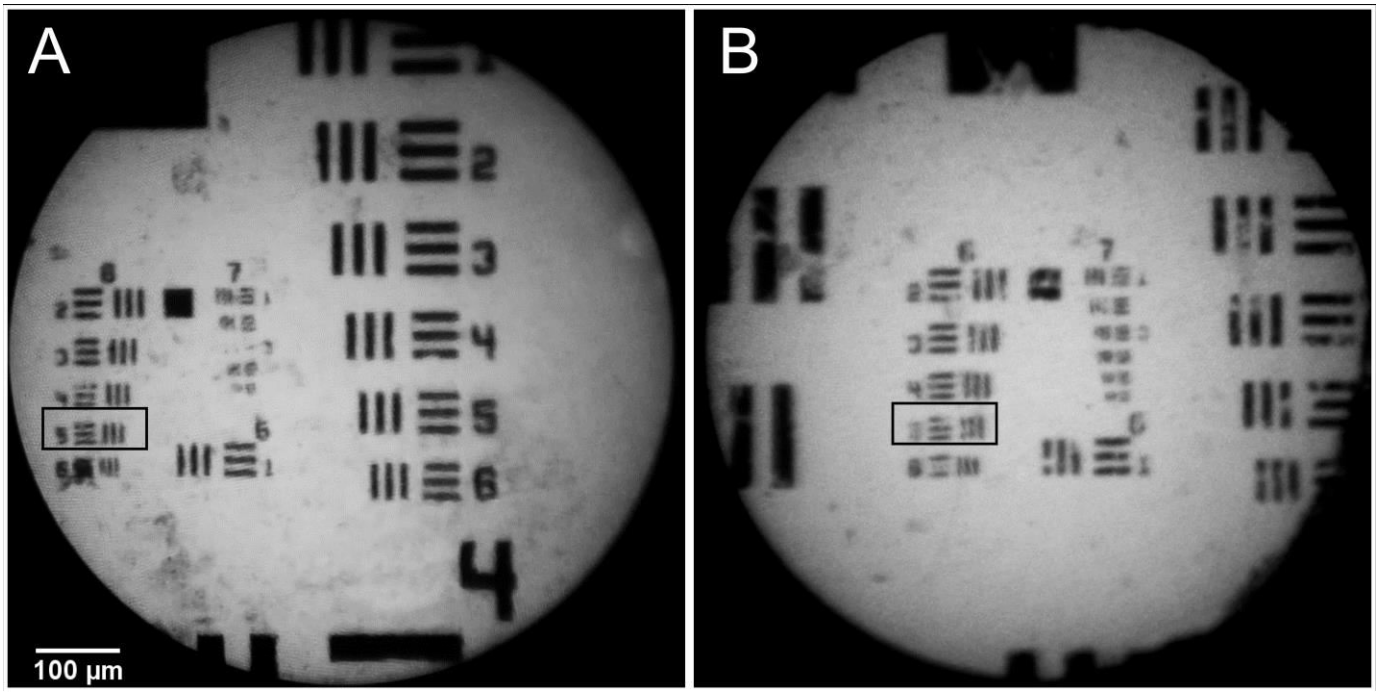

Figure 5-2: System resolution evaluation. Air-Force Resolution Target image taken with the mHRME system using **(A)** the Galaxy Note 3 and **(B)** The HTC One X+ The smallest target the system can resolve is group 6, element 5 (boxed) corresponding to a resolution of 4.9 µm

5.3.2. Cultured Cell Imaging

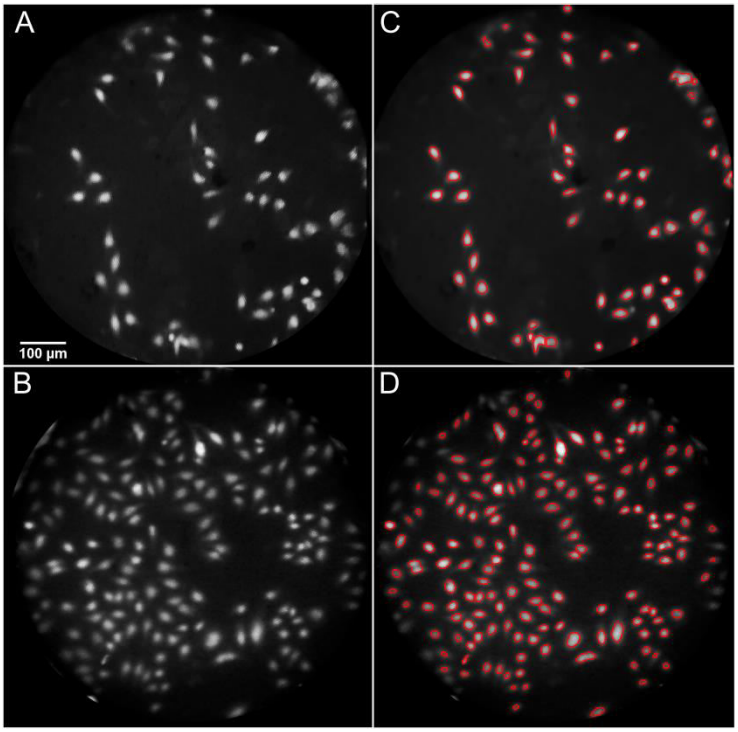

Figure 5-3 HeLa cell imaging. Raw images of cultured HeLa cells taken with the **(A)** Galaxy Note 3 and **(B)** HTC One X+ mobile high-resolution microendoscopes. Nuclei from **(A)** and **(B)** are automatically selected from the background and outlined in **(C)** and **(D)**, respectively.

Images of proflavine-stained HeLa cells taken with the Galaxy Note 3 and HTC One X+ are shown in **Figure 5-3.** The figure shows the green channel from an otherwise unprocessed mHRME image. In order to evaluate the signal-to-background ratio, the cells were segmented automatically from the background using a custom MATLAB script. First, a top hat filter was applied reduce the background and correct any uneven illumination. Next, a threshold was determined using Otsu's method [95] to separate nuclei from the background of the image. The resulting segmentation corresponding is shown in **Figure 5-3**. The signal-to-background ratio was calculated by dividing the mean intensity of pixels within the segmented cell nuclei by the mean intensity of pixels within the fiber bundle not classified as nuclei. The resulting signal-to-background ratio is 5.3 for

the Galaxy Note 3 system and 4.4 for the HTC One X+ system, comparing favorably to that obtained with previous standard HRME systems [57,67].

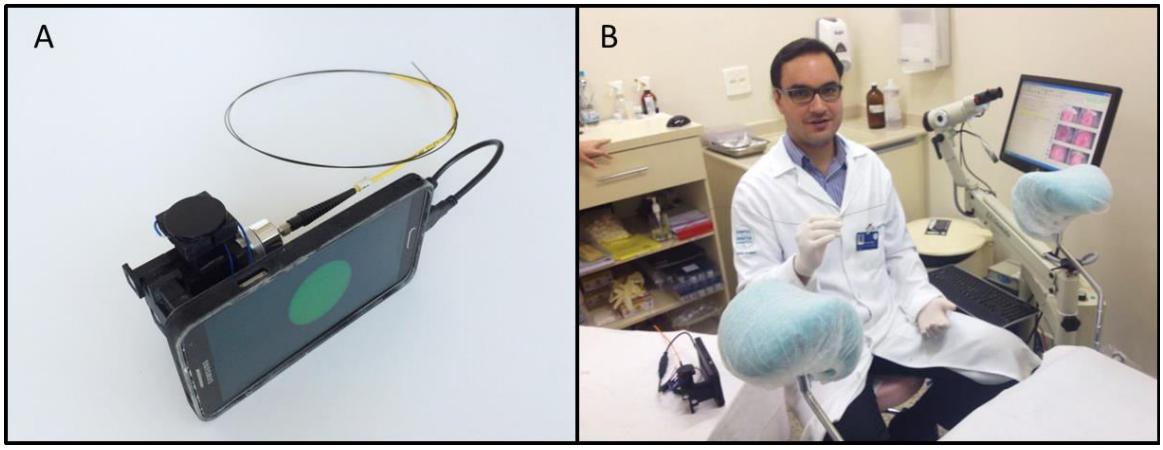

Figure 5-4 Photographs of the mHRME prototype. (A) Photograph of the completed mHRME Galaxy Note 3 prototype**. (B)** Photograph of the mHRME in a coloposcopy clinic at Hospital de Câncer de Barretos.

5.3.3. In Vivo Imaging

The mHRME was tested by colposcopists at Hospital de Câncer de Barretos to determine its ability to image squamous epithelium *in vivo*. **Figure 5-4** shows the completed prototype with the Galaxy Note 3 and a photograph of the mHRME in the colposcopy clinic prior to *in vivo* use. **Figure 5-5** provides representative *in vivo* mHRME images obtained from colposcopically normal and colposcopically abnormal squamous epithelium. The mHRME image of colposcopically normal

tissue, shown in **Figure 5-5A** shows round, well-spaced and small nuclei, consistent with the histological diagnosis of normal squamous epithelium. In contrast, the majority of the mHRME image of colposcopically abnormal tissue, shown in **Figure 5-5B** shows large, pleomorphic, crowded nuclei, consistent with the histological diagnosis of high grade dysplasia. This image was taken at the edge of a lesion; the junction between abnormal and normal epithelium is evident in the bottom left hand region of **Figure 5B** and is marked with arrows. Both mHRME images in **Figure 5-5** have been post-processed identically by selecting only the green channel, applying a top hat filter, and enhancing the contrast. In the future, this

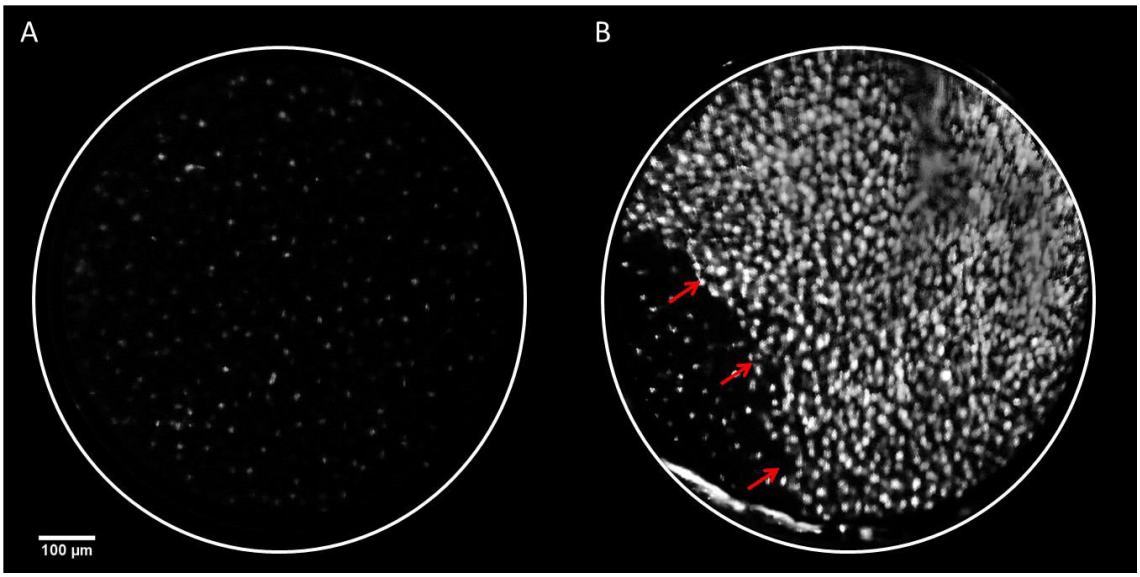

Figure 5-5 In Vivo imaging of the cervix with the mHRME of (A) normal squamous epithelium and **(B)** high grade dysplasia. The white circle indicates the boundary of the fiber bundle. The red arrows in **(B)** indicate the junction between the lesion and surrounding normal tissue

post-processing could be achieved in near real-time with a custom android camera application.

5.4. Discussion

We developed a mobile phone high-resolution microendoscope capable of imaging epithelial cells *in vivo*. At 4.9 μm, the resolution is slightly inferior to that of the standard HRME system (4.4 μm), likely due to the lower quality, smaller camera sensor. However, the resolution is sufficient to acquire sub-cellular resolution images of cervical tissue *in vivo*. Using a mobile phone eliminates the need for a scientific-grade camera and laptop, thereby significantly reducing both size and cost. The battery powered system can be used in settings without wall electricity. Using the Galaxy Note 3's built-in battery provides two hours of imaging, while the economical(~$30) Anker external USB battery pack allows for ten hours of imaging.

System cost could be reduced substantially if produced in large quantities. First, 3D printed components could be made by injection molding, at a fraction of the price. Second, the optical lenses and LEDs drop markedly in price when purchased in bulk. With large-scale production the price of the mHRME would be under $500, exclusive of the cell phone. Because the device does not have any associated consumables, we believe this price target is reasonable even for use in low-resource settings.

The device is also designed to be flexible to allow for different applications. The LED, filters and dichroic mirror can be changed in order to utilize other fluorescent dyes without any additional system modifications. The field-of-view can be changed depending on the application by using different fiber bundles. For applications in which a much larger field-of-view is desirable, mosaicking approaches can be implemented[99]. Finally, the optics of the system are designed to interface with a variety of mobile phones. The magnification was chosen such that the CMOS is underfilled. This ensures that if other mobile phones were selected with smaller sensor sizes, the fiber image would still fit on the sensor. The mHRME sends a collimated signal to the cell phone camera. A cell phone with a camera of at least 8 megapixels that can be set to infinity or landscape mode is sufficient to acquire in-focus images with subcellular resolution.

In conclusion, we have demonstrated a mobile phone based microscope capable of achieving sub-cellular resolution *in vivo*. While initial results are promising, further studies are necessary to validate that the device can identify cervical precancer with high sensitivity and specificity to evaluate its diagnostic performance. Advances in mobile phone technology and rapid prototyping techniques present an exciting opportunity to develop new diagnostic imaging techniques tailored for use in low-resource settings. We believe this device may have particular utility in countries in which traditional cervical cancer screening techniques are difficult to implement.

Chapter 6: Highly Sensitive Two-Dimensional Paper Network Incorporating Biotin-Streptavidin for the Detection of Malaria[++]

6.1. Introduction

Microfluidic paper-based devices are a novel class of point-of-care rapid diagnostic test (RDT) capitalizing on paper's low cost, ubiquity, and wicking properties[78]. A subset of microfluidic paper-based devices, lateral flow tests (LFTs), are a staple of clinical point-of-care (POC) diagnostics due to their simplicity, speed and low cost[105]. LFTs are typically simple sandwich immunoassays designed to

[++] This chapter has been published in Grant BD, Smith CA, Karvonen K, Richards-Kortum R. Highly Sensitive Two-Dimensional Paper Network Incorporating Biotin–Streptavidin for the Detection of Malaria. Anal Chem [Internet] 2016;88(5):2553–7[130].

detect proteins of clinical importance. They often have higher limits-of-detection than their conventional enzyme linked immunoassay (ELISA) counterparts, reducing their clinical utility[81,106]. Increased sensitivity requires the ability to implement more complicated, multistep assays, i.e. utilizing chemical amplification techniques. Recently, two dimensional paper networks (2DPN) have been developed to expand the utility of traditional LFTs[106]. These 2DPNs provide the ability to run multistep immunoassays with minimal user interaction and do not require additional instruments or significantly increase cost[106]. These devices allow for the inclusion of strategies which improve the limit-of-detection (LOD) relative to "one-dimensional" LFTS[81–85,106], providing the means to develop highly sensitive POC assays for clinically relevant targets.

One potential application of highly sensitive RDTs is the diagnosis of malaria. The World Health Organization (WHO) reports that half the world's population is at risk for malaria[107]. Malaria causes an estimated 627,000 deaths annually with 90% occurring in sub-Saharan Africa[107]. Most of these deaths result from infections with the *Plasmodium falciparum* (*Pf*) parasite, making its detection particularly important[108]. RDTs that diagnose *Pf* malaria often target the *Pf* histidine-rich protein 2 (*Pf* HRP2), an antigen released by blood stages of *Pf* parasites[109]. Using traditional ELISA techniques, researchers have been able to reliably measure *Pf* HRP2 levels as low as 0.11 ng/mL[86], corresponding to approximately 0.7 parasites/μL, using the maximum circulating approximation developed by Marquart et al[110]. In contrast, traditional lateral flow RDTs for *Pf* HRP2 are able to achieve

limits-of-detection as low as 6.94 ng/mL (8 parasites/μL)[83,110]. Fu et al. demonstrated that by implementing a 2DPN gold enhancement immunoassay, they could achieve a limit-of-detection of 2.9 ng/mL (4 parasites/μL)[82,110]. While a significant improvement, additional steps are necessary to achieve a LOD comparable to the best reported traditional ELISAs. Malaria elimination programs, which aim to detect subclinical malaria infections, require low LODs equivalent to standard HRP2 ELISAs[111].

Incorporating a streptavidin-biotin detection system can improve the limit-of-detection of immunoassays. Streptavidin-biotin detection strategies have been used for decades in ELISAs due to their many advantages[112]. Briefly, streptavidin has an extremely high affinity for biotin[113] (Kd $\sim 4 \times 10^{-14}$), streptavidin binds to biotin with high specificity, and biotin is small (244 Da) allowing it to be readily covalently linked to molecules without altering biological activity[112]. Streptavidin is available with a variety of detection labels that produce additional amplification, including the enzyme horse-radish peroxidase[112], enabling the detection of biotinylated molecules. Furthermore, streptavidin-biotin detection strategies offer an inherently amplified signal versus direct detection strategies because streptavidin and biotin both provide four binding sites for one another[112]. Additional sensitivity can be achieved by utilizing streptavidin conjugated to polymers of horse-radish peroxidase, providing a larger number of enzyme molecules per bound molecule. Here we demonstrate that by using a larger sample size than previously reported 2DPN RDTs and employing a streptavidin poly- horse-

radish peroxidase detection comparable to the lowest reported limit-of-detection by traditional ELISA.

6.2. Materials and Methods

6.2.1. Two-Dimensional Paper Network Device

The two-dimensional paper network (2DPN) devices, depicted in **Figure 6-1**, are constructed on a plastic backbone consisting of 10 mil Dura-Lar (Blick Art Supplies, Galesburg, Illinois) and 5 mil adhesive-backed Dura-Lar (Blick Art Supplies, Galesburg, Illinois). The five reagent storage and release pads and the sample pad are cut from glass fiber pads (grade 8951, Ahlstrom, Helsinki, Finland). The wicking pad is made from cellulose (C083, Millipore, Billerica, MA). The

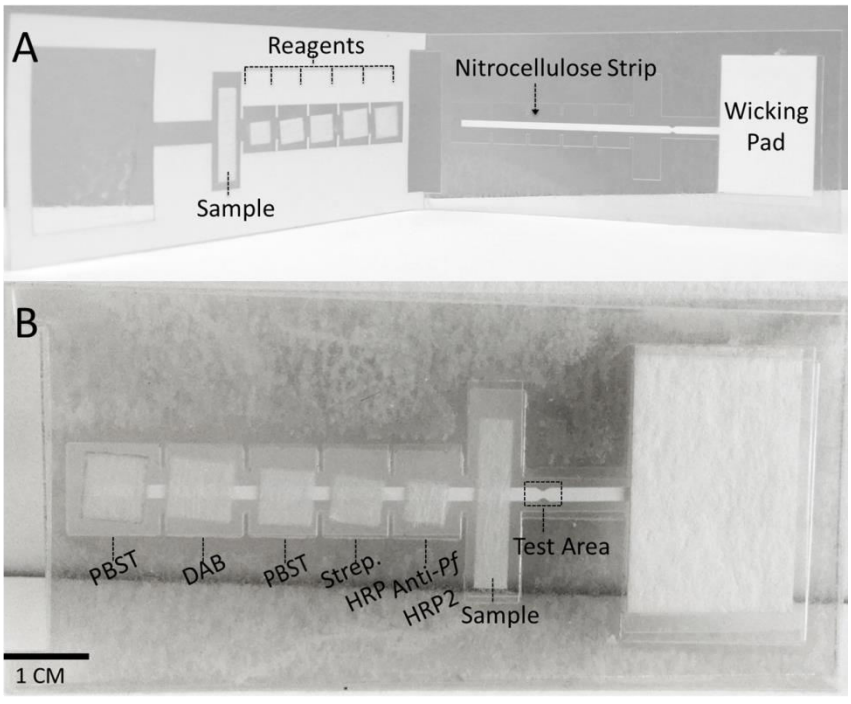

Figure 6-1 : Device diagram. (A) Device prior to folding with key components labeled. **(B)** Device folded to initiate flow with reagents and test area highlighted.

primary lateral flow channel consists of 4 mil backed high flow nitrocellulose (HF135, Millipore, Billerica, MA). All materials were cut using a CO2 laser cutter (Universal Laser Systems, Scottsdale, Arizona).

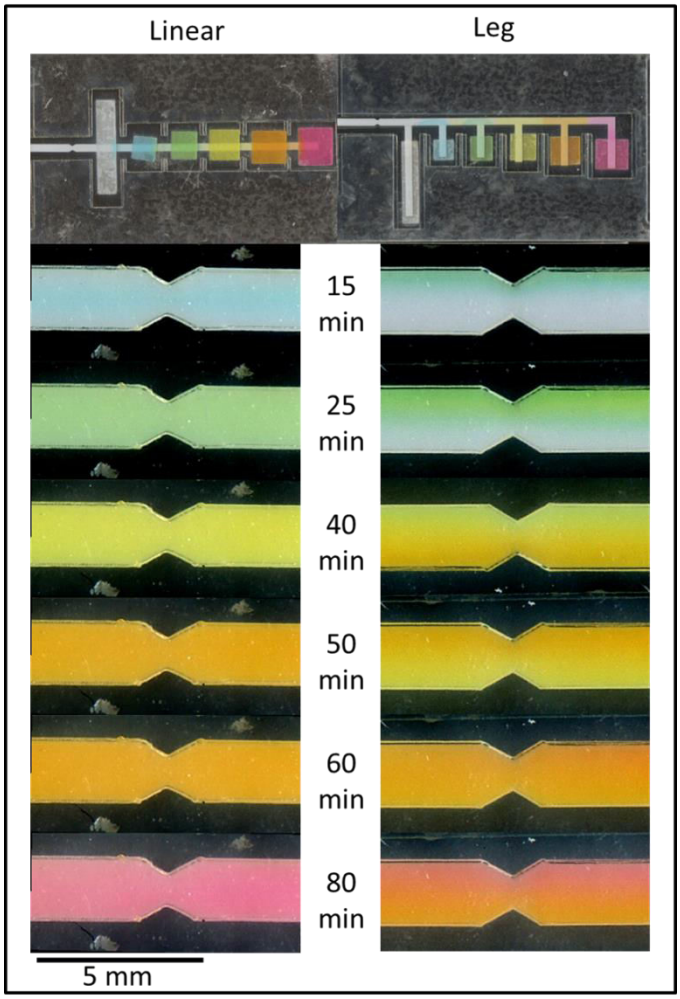

Figure 6-2: Flow profile comparison between devices. Food coloring was used to compare the flow between two device designs. The linear device showed consistently sequential reagent delivery, while the leg device showed parallel reagent flow at the 25, 50 and 80 minute time points.

6.2.2. Sequential Fluid Flow Experiment

We performed experiments to evaluate the flow of reagents in two different 2DPNs designed to deliver six reagents sequentially. The first device was modeled after the device described by Fu et al[82]. Reagent pads were placed on "legs" extending at a ninety-degree angle off the main lateral flow body (**Figure 6-2**). This device is referred to as the "leg design" in the remainder of this manuscript. The second device consists of the same reagent pads placed directly on the main body of the device. Due to the fact that this device consists of a linear piece of nitrocellulose, it is referred to as the "linear device".

In order to visualize the flow of reagents, we used food dye (McCormick, Sparks, Maryland) diluted in Phosphate Buffered Saline (PBS) with .05% Tween® 20 (PBST). Glass fiber pads with capacities of 50 µL, 15 µL, 20 µL, 25 µL, 30 µL and 35 µL were placed in their respective positions on the device. Different colors of food coloring, diluted in PBST, were dispensed with the appropriate volume on each pad, as shown in **Figure 6-1**. The device was folded in half to initiate fluid flow. Images were acquired with a flatbed scanner at 600 dots-per-inch (DPI) at 15, 25, 40, 50, 60 and 80 minutes after flow initiation.

6.2.3. *Pf* HRP2 2DPN Assay Preparation

Prior to device assembly, we pipetted 0.4 µL of the capture antibody, a murine antibody to *Pf* HRP2 (Immunology Consultants Laboratory, Portland, OR), directly onto the nitrocellulose strip at the test location. The strip was allowed to

dry for ten minutes before applying another 0.4 μL of antibody to the same spot. It was then dried for 90 minutes at 37 ˚C.

To prevent nonspecific binding, the nitrocellulose strip was blocked in a similar fashion to that described by Fu et al.[82]. The device was completely submerged for twenty minutes in PBS containing 5% sucrose, 2% bovine serum albumin (BSA), 0.25% PVP (40KD mW, Sigma Aldrich, St. Louis, Missouri), and .05% Tween 20. The nitrocellulose was dried for 60 minutes at 37˚C before completely assembling the device. Finally, the device was assembled as shown in **Figure 6-1**.

The unconjugated murine detection antibody (Immunology Consultants Laboratory, Portland, OR) was conjugated to biotin using EZ-link biotinylation kit (Thermo Fisher Scientific, Waltham, Massachusetts). The biotin conjugated detection antibody was desalted using Zeba columns (Thermo Fisher Scientific, Waltham, Massachusetts) to remove any unbound biotin. A streptavidin- horse-radish peroxidase polymer consisting of 400 horse-radish peroxidase monomer molecules (poly-HRP80, Fitzgerald, Acton, Massachusetts) was used as the secondary detection mechanism. Diaminobenzidine (Sigma-Aldrich, St. Louis, Missouri) served as the colorimetric substrate.

6.2.4. Running the 2DPN Assay

The biotinylated detection antibody was diluted to 40 μg/mL in PBST. The streptavidin-horse-radish peroxidase polymer was diluted to 8 μg/mL in PBST. DAB was dissolved in Millipore water at a concentration of 0.5 mg/mL. Samples

were created by spiking recombinant *Pf* HRP2 (CTK Biotech, San Diego, CA) in fetal bovine serum (FBS). We tested concentrations of 0, 0.1 ng/mL, 0.25 ng/mL, 0.5 ng/mL, 1 ng/mL *Pf* HRP2 in triplicate on both the linear and leg 2DPNs. Immediately prior to running the assay, sodium percarbonate (Sigma-Aldrich, St. Louis, Missouri) was added to the DAB solution to a concentration of 5.7 mg/mL. Sodium percarbonate provides the necessary hydrogen peroxide for the DAB colorimetric reaction to occur.

To run the assay, 50 µL of sample was pipetted onto the first pad. Next, 15 µL detection antibody was applied to the second pad, followed by 20 µL streptavidin-horse-radish peroxidase, 25 µL PBST, 30 µL DAB-sodium percarbonate solution, and 35 µL PBST. The device was then folded in half to initiate fluid flow. Each device was scanned in black and white at 600 DPI using a flatbed scanner at 60 minutes and 90 minutes after assay initiation.

6.2.5. Running Standard ELISA Kit

We also tested all spiked FBS samples using the Malaria Ag CELISA (Cellabs, Sydney, Australia). We additionally tested 0.05 ng/mL of HRP2 spiked in FBS with the CELISA. The CELISA is the primary commercialized HRP2 ELISA[111] and has reported sensitivity and specificity equivalent to quantitative polymerase chain reaction (qPCR) in symptomatic patients[114].

The assay was run in accordance with the provided protocol. Briefly, 100 µL spiked FBS sample was added into each well and incubated for one hour at room

temperature in a humid chamber. The wells were manually washed five times with 300 µL PBST. Next, 100 µL of detection antibody was added to each well, and the plate was incubated for 1 hour at room temperature in a humid chamber. After incubation, the wells were washed another five times with 300 µL PBST. Finally, 100 µL of substrate was added to each well, and the plate was incubated in the dark at room temperature for fifteen minutes. 50 µL of stop solution was added to each well, and the plate was imaged at 450 nm using a plate reader (Tecan, Zürich, Switzerland). A two-sided t-test was used to test for significant differences in mean absorbance between different HRP2 concentrations. P-values of less than 0.05 were considered significant.

6.2.6. Analysis of 2DPN Assay Signal

A fixed size rectangular region of interest (ROI) was placed at the capture region of each image. An additional background ROI of identical size was selected automatically halfway between the signal ROI and the wicking pad. To determine the signal, the complement of the image was first computed such that higher pixel intensity corresponded to a higher signal. The test signal was defined by calculating the mean of the maximum pixel intensity for each row of the test ROI. The background signal was calculated identically using the background ROI. Finally, the test ROI signal was divided by the background ROI signal to determine a signal-to-background ratio. A two-sided t-test assuming unequal variances was used to test whether differences in the signal-to-background ratio for different antigen

concentrations were statistically significant; p-values of less than 0.05 were considered significant.

6.3. Results and discussion

6.3.1. Sequential Flow Comparison

The flow comparison between the leg and linear is shown in **Figure 6-2**. An image of each device is shown immediately after folding. Additional images of the test zone of each device are shown at various time points after folding to assess flow. In both devices, the final reagent reached the test zone in 80 minutes. However, the leg device resulted in parallel flow of consecutive reagents as opposed to sequential reagent delivery. This is particularly apparent at the 25, 50 and 80-minute time points. Conversely, the linear device shows consistent sequential reagent delivery at all time points.

Results suggest that the nitrocellulose inlets of the leg device, which are perpendicular to fluid flow, disrupt the desired sequential laminar flow. This effect is exacerbated relative to previously published 2DPNs by having a larger sample pad. In previously published devices, each sequential reagent pad is designed to hold a larger volume than the previous pad[81–85,106]. By placing the largest pad first, we introduced a strong force perpendicular to the desired flow immediately prior to the test area. Furthermore, we extended the total number of reagent pads. This increases the number of inlets perpendicular to the device, further exacerbating the

effect. The linear device solves this challenge by placing reagent pads symmetrically centered on the device, resulting in no net force perpendicular to the primary nitrocellulose channel.

6.3.2. *Pf* HRP2 Assay

Example images for 0.5 ng/mL, 0.1 ng/mL and 0 ng/mL HRP2 concentrations are provided for both the linear and leg devices in **Figure 6-3** In **Figure 6-3G,** the signal ROI is outlined in a solid black box and the background ROI in the dotted black box. **Figure 6-3** also shows a scatter plot of the calculated signal-to-background ratios for concentrations ranging from 0 to 1 ng/mL with their standard deviations for both linear and leg devices. For the linear 2DPN, at 60 minutes, the mean SBR between 0 ng/mL and 0.1 ng/mL were not statistically different. The SBR between 0.5 ng/mL and 0.25 ng/mL were also not statistically different. The mean SBR for all other concentrations were significantly different at 60 minutes for the linear 2DPN. At 90 minutes, the mean SBR for all antigen concentrations were significantly different from one another for the linear 2DPN. For the leg 2DPN, there were no significant differences in mean SBR between HRP2 concentrations at 60 or 90 minutes. Although signal was present for 0.5 ng/mL and 1.0 ng/mL after 90 minutes, the large variability in SBR prevented differences from reaching statistical significance. We believe the inferior performance for the leg device is due to the parallel reagent delivery illustrated with the food coloring experiments. When signal is present for the leg device, it is only present in the middle of the test zone as

shown in **Figure 6-3D.** This is likely the only location where all reagents are delivered in sufficient quantity.

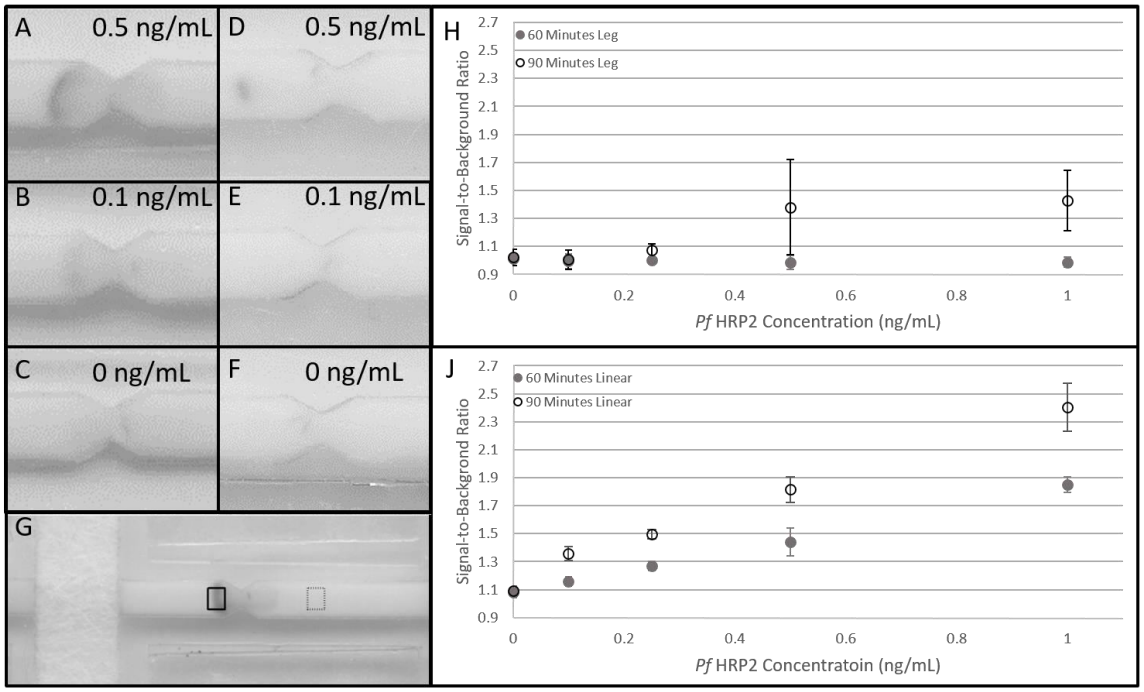

Figure 6-3 : Results of Pf HRP2 assay. Representative scanned image for the linear device of (A) 0.5 ng/mL Pf HRP2. (B) 0.1 ng/mL and (C) 0 ng/mL after 90 minutes. Representative scanned images for the leg device are shown in (D), (E) and (F) for the same concentrations. (G) Signal and background regions-of-interest. The solid black box corresponds to the signal region-of-interest and the dotted black box to the background region-of-interest. (H) A plot of the signal-to-background ratio for the leg 2DPN for concentrations ranging from 0 to 1 ng/mL Pf HRP2 at 60 and 90 minutes after assay initiation. Each data point corresponds to the average of three separate tests. There is no significant difference in mean SBR between any antigen concentration at 60 or 90 minutes. (J) Presents the same plot for the linear 2DPN. At 60 minutes, there is no significant difference between 0.1 ng/mL and 0 ng/mL or between 0.5 ng/mL and 0.25 ng/mL. The mean SBR is significantly different between all other antigen concentrations. At 90 minutes, the mean SBR is significantly different between all antigen concentrations for the linear device.

For the CELISA kit, there was no significant difference between the mean absorbance for 0.05 ng/mL and 0 ng/mL. Mean absorbance were significantly different between all other concentrations. The LOD for the linear device at 90 minutes is 0.1 ng/mL, comparable to the lowest reported ELISA LOD of 0.11 ng/mL[86], corresponding to approximately 0.7 parasites/μL[110]. The CELISA HRP2 ELISA kit used here also produced a LOD of 0.1 ng/mL. Results using this kit are shown in **Figure 6-4**.

The improvement in limit-of-detection is due to both the use of polymerized horse-radish peroxidase conjugated streptavidin in tandem with a biotinylated detection antibody and the 50 μL sample size. Ramachandran et al. reported a 2DPN achieving a LOD of 6.5 ng/mL using 10 μL of spiked FBS sample employing the same capture and detection antibody and the same colorimetric substrate reported here[85]. Increasing the sample size would have maximally improved the LOD to 1.3 ng/mL. The additional improvement in limit-of-detection is attributable to the streptavidin-biotin detection system. A 50 μL plasma sample size is obtainable from a finger prick using a high-flow lancet, e.g. the BD Microtainer Contact-Activated Blue Lancet which provides up to 500 μL of blood per single puncture[115].

6.4. Conclusions

We have demonstrated an extended 2DPN capable of delivering the sample and five reagents sequentially with a limit-of-detection equivalent to the Cellabs CELISA Malaria Antigen Kit. Improvements for this device could be made by incorporating dry reagent storage[83,85] and a plasma separating membrane, allowing for whole blood analysis. Because of the ease of biotinylation, the device can be readily modified for the detection of other antigens that require a highly sensitive point-of-care test. The improvement LOD comes at the cost of increased assay time. However, for assays in which clinically necessary LOD cannot be achieved by conventional lateral flow tests, this method offers a novel point-of-care strategy.

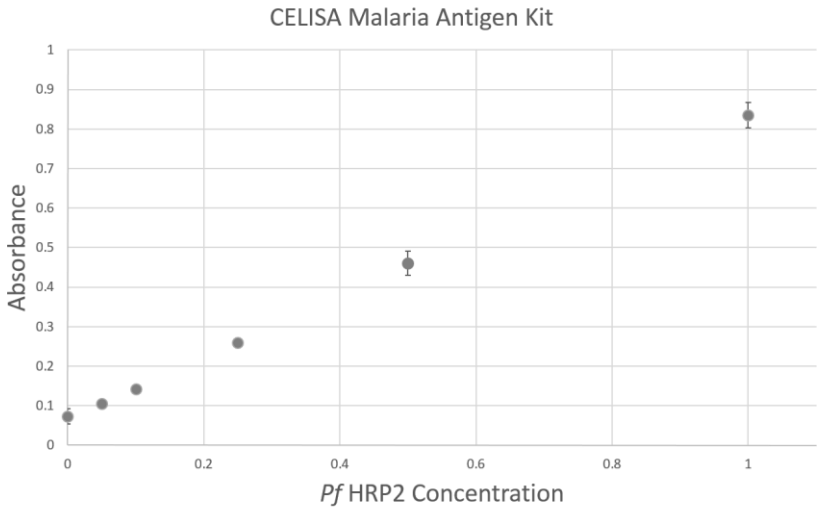

Figure 6-4: Results of Pf HRP2 CELISA kit. A plot of the Pf HRP2 CELISA for sample concentrations ranging from 0 to 1 ng/mL run in triplicate Error bars represent one standard deviation. There is a significant difference ($p<0.05$) between all concentrations except between 0.05 ng/mL and 0 ng/mL.

Chapter 7: A paper-based HPV VLP immunoassay for determining HPV vaccination status

7.1. Introduction

More than 520,000 new cases of cervical cancer and 265,000 related deaths occur annually [1]. Over 85% of cases of and deaths due to cervical cancer occur in low- and middle-income countries (LMICs), where cervical cancer is the third leading cause of cancer death among women[1]. LMICs bear a disproportional burden of cervical cancer primary due to the difficulty of implementing prevention and screening programs in these locations [33]. Infection with the human papillomavirus (HPV) is the cause of virtually all cases of cervical cancer [7]; globally, HPV16 and HPV18 are responsible for 70% of cervical invasive squamous cell carcinoma of the cervix [116]. Vaccines to prevent HPV infection have the potential to drastically

reduce the global burden of cervical cancer [70]. Three HPV vaccines, Cervarix, Gardasil, and Gardasil-9, are commercially available to protect against HPV16 and HPV18 [68,70,117]. Gardasil also protects against HPV 6 and HPV11 which cause 90% of genital warts [69]. Randomized, prospective studies have demonstrated the efficacy of Cervarix and Gardasil to preventing HPV16 and HPV18 infections, and HPV16- or HPV18-related cervical intraepithelial neoplasia (CIN) [69–71]. More recently a nonavalent vaccine, Gardasil-9, was developed that provides protection against nine HPV types including 6, 11, 16 and 18 and five additional oncogenic HPV types (31, 33, 45, 52 and 58)[73]. Together these HPV types cause 90% of all cervical cancer, thus mass immunization with Gardasil-9 may potentially prevent 90% of cervical cancers [73].

Wide-scale adoption of HPV vaccines is predicted to significantly lower the incidence of cervical cancer worldwide, and reduce global disparities in cervical cancer incidence [117]. The cost of the three-dose HPV series is approximately $390 for the Cervarix Vaccine, $480 for Gardasil and $530 for Gardasil-9[118]. Cost is the biggest barrier to national implementation of the HPV vaccine in LMICs [75]. Recent studies suggest that two doses of vaccine may provide protective immunity [119,120] and be more cost-effective than the three-dose series [121]. Lack of comprehensive medical records in LMICs [122] presents another challenge to national HPV immunization programs. Absent medical records, providers must rely on patient self-reporting to assess whether a patient has received all recommended doses of vaccine. This can lead to vaccination of individuals who have previously received

sufficient doses of the vaccine. In order to optimize cost-effectiveness, it is critical that vaccines are provided only to those who have not received the full series of the vaccine. The accuracy of self-reported vaccine history varies depending on the vaccine [123]. HPV vaccine self-reporting is particularly poor due to the multiple dose requirements. A study evaluating the accuracy of self-reported of HPV vaccination history among adolescents revealed major inaccuracies [2]. Only 54% (36/66) of those who had received at least one vaccine correctly reported having had the vaccine and only 35% (17/48) of those who had received all three vaccines correctly self-reported having all three doses [2]. Due to the under-reporting of HPV vaccine status and the lack of reliable medical records in many developing countries, there is a significant possibility of unnecessary revaccination.

HPV immunization status can be determined by measuring the serum concentration of HPV antibodies Currently, serum HPV antibody concentration can only be measured using a virus like particle (VLP) enzyme-linked immunosorbent assay (ELISA) or a neutralization assay [77]. However, both of these assays traditionally require sophisticated laboratory equipment and highly trained personnel. Low-cost, point-of-care alternatives to these tests are needed to help assess whether patients have previously received 2 or more doses of HPV vaccine in order to facilitate efficient vaccination programs. Recently, Fu et al. reported instrument-free two-dimensional paper networks (2DPNs) to perform multistep immunoassays at the point-of-care[82]. In this paper, we build on this approach to develop an equipment-free rapid paper immunoassay to detect antibodies to HPV-

16 from a finger prick sample of capillary blood to rapidly determine HPV immunization status at the point-of-care. We report results from a pilot study of 28 subjects to evaluate the whether an individual has received two or more doses of the Gardasil or Cervarix vaccines.

7.2. Methods

Figure 7-1 shows a photograph of the two-dimensional lateral flow assay to detect HPV antibodies from a drop of capillary blood. An important design consideration is to discriminate between vaccinated individuals and individuals with a history of PHV infection. The assay is designed to detect HPV16 antibodies because of the significantly higher HPV16 antibody geometric mean titers seen in vaccinated individuals relative to those with a history of natural HPV16 infection [124]. This difference is much greater for HPV16 than for HPV18 [124]. The assay consists of a lateral flow strip with three capture zones to capture HPV16 antibodies from the serum and a positive control zone. HPV16 L1 virus like particles (VLPs) are immobilized at the capture zones and human immunoglobin (IgG) is immobilized at the positive control zone. Three test zones were included to aid in discrimination between vaccinated individuals and those with a history of natural HPV infection. Preliminary tests were performed with pooled serum from individuals with a history of HPV16 infection (provided by the National Institute of Biological Safety and Controls) and serum from an individual who had received three doses of the Gardasil vaccine. These tests revealed using a single test zone did not allow for

visual discrimination between serum from an individual with a natural HPV16 infection and one who had received three HPV vaccines. However, by using three test zones a difference was visually apparent (data not shown).

As shown in **Figure 7-1A,** the device consists of a nitrocellulose membrane with HPV16 VLPs immobilized at three test zones and human IgG immobilized at the positive control zone, a cellulose picking pad, a plasma separation membrane (right side) and three glad fiber pads, one of which contains dried detection antibody (left side) all adhered to a thin acetate sheet. On the right side of the device, the plasma separation membrane is connected via a nitrocellulose leg to the main lateral flow strip. On the left side of the device, three glass fiber pads are placed on exposed adhesive. The middle pad contains dried anti-Human IgG conjugated to colloidal gold. The device is operated by placing a blood sample on the plasma separation membrane and rehydrating the three glass fiber pads with buffer (PBST). The plasma separation membrane allows the plasma to pass on to the nitrocellulose strip but retains red blood cells. The adhesive cover is removed from the left side of the device. Once the plasma reaches the plasma separation line, shown in **Figure 7-1A** , the device is folded in half along the midline. This places the glass fiber pads in direct contact with the main lateral flow strip and initiates sequential flow of the first wash buffer, labeled detection antibody and final wash buffer.

7.2.1. Production of HPV16 L1 virus-like particles

HPV16 L1 virus-like-particles were produced by transfecting 293TT cells with a plasmid expressing codon-modified HPV16L1 (p16L1h) gene[125]. The plasmid was supplied from Dr. Susanna Pang from the National Cancer Institute Laboratory of Cellular Oncology. The methods to produce human papillomavirus pseudoviruses have been published in detail previously [126–129].

Twenty-four hours prior to transfection, 2 x 10^7 293TT cells (National Cancer Institute Laboratory of Cellular Oncology) were plated on a 225cm^2 flask in 50 mL of Dulbecco's Modified Eagle Medium (DMEM) with 10% fetal bovine serum, 1% non-essential amino acids and 1% Glutamax-I (Thermo Fisher Scientific). Immediately prior to transfection, 112.5 µg p16l1h DNA was added to 5.6 mL Opti-MEM (Thermo Fisher Scientific) and in a separate tube 247.5 µL of Lipofectamine 2000 (Thermo Fisher Scientific) was added to 5.6 mL of Opti-MEM. The solutions were incubated separately for 10 minutes at room temperature and then combined. After gentle mixing the combined solution was incubated for 20 minutes and then added directly to the cultured cells. The cells were transfected for 48 hours at 37˚C before harvesting.

Cells were collected, centrifuged and placed in a siliconized 1.5 mL tube. Cells were lysed by resuspension in Dulbecco's phosphate buffered saline with calcium and magnesium (DPBS, Thermo Fisher Scientific) with 2.5% of 1 M ammonium sulfate, 0.5% Triton X-100 (Thermo Fisher Scientific), 0.1% Benzonase

(Sigma) and 0.1% Plasmid safe (Epicentre). The lysis was then incubated overnight at 37˚C to allow for capsid maturation. The following day, the solution was adjusted to 0.8 M NaCl and incubated on ice for 10 minutes. The salt lysate was double-clarified by centrifugation at 5,000 x g for five minutes. Capsids were purified by ultracentrifugation with an Optiprep gradient[126]. SDS-PAGE gels were run on each gradient fraction to determine if the fraction contained a significant amount of L1. Fractions containing L1 were pooled for use in the HPV antibody immunoassay.

7.2.2. Fabrication of paper-based HPV VLP immunoassay

All materials for the paper-based HPV antibody immunoassay were cut using a CO_2 laser cutter (Universal Laser Systems). Devices were constructed from 10 mil Dura-lar (Blick Art Supplies) and 5 mil adhesive-backed Dura-lar (Blick Art Supplies). The lateral flow channel was cut from 2 mil backed high-flow nitrocellulose (HF090, Millipore). The reagent storage and release pads were cut glass fiber pads (Grade 8951, Alhstrom). The wicking pad was cut from cellulose (C083, Millipore). The plasma separation membrane was cut from a commercially available glass fiber filter (LF1, GE Healthcare Life Sciences).

The paper-based HPV antibody immunoassays were assembled as shown in **Figure 7-1.** The nitrocellulose strip has three consecutive test zones to capture anti-HPV 16 antibodies and one positive control capture location. The test zones were created by pipetting 0.4 µL of HPV16 L1 VLPs on each test location. After drying the devices at 37°C for ten minutes, 0.4 µL of HPV16 L1 VLPs were again

pipetted on each test location. The first capture location was spotted with HPV16 L1 VLPs diluted one to four (25 μg/mL) in phosphate buffered saline (PBS) and the second and third locations were spotted with HPV16 L1 VLPs diluted one to two in PBS (50 μg/mL). The positive control location was spotted once with 0.4 μL of 44 μg/mL human IgG (Thermo Fisher Scientific) diluted in PBS.

The nitrocellulose strips were dried for one hour at 37°C. The nitrocellulose strips were then blocked by completely submerging in PBS with .05% v/v Tween 20 (Biolegend) , 5% w/v sucrose (Sigma Aldrich) and 0.25% w/v Polyvinylpyrrolidone (40 kD, Sigma Aldrich). After blocking for 30 minutes, the strips were dried for 30 minutes at 37°C. The devices were then completely assembled by placing the glass fiber pads, nitrocellulose strips, plasma separation membrane and wicking pad as depicted in **Figure 7-1**. To create stable detection antibody, 40 nm diameter gold conjugated goat anti-Human IgG (50 OD, BioAssay Works) was diluted one-to-five in PBS with 1% w/v bovine serum albumin (BSA), 5% sucrose (Sigma Aldrich) and 5% trehalose (Sigma Aldrich). Five microliters of the diluted antibody gold conjugate was spotted on the detection antibody glass fiber pad. The entire device was then dried overnight at room temperature. All devices were fabricated one day prior to clinical testing and stored at room temperature until use.

7.2.3. Clinical Testing

The pilot study was performed with the approval of the Institutional Review Board of Baylor College of Medicine. Informed consent was obtained from each subject. Subjects were eligible for inclusion if they were 18 or older and had a history of being sexually active. Subjects were ineligible if they had a history of diagnosis of any immunodeficiency disorder, diagnosis of HIV, Hepatitis B or Hepatitis C or if they were currently using steroids or other immune-suppressive medications. After consent, subjects were asked a brief series of questions including the number of HPV vaccines he/she has received, the type of HPV vaccine and the number of sexual partners he/she had in the last six months.

The complete supplies required for each test are shown in **Figure 7-1**. A finger prick was performed using a high-flow microtainer lancet (BD Diagnostics). Blood was collected using a 20 µL microsafe capillary tube (Safe-Tec) and immediately dispensed onto the plasma separation membrane. While the plasma separated, PBS with .05% Tween 20 (PBST) was dispensed onto the glass fiber reagent pads. A 20 µL exact volume transfer pipette was used to place 20 µL of PBST on both the first wash glass fiber pad and the detection antibody pad. A 40 µL exact volume transfer pipette was used to dispense PBST on the second wash pad. Next, the adhesive was exposed by peeling back the paper covering. Once the plasma reached the minimum plasma line, shown in **Figure 7-1**, the device was folded in half to initiate the test by placing the glass fiber pads in direct contact with the main lateral flow strip. If the plasma did not reach the minimum plasma line, the

test was considered invalid. Plasma reached the plasma line after one to two minutes. Completed tests were scanned at 800 dots per inch (DPI) using a flatbed color scanner 35 minutes after folding the device.

Images were analyzed both subjectively and objectively to determine if the test result was positive or negative. The images were randomized and given to three independent reviewers blinded to the HPV vaccine status of the tested

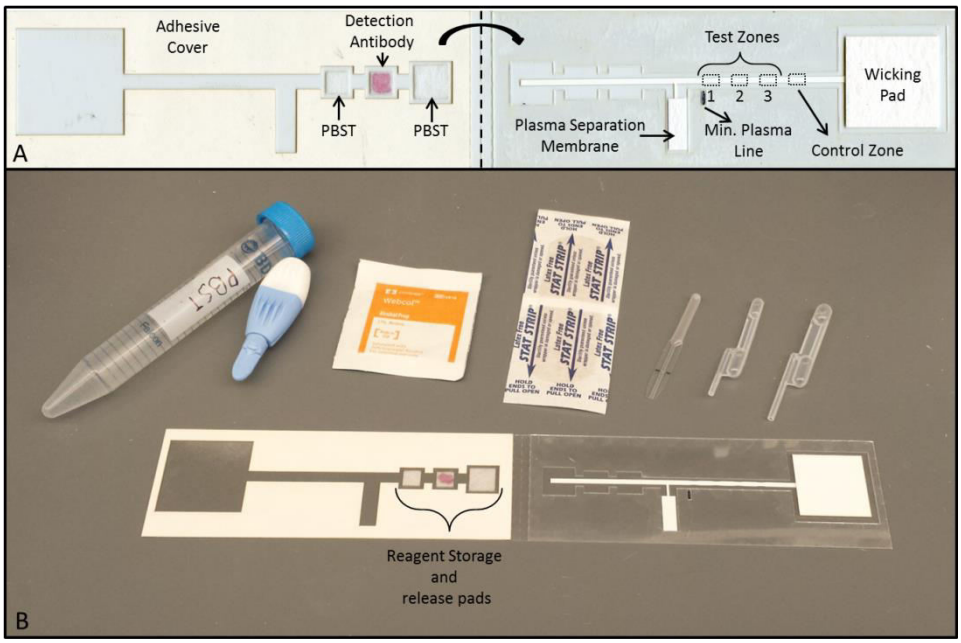

Figure 7-1 Two-dimensional paper network for detecting human antibodies against HPV 16. (A) Device overview. The device consists of a nitrocellulose membrane with HPV16 virus-like particles immobilized at three test zones, a cellulose wicking pad, a plasma separation membrane, and three glass fiber pads, one of which contains dried detection antibody, all adhered to a thin acetate sheet. **(B)** All supplies needed to perform the assay at the point-of care. The supplies consist of the paper immunoassay device, 15 mL of phosphate-buffered saline with 0.05% Tween-20, an alcohol prep pad, a Band-Aid, a high-flow lancet, a 20 µL microsafe capillary tube and a 20µL and 40 µL exact volume transfer pipette

individual. The reviewers were told to determine whether each test was positive based on the presence of signal at two or more test zones. Images were also analyzed quantitatively; analysis was performed only on the green channel, where contrast is greatest for the gold detection system. After selecting the green channel, the image was inverted so that higher pixel intensities corresponded to higher signal. A fixed-size region of interest (ROI) was manually placed at each test zone and at the positive control site. Three background ROIs, equal in size to the test zone ROIs, were automatically placed halfway between successive capture locations. In each row of the ROI, the pixel value corresponding to the 95^{th} percentile was calculated. The signal in each ROI was defined as the average of the 95^{th} percentile value calculated for each row. The 95^{th} percentile was chosen instead of the maximum value to mitigate the effect of debris in the test ROI. Signal from the three background ROIs were averaged together to define the background signal for each device. The signal-to-background ratio (SBR) was defined for each test zone location and positive control location by dividing the signal at each corresponding ROI by the mean background signal. We plotted the mean signal to background ratio for each capture zone location and compared results for unvaccinated subjects and those who reported receiving one, two or three doses of the HPV vaccine. Differences in mean signal-to-background ratios were evaluated using an unpaired two-tailed Student's t-test; p-values of less than 0.05 were considered statistically significant.

7.2.4. Dried Reagent Storage

To determine the stability of the dried reagents, a simplified device with only a single test zone location, shown in **Figure 7-3**, was fabricated. The test zone was created by pipetting 0.4 µL of 50 µg/mL HPV16 L1 VLPs in PBS on the nitrocellulose test location. The positive control was created by spotting 0.4 µL of 44 µg/mL anti-human IgG at the control location. The nitrocellulose was then dried for 10 minutes at 37˚C. Another 0.4 µL of 50 µg/mL HPV16 L1 VLPs was pipetted onto the test zone and the nitrocellulose was dried for an additional 60 minutes at 37˚C. The nitrocellulose was blocked and dried reagent pads were prepared identically to the paper-based HPV antibody immunoassay used for clinical testing. After the devices dried overnight, they were placed in a 4.5 mil thick Mylar foil pouch (Impak, Los Angeles) with two grams of molecular sieve (Impak, Los Angeles). Three assembled stability testing devices were placed in each bag. The foil pouches were sealed using a constant heat bag sealer. Three of the devices were tested immediately and the remaining devices were then placed in a chamber at 37°C with 85% relative humidity. The remaining devices were tested at 10, 15, 20 and 30 days after being exposed to high heat and humidity.

Plasma from an individual who had received three Gardasil HPV vaccines was used as the sample for all devices. Collection of blood was approved by the Rice University Institutional Review Board. 10 mL of blood was collected into a citrate dextrose solution A tube from a venous draw by a certified phlebotomist. The blood was then centrifuged at 1,000 x g for 10 minutes at 4°C. The supernatant

plasma was collected and centrifuged at 10,000 x g for 10 minutes at 4°C. The plasma was then aliquoted and stored at -20°C until needed for testing.

To test the devices at each time point, the glass fiber pads were rehydrated using the exact volume transfer pipettes as described above. Then, 5 µL of the collected plasma was pipetted onto the sample glass fiber pad. Once the plasma reached the minimum plasma line, the sample glass fiber pad was removed and the device was folded to initiate flow. This is to prevent the presence of the glass fiber pad from affecting the flow profiled of the stability testing lateral flow strip. This step is not needed in the paper-based HPV antibody clinical test because flow from the plasma separation membrane ceases after red blood cells reach the nitrocellulose. After 35 minutes, images were obtained at 800 DPI using a flatbed scanner. Image analysis was performed similarly to the procedure using for the standard device. Fixed-size ROIs were manually placed at the test capture location and positive control location. Background ROIs of the same size as the test ROIs were automatically selected midway between the test zone and positive control location and midway between the positive control location and wicking pad. Analysis was then performed identically to the standard device.

7.3. Results and Discussion

Thirty-five subjects were enrolled in the study to evaluate the ability of the paper based HPV antibody immunoassay to determine HPV vaccination status. After the first five subjects, the device blocking method was modified to improve

device stability at 37˚C. The original blocking solution included 2% BSA which degraded in the presence of high heat. The blocking procedure was modified as described in the methods. Results from the first five subjects are thus not included in the analysis. For the remaining 30 tests, the plasma failed to reach the minimum plasma line for two subjects. A summary of the data from the remaining 28 patients is provided in **Table 7-1.** After 35 minutes, the positive control signal was visible in all 28 devices, indicating completion of the assay.

	No HPV Vaccines	One HPV Vaccine	Two HPV Vaccines	Three HPV Vaccines
Number of Volunteers	10	3	5	10
Median age (years) (range)	28 (23-43)	24 (23-25)	28.5 (22 – 34)	25 (23 – 35)
Average time since last vaccine (years) (range)	-	3.5 (0.5-8)	7.9 (0.75-16)	4.8 (0 – 12)

Table 7-1: Summary of subjects in paper-based HPV VLP immunoassay pilot study

Example images of completed paper-based HPV antibody immunoassays for individuals who reported receiving zero, one, two and three HPV vaccines are provided in **Figure 7-2**. All 15 tests from subjects who reported receiving two or three doses of the HPV vaccine, were judged positive by all three observers based on the presence of signal at least two test zones. Twelve of the thirteen tests from subjects who reported receiving one or zero doses of the HPV vaccine were judged negative by all three observers. One test from an unvaccinated subject was judged negative by one reviewer and positive by two reviewers.

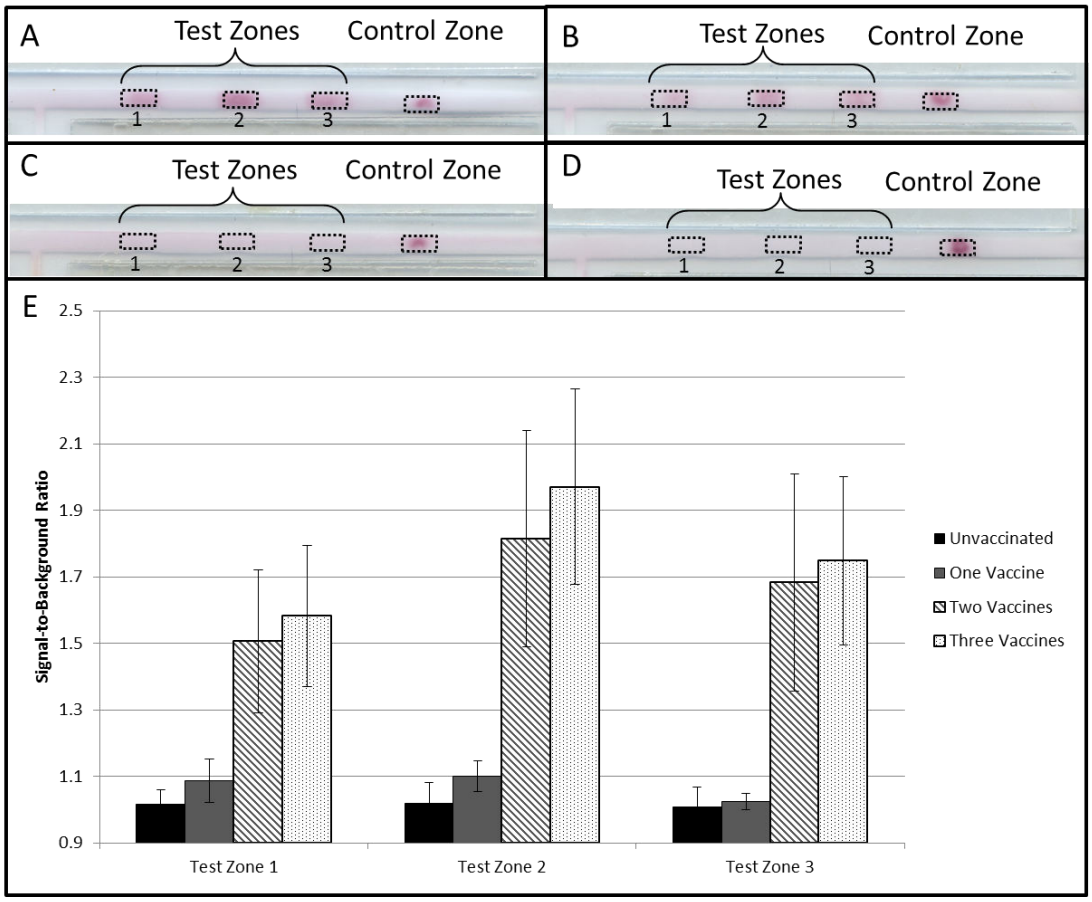

Figure 7-2 Quantitative results of the pilot study. Representative images of the paper-based HPV VLP immunoassay after 35 minutes for individuals who received **(A)** Three doses of HPV Vaccine, **(B)** Two doses of HPV vaccines, **(C)** One dose of HPV Vaccine and **(D)** No HPV vaccine. **(E)** Average signal-to-background ratio at each test zone stratified by number of HPV vaccines received

Figure 7-2E shows a quantitative comparison of the signal-to-background at each capture location for subjects stratified by the number of HPV vaccines they reported receiving The mean SBR is significantly higher for individuals who reported receiving three vaccines than for unvaccinated individuals and individuals

who reported receiving one vaccine ($p<0.01$) The mean SBR from subjects who received two vaccines was significantly higher than that for unvaccinated subjects and for subjects who reported receiving a single HPV vaccine ($p<0.01$). There were no statistically significant differences in the SBR at any test zone between subjects who received two or three HPV vaccines. Similarly, there were no significant differences between the mean SBR of tests from unvaccinated subjects in comparison to subjects who had received a single HPV vaccine.

The results of stability testing are shown in **Figure 7-3**. After 10 days of storage, the SBR decreased by 7% at the test zone and by 17% at the positive control zone. From day 10 to day signal decreased by 3.3% at the test zone and 6.8% at the control zone. Fluctuations in the SBR between these two time points are likely a result of device-to-device variability. The Eppendorf Research Plus pipette used for spotting the capture antibodies on the nitrocellulose strips has a random error of ± 6% at the volume being dispensed. To reduce the variability between devices, automated liquid dispensers are needed. However, despite this variably the test could still discriminate unvaccinated individuals and individuals who reported having a single vaccine from those who reported receiving two or more HPV vaccines.

The initial results of this test are promising; however, a large-scale study is necessary to understand the repeatability and robustness of the paper-based HPV VLP immunoassay. A false positive was recorded by two reviewers. It is possible the faint signal seen in this device was due to a previous natural HPV16 infection.

We chose to include only subjects with a history of sexual activity to increase the likelihood of participants having a history of natural HPV infection; however, we do not know the natural history of infection for any participants. To reduce the likelihood of false positives, future iterations of the immunoassay could use HPV16 L1 VLPs at one test zone and HPV18 L1 VLPs at a second test zone. In future testing, device imaging or visual interpretation should occur as soon as the positive control signal is visible instead of a fixed duration of 35 minutes. This will allow for a faster time to result in most cases. The appropriateness of this assay design also depends on ongoing research evaluating long-term efficacy of two versus three dose HPV vaccination regimens.

A primary limitation of this study was reliance of self-reporting of HPV vaccine status. There are several factors which lead us to believe that the accuracy of this self-reporting is higher than that in the study reported by Stupiansky et al.[2]. The subjects in the Stupiansky et al. study were ages 14 to 17. In this study, all participants were pursuing or had completed post-graduate education in biomedical sciences and actively volunteered to participate in an HPV-vaccine related study. Two subjects reported they were unsure if they had received two or three HPV vaccines. They called their primary care physician and verified the number of HPV vaccines they had received before participating. All other subjects reported being confident in their HPV vaccination history. In future studies, medical records should be obtained to ensure accuracy of the participants HPV vaccination history.

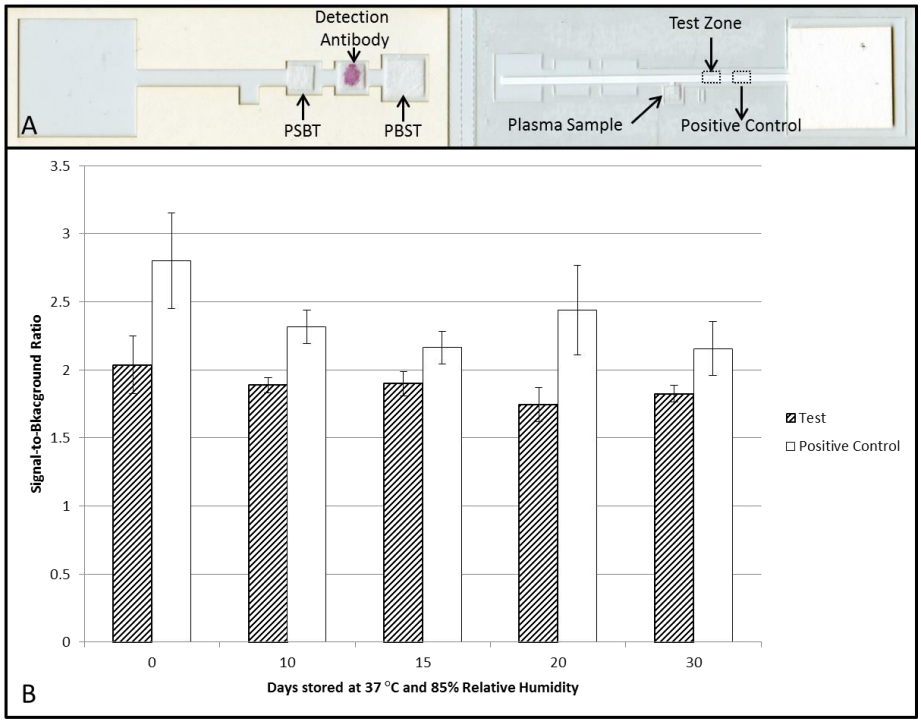

Figure 7-3: Stability testing of paper-based HPV VLP immunoassays. Devices were stored at 37˚C and 85% relative humidity for 30 days. Each device contained a test zone and positive control zone. The same sample, plasma from an individual who had received 3 HPV vaccine, was used for to evaluate the performance of the devices. The mean signal-to-background ratio decreased 10% over the course of 30 days at the test zone and 23% at the positive control zone.

Chapter 8: Conclusions

8.1. Summary

Cervical cancer is a major global health concern that disproportionately affects those living in low resource settings. Novel screening and diagnostic techniques are needed to reduce the burden of disease globally. *In vivo* imaging techniques and point-of-care molecular diagnostics can be used in tandem to help achieve this goal. Simultaneously, HPV vaccination programs must be efficiently implemented globally to reduce the future impact of HPV-related cancer. Rapid immunoassays can also help to achieve this goal.

This dissertation begins by evaluating the diagnostic accuracy of the HRME to identify precancerous lesions of the cervix. Several different morphological parameters were evaluated. In a study evaluating HRME images from 59 patients referred for colposcopy based on an abnormal Pap test, HRME images from

colposcopically abnormal sites were classified as neoplastic or non-neoplastic with 92% sensitivity and 77% specificity using median nuclear eccentricity and mean nuclear area. A second study evaluating HRME images from an additional 228 patients found similar sensitivity using four classification methods. However, while multiple methods showed high sensitivity, they were all limited in terms of specificity. Classification using the number of abnormal nuclei per unit area and using nuclear-to-cytoplasmic ratio both showed 98% sensitivity in detecting lesions of grade CIN3 or higher. Due to the critical nature of detecting these neoplastic cases, both of these modalities show promise for future studies. Additional parameters may be necessary to increase specificity.

In addition to evaluating the diagnostic performance of the standard HRME system, a smaller, less expensive cell-phone based mHRME was developed and characterized. Rapid improvement in mobile phone technology provides a unique opportunity to create point-of-care optical diagnostic tools. The mHRME achieves sub-cellular resolution and was successfully used to image normal and dysplastic cervical squamous epithelium *in vivo*.

This dissertation also reports the design and testing two paper-based immunoassays. Paper-based rapid diagnostic tests offer unique attributes making them amenable to low-cost point-of-care diagnostics. The first immunoassay reported in this dissertation is a highly-sensitive two-dimensional paper network for the detection of the malarial antigen *Pf* HRP2. This test achieves a limit of detection comparable to the best reported standard ELISA for this antigen. With the

development of HPV E7 antibodies, this platform could be utilized to create a unique HPV oncoprotein screening test. A similar paper-based immunoassay was also developed for the evaluation of an individual's HPV16 VLP immune response in order to ascertain HPV vaccination status. Initial results suggest this test could help to distinguish between those who have received more than one HPV vaccine and those who have not.

8.2. Future Work

The work in this dissertation provides the groundwork for developing new low-cost cervical cancer screening and diagnostic tests. In order to develop clinically impactful tools, several important steps remain. First, the HRME must continue to be refined to optimize cost, user-friendliness and diagnostic performance. Increasing specificity while maintaining sensitivity is paramount to the success of the device. Alternative morphological parameters or additional contrast agents may be necessary in order to discriminate between high grade dysplasia and benign abnormalities of the cervix. In future studies, a single image should be taken from each macroscopically abnormal location of the cervix instead of a short video. Analysis should then be performed immediately and the HRME diagnosis recorded. These changes are critical to move towards a more fully-automated approach.

The mHRME offers a lower cost, smaller device, but has several limitations. First, the mHRME requires modifications to work for different mobile phones.

Second, it is not as robust as the standard HRME. If the mHRME is to be used in clinical settings, a collaborative effort is needed consisting of clinicians, mechanical engineers and software engineers. The clinicians are needed to guide the design process to create a practical, user-friendly device. Mechanical engineers are needed to improve device stability and compatibility with multiple phones. Finally, software engineers are needed to write a custom Android application capable of quantifying nuclear morphological features in near real time.

The highly-sensitive 2DPN presented for malaria is a promising first step to create an HPV oncoprotein screening test. However, a substantial amount of research is left to meet this goal. First, high quality antibodies for the detection of high-risk HPV E7 proteins are needed. Commercially available antibodies for this antigen are very limited. Second, spiked FBS samples were used in the malarial antigen 2DPN proof-of-concept. For the HPV oncoprotein immunoassay, samples would be obtained from cervical swabs. Before running these samples on a 2DPN, samples would need to be lysed, purified and possibly concentrated. Research is needed to develop sample preparation amenable to the point-of-care in order to produce an HPV oncoprotein immunoassay.

Finally, the proof-of-principle paper-based HPV VLP immunoassay provides initial results suggesting utility in rapidly assessing an individual's immune response to HPV16. However, a large-scale study including verification with patient medical records and HPV DNA testing is necessary to fully understand the repeatability, robustness and limitations of this assay. A new immunoassay using

one HPV16 test zone and one HPV18 test zone should be explored in order to help differentiate between individuals with a history of HPV infection and those who have received the vaccine.

References

1. Torre LA, Bray F, Siegel RL, Ferlay J, Lortet-Tieulent J, Jemal A. Global Cancer Statistics, 2012. CA Cancer J Clin 2015;65(2):87–108.
2. Stupiansky N, Zimet G, Cummings T, Fortenberry J, Shew M. Accuracy of self-reported HPV Vaccine Receipt Among Adolescent Girls and Their Mothers. J Adolesc Heal 2012;50(1):103–5.
3. GLOBOCAN 2012 (IARC) [Internet]. 2012 [cited 2015 Dec 11];Available from: http://globocan.iarc.fr/Pages/fact_sheets_cancer.aspx
4. Bray F, Jemal A, Grey N, Ferlay J, Forman D. Global cancer transitions according to the Human Development Index (2008-2030): A population-based study. Lancet Oncol 2012;13(8):790–801.
5. International Agency on Cancer (IARC). Effectiveness of screening in populations. In: IARC Handbooks of Cancer Prevention. Volume 10: Cervix Cancer Screening. Lyon, France: IARCPress; 2005. p. 201–25.
6. Khan MJ, Castle PE, Lorincz AT, Wacholder S, Sherman M, Scott DR, et al. The elevated 10-year risk of cervical precancer and cancer in women with human papillomavirus (HPV) type 16 or 18 and the possible utility of type-specific HPV testing in clinical practice. J Natl Cancer Inst 2005;97(14):1072–9.
7. Walboomers JM, Jacobs M V, Manos MM, Bosch FX, Kummer JA, Shah K V, et al. Human Papillomavirus is a necessary cause of invasive cervical cancer worldwide. J Pathol 1999;189(May):12–9.
8. Schiff M, Castle PE, Jeronimo J, Rodriguez AC, Wacholder S. Human papillomavirus and cervical cancer. Lancet 2007;370:890–907.
9. Ault K a. Human papillomavirus vaccines and the potential for cross-protection between related HPV types. Gynecol Oncol 2007;107(2):S31–3.
10. Muñoz N, Castellsagué X, de González AB, Gissmann L. Chapter 1: HPV in the etiology of human cancer. Vaccine 2006;24 Suppl 3:S3/1–10.
11. McLaughlin-Drubin ME, Meyers J, Munger K. Cancer associated human papillomaviruses. Curr Opin Virol 2012;2(4):459–66.
12. Münger K, Phelps WC, Bubb V, Howley PM, Schlegel R. The E6 and E7 genes of the human papillomavirus type 16 together are necessary and sufficient for transformation of primary human keratinocytes. J Virol 1989;63(10):4417–21.

13. Moody C, Laimins L. Human papillomavirus oncoproteins: pathways to transformation. Nat Rev Cancer 2010;10(8):550–60.

14. Boyer SN, Wazer DE, Band V. E7 Protein of Human Papilloma Virus-16 Induces Degradation of Retinoblastoma Protein through the Ubiquitin-Proteasome Pathway Advances in Brief E7 Protein of Human Papilloma Virus-16 Induces Degradation of Retinoblastoma Protein through the Ubiquitin-Prot. 1996;4620–4.

15. Dyson N, Howley PM, Münger K, Harlow E, Product G. The Human Papilloma Virus -16 E7 Oncoprotein is Able to Bind to the Retinoblastoma Gene Product. Science (80-) 1989;243(4893):934–7.

16. Dong WL, Caldeira S, Sehr P, Pawlita M, Tommasino M. Determination of the binding affinity of different human papillomavirus E7 proteins for the tumour suppressor pRb by a plate-binding assay. J Virol Methods 2001;98(1):91–8.

17. Scheffner M, Werness B, Huibregtse J, Levine A, Howley P. The E6 oncoprotein encoded by human papillomavirus types 16 and 18 promotes the degradation of p53. Cell 1990;63(6):1129–36.

18. Buckley CH, Butler EB, Fox H. Cervical intraepithelial neoplasia. J Clin Pathol 1982;35:1–13.

19. Sellors JW, Sankaranarayanan R. An introduction to cervical intraepithelial neoplasia. In: Sellors JW, Sankaranarayanan R, editors. Colposcopy and Treatment of Cervical Intraepithelial Neoplasia. A Beginner's Manual. 2003. p. 13–20.

20. Wei J. Pathology of Cervical Carcinoma. In: Global Library of Women's Medicine. 2009.

21. Woodman CBJ, Collins SI, Young LS. The natural history of cervical HPV infection: unresolved issues. Nat Rev Cancer 2007;7(1):11–22.

22. Saslow D, Solomon D, Lawson HW, Killackey M, Kulasingam SL, Cain J, et al. American Cancer Society , American Society for Colposcopy and Cervical Pathology , and American Society for Clinical Pathology Screening Guidelines for the Prevention and Early Detection of Cervical Cancer. CA - A Cancer J Clin 2012;62(3):147–72.

23. Siegel RL, Miller KD, Jemal A. Cancer Statistics, 2015. CA Cancer J Clin 2015;65(65):5–29.

24. Läärä E, Day NE, Hakama M. Trends in mortality from cervical cancer in the Nordic countries: association with organised screening programmes. Lancet 1987;1(8544):1247–9.

25. Hakama M. Trends in the incidence of cervical cancer in the Nordic countries. Trends cancer Incid New York Hemisph Publ Corp 1982;279–92.

26. Lynge E, Madsen M, Engholm G. Effect of Organized Screening on Incidence and Mortality of Cervical Cancer in Denmark. Cancer Res 1989;49(c):2157–60.

27. Devesa SS, Young JL, Brinton L a, Fraumeni JF. Recent trends in cervix uteri cancer. Cancer 1989;64(10):2184–90.

28. Dunne EF, Unger ER, Sternberg M, McQuillan G, Swan DC, Patel SS, et al. Prevalence of HPV infection among females in the United States. JAMA 2007;297(8):813–9.

29. Ronco G, Dillner J, Elfström KM, Tunesi S, Snijders PJF, Arbyn M, et al. Efficacy of HPV-based screening for prevention of invasive cervical cancer: Follow-up of four European randomised controlled trials. Lancet 2014;383(9916):524–32.

30. Sellors JW, Sankaranarayanan R. Colposcopy and Treatment of Cervical Intraepihtelial Neoplasia: A beginner's manual. Lyon: International Agency for Research on Cancer; 2003.

31. Marina OC. Effects of acetic acid on light scattering from cells. J Biomed Opt 2012;17:085002.

32. Mitchell MF, Schottenfeld D, Tortolero-Luna G, Cantor SB, Richards-Kortum R. Colposcopy for the diagnosis of squamous intraepithelial lesions: A meta-analysis. Obstet. Gynecol. 1998;91(4):626–31.

33. Denny L, Quinn M, Sankaranarayanan R. Chapter 8: Screening for cervical cancer in developing countries. Vaccine 2006;24(SUPPL. 3):71–7.

34. Sherris J, Herdman C, Elias C. Cervical cancer in the developing world. West J Med 2001;175(4):231–3.

35. Adesina A, Chumba D, Nelson AM, Orem J, Roberts DJ, Wabinga H, et al. Improvement of pathology in sub-Saharan Africa. Lancet Oncol 2013;14(4):e152–7.

36. Lazcano-Ponce EC, Moss S, Alonso de Ruíz P, Salmerón Castro J, Hernández Avila M. Cervical cancer screening in developing countries: why is it ineffective? The case of Mexico. Arch Med Res 1999;30(3):240–50.

37. Gage JC, Ferreccio C, Gonzales M, Arroyo R, Huivín M, Robles SC. Follow-up care of women with an abnormal cytology in a low-resource setting. Cancer Detect Prev 2003;27(6):466–71.

38. Graffikin L, Chirenje ZM, Blumenthal PD, Sanghvi H, Chipato T, McGrath J, et al. Visual inspection with acetic acid for cervical-cancer screening: test qualities in a primary-care setting. Lancet 1999;353:869–73.

39. Sankaranarayanan R, Wesley R, Somanathan T, Dhakad N, Shyamalakumary B, Amma NS, et al. Visual inspection of the uterine cervix after the application of

acetic acid in the detection of cervical carcinoma and its precursors. Cancer 1998;83(10):2150–6.

40. Ottaviano M, La Torre P. Examination of the cervix with the naked eye using acetic acid test. Am J Obstet Gynecol 1982;143(2):139–42.

41. Denny L, Kuhn L, Pollack a, Wainwright H, Wright TC. Evaluation of alternative methods of cervical cancer screening for resource-poor settings. Cancer 2000;89(4):826–33.

42. Denny L, Kuhn L, Pollack A, Wright T. Direct visual inspection for cervical cancer screening. Cancer 2002;94(6):1699–707.

43. World Health Organization. Guidelines for screening and treatment of precancerous leasions for cervical cancer protection. Geneva: World Health Organization; 2013.

44. Sankaranarayanan R, Wesley R, Thara S, Dhakad N, Chandralekha B, Sebastian P, et al. Test characteristics of visual inspection with 4% acetic acid (VIA) and Lugol's iodine (VILI) in cervical cancer screening in Kerala, India. Int J Cancer 2003;106(3):404–8.

45. Sarian LO, Derchain SF, Naud P, Tatti S, Branca M, Matos J, et al. Evaluation of visual inspection with acetic acid (VIA), Lugol ' s iodine (VILI), cervical cytology and HPV testing as cervical screening tools in Latin America This report refers to partial results from the LAMS (Latin AMerican Screening) study Stud. 2005;12(3):142–9.

46. Jacob M, Broekhuizen FF, Castro W, Sellors J. Experience using cryotherapy for treatment of cervical precancerous lesions in low-resource settings. Int J Gynecol Obstet 2005;89(SUPPL. 2):13–20.

47. Luciani S, Gonzales M, Munoz S, Jeronimo J, Robles S. Effectiveness of cryotherapy treatment for cervical intraepithelial neoplasia. Int J Gynaecol Obstet 2008;101(2):172–7.

48. Qiao Y-L, Sellors JW, Eder PS, Bao Y-P, Lim JM, Zhao F-H, et al. A new HPV-DNA test for cervical-cancer screening in developing regions: a cross-sectional study of clinical accuracy in rural China. Lancet Oncol 2008;9(10):929–36.

49. Sankaranarayanan R, Esmy PO, Rajkumar R, Muwonge R, Swaminathan R, Shanthakumari S, et al. Effect of visual screening on cervical cancer incidence and mortality in Tamil Nadu, India: a cluster-randomised trial. Lancet 2007;370(9585):398–406.

50. Mwanahamuntu MH, Sahasrabuddhe V V, Parham GP. HPV screening for cervical cancer in rural India. N Engl J Med 2009;361(3):305.

51. Castle PE. Invited commentary: is monitoring of human papillomavirus infection for viral persistence ready for use in cervical cancer screening? Am J

Epidemiol 2008;168(2):138–44; discussion 145–8.

52. Lidqvist M, Nilsson O, Holmgren J, Hölters S, Röijer E, Dürst M, et al. Detection of human papillomavirus oncoprotein E7 in liquid-based cytology. J Gen Virol 2012;93(Pt 2):356–63.

53. Thekkek N, Richards-Kortum R. Optical Imaging for Cervical Cancer Detection: Solutions for a Continuing Global Problem. Nat Rev Cancer 2008;8(9):725–31.

54. Collier T, Lacy A, Richards-Kortum R, Malpica A, Follen M. Near Real-Time Confocal Microscopy of Amelanotic Tissue. Acad Radiol 2002;9(5):504–12.

55. Sung K, Liang C, Descour M, Collier T, Follen M, Malpica A, et al. Near real time in vivo fibre optic confocal microscopy: sub-cellular structure resolved. J Microsc 2002;207(Pt 2):137–45.

56. Tan J, Quinn M a, Pyman JM, Delaney PM, McLaren WJ. Detection of cervical intraepithelial neoplasia in vivo using confocal endomicroscopy. BJOG 2009;116(12):1663–70.

57. Muldoon TJ, Pierce MC, Nida DL, Williams MD, Richards-Kortum R. Subcellular-resolution molecular imaging within living tissue by fiber microendoscopy. Opt Express 2007;15(25):16413–23.

58. Pierce M, Yu D, Richards-Kortum R. High-resolution fiber-optic microendoscopy for in situ cellular imaging. J Vis Exp 2011;47:2306.

59. Grant BD, Schwarz RA, Quang T, Schmeler KM, Richards-Kortum R. High-Resolution Microendoscope for the Detection of Cervical Neoplasia. Mob Heal Technol Methods Protoc 2015;421–34.

60. Pierce MC, Guan Y, Quinn MK, Zhang X, Zhang W-H, Qiao Y-L, et al. A pilot study of low-cost, high-resolution microendoscopy as a tool for identifying women with cervical precancer. Cancer Prev Res 2012;5(11):1273–9.

61. Thekkek N, Muldoon T, Polydorides AD, Maru DM, Harpaz N, Harris MT, et al. Vital-dye enhanced fluorescence imaging of GI mucosa: metaplasia, neoplasia, inflammation. Gastrointest Endosc 2012;75(4):877–87.

62. Pierce MC, Vila PM, Polydorides AD, Richards-Kortum R, Anandasabapathy S. Low-Cost endomicroscopy in the esophagus and colon. Am J Gastroenterol 2011;106(9):1722–4.

63. Muldoon TJ, Anandasabapathy S, Maru D, Richards-Kortum R. High-resolution imaging in Barrett's esophagus: a novel, low-cost endoscopic microscope. Gastrointest Endosc 2008;68(4):737–44.

64. Muldoon TJ, Roblyer D, Williams MD, Stepanek VMT, Kortum RR, Gillenwater AM. Noninvasive imaging of oral neoplasia with a high-resolution fiber-optic microendoscope. Head Neck 2012;34(3):305–12.

65. Pierce MC, Schwarz RA, Bhattar VS, Mondrik S, Williams MD, Lee JJ, et al. Accuracy of in vivo multimodal optical imaging for detection of oral neoplasia. Cancer Prev Res 2012;5(6):801–9.

66. Quinn MK, Bubi TC, Pierce MC, Kayembe MK, Ramogola-Masire D, Richards-Kortum R. High-resolution microendoscopy for the detection of cervical neoplasia in low-resource settings. PLoS One 2012;7(9):e44924.

67. Shin D, Pierce MC, Gillenwater AM, Williams MD, Richards-Kortum R. A fiber-optic fluorescence microscope using a consumer-grade digital camera for in vivo cellular imaging. PLoS One 2010;5(6):e11218.

68. Harper DM, Franco EL, Wheeler C, Ferris DG, Jenkins D, Schuind A, et al. Efficacy of a bivalent L1 virus-like particle vaccine in prevention of infection with human papillomavirus types 16 and 18 in young women: a randomised controlled trial. Lancet 2004;364(9447):1757–65.

69. Villa LL, Costa RLR, Petta C a., Andrade RP, Ault K a., Giuliano AR, et al. Prophylactic quadrivalent human papillomavirus (types 6, 11, 16, and 18) L1 virus-like particle vaccine in young women: A randomised double-blind placebo-controlled multicentre phase II efficacy trial. Lancet Oncol 2005;6(5):271–8.

70. Pasquié J, Ph D, Scavée C, Bordachar P, Clémenty J, Haïssaguerre M. Quadrivalent Vaccine against Human Papillomavirus to Prevent High-Grade Cervical Lesions. N Engl J Med 2007;356(19):1915–27.

71. Paavonen J, Naud P, Salmerón J, Wheeler CM, Chow S-N, Apter D, et al. Efficacy of human papillomavirus (HPV)-16/18 AS04-adjuvanted vaccine against cervical infection and precancer caused by oncogenic HPV types (PATRICIA): final analysis of a double-blind, randomised study in young women. Lancet 2009;374(9686):301–14.

72. Markowitz LE, Dunne EF, Chesson HW, Curtis CR, Gee J, Bocchini Jr. JA, et al. Human Papillomavirus Vaccination: Recommendations of the Advisory Committee on Immunization Practices (ACIP). Mmwr. 2014;63(No. RR 5):1–29.

73. Joura E a, Giuliano AR, Iversen O-E, Bouchard C, Mao C, Mehlsen J, et al. A 9-Valent HPV Vaccine against Infection and Intraepithelial Neoplasia in Women. N Engl J Med 2015;372(8):711–23.

74. Roden R, Wu T-C. How will HPV vaccines affect cervical cancer? Nat Rev Cancer 2006;6(10):753–63.

75. Agosti JM, Goldie SJ. Introducing HPV Vaccine in Developing Countries — Key Challenges and Issues. N Engl J Med 2007;356(19):1908–10.

76. Hopkins TG, Wood N. Female human papillomavirus (HPV) vaccination: Global uptake and the impact of attitudes. Vaccine 2013;31(13):1673–9.

77. Pastrana D V., Buck CB, Pang YYS, Thompson CD, Castle PE, FitzGerald PC, et al. Reactivity of human sera in a sensitive, high-throughput pseudovirus-based papillomavirus neutralization assay for HPV16 and HPV18. Virology 2004;321(2):205–16.

78. Martinez AW, Phillips ST, Whitesides GM, Carrilho E. Diagnostics for the developing world: microfluidic paper-based analytical devices. Anal Chem 2010;82(1):3–10.

79. Peeling RW, Holmes KK, Mabey D, Ronald a. Rapid tests for sexually transmitted infections (STIs): the way forward. Sex Transm Infect 2006;82 Suppl 5:v1–6.

80. Wong RC, Tse HY, editors. Lateral Flow Immunoassay. New York: Humana Press; 2009.

81. Fu E, Lutz B, Kauffman P, Yager P. Controlled reagent transport in disposable 2D paper networks. Lab Chip 2010;10(7):918–20.

82. Fu E, Liang T, Spicar-Mihalic P, Houghtaling J, Ramachandran S, Yager P. Two-dimensional paper network format that enables simple multistep assays for use in low-resource settings in the context of malaria antigen detection. Anal Chem 2012;84(10):4574–9.

83. Fridley GE, Le H, Yager P. Highly sensitive immunoassay based on controlled rehydration of patterned reagents in a 2-dimensional paper network. Anal Chem 2014;86(13):6447–53.

84. Fu E, Liang T, Houghtaling J, Ramachandran S, Ramsey S a, Lutz B, et al. Enhanced sensitivity of lateral flow tests using a two-dimensional paper network format. Anal Chem 2011;83(20):7941–6.

85. Ramachandran S, Fu E, Lutz B, Yager P. Long-term dry storage of an enzyme-based reagent system for ELISA in point-of-care devices. Analyst 2014;1456–62.

86. Butterworth AS, Robertson AJ, Ho M-F, Gatton ML, McCarthy JS, Trenholme KR. An improved method for undertaking limiting dilution assays for in vitro cloning of Plasmodium falciparum parasites. Malar J 2011;10:95.

87. López-Gómez M, Malmierca E, de Górgolas M, Casado E. Cancer in developing countries: The next most preventable pandemic. The global problem of cancer. Crit. Rev. Oncol. Hematol. 2013;88(1):117–22.

88. Wright TC, Kuhn L. Alternative approaches to cervical cancer screening for developing countries. Best Pract Res Clin Obstet Gynaecol 2012;26(2):197–208.

89. Sankaranarayanan R, Nene BM, Shastri SS, Jayant K, Muwonge R, Budukh AM, et al. HPV screening for cervical cancer in rural India. N Engl J Med

2009;360(14):1385–94.

90. Shin D, Protano M-A, Polydorides AD, Dawsey SM, Pierce MC, Kim MK, et al. Quantitative analysis of high-resolution microendoscopic images for diagnosis of esophageal squamous cell carcinoma. Clin Gastroenterol Hepatol 2015;13(2):272–9.e2.

91. Miles B a., Patsias A, Quang T, Polydorides AD, Richards-Kortum R, Sikora AG. Operative margin control with high-resolution optical microendoscopy for head and neck squamous cell carcinoma. Laryngoscope 2015;n/a – n/a.

92. Parikh ND, Perl D, Lee MH, Chang SS, Polydorides AD, Moshier E, et al. In vivo classification of colorectal neoplasia using high-resolution microendoscopy: Improvement with experience. J Gastroenterol Hepatol 2015;30(7):1155–60.

93. Wainwright M. Acridine-a neglected antibacterial chromophore. J Antimicrob Chemother 2001;47(1):1–13.

94. Richart RM. Cervical intraepithelial neoplasia: a review. Pathol Annu 1973;8:301–28.

95. Otsu N. A Threshold Selection Method from Gray-Level Histograms. IEEE Trans Syst Man Cybern 1979;9(1):62–6.

96. Cuzick J. A wilcoxon-type test for trend. Stat Med 1985;4(4):543–7.

97. Drezek R, Guillaud M, Collier T, Boiko I, Malpica A, Macaulay C, et al. Light scattering from cervical cells throughout neoplastic progression: influence of nuclear morphology, DNA content, and chromatin texture. J Biomed Opt 2003;8:7–16.

98. Carreon JD, Sherman ME, Guillén D, Solomon D, Herrero R, Jerónimo J, et al. CIN2 Is a Much Less Reproducible and Less Valid Diagnosis than CIN3: Results from a Histological Review of Population-Based Cervical Samples. Int J Gynecol Pathol 2007;26(4):441–6.

99. Bedard N, Quang T, Schmeler K, Richards-Kortum R, Tkaczyk TS. Real-time video mosaicing with a high-resolution microendoscope. Biomed Opt Express 2012;3(10):2428–35.

100. Grant B, Guerreiro-Fregnani J, Possati-Resende J, Scapulatempo-Neto C, Matsushita G, Mauad E, et al. High-resolution microendoscopy: A point-of-care diagnostic for cervical dysplasia in low-resource settings. Eur J Cancer Prev 2015;

101. Cuzick J, Arbyn M, Sankaranarayanan R, Tsu V, Ronco G, Mayrand M-H, et al. Overview of human papillomavirus-based and other novel options for cervical cancer screening in developed and developing countries. Vaccine 2008;26 Suppl 1:K29–41.

102. Sankaranarayanan R, Nessa A, Esmy PO, Dangou J-M. Visual inspection

methods for cervical cancer prevention. Best Pract Res Clin Obstet Gynaecol 2012;26(2):221–32.

103. Breslauer DN, Maamari RN, Switz N a., Lam W a., Fletcher D a. Mobile phone based clinical microscopy for global health applications. PLoS One 2009;4(7):1–7.

104. Tseng D, Mudanyali O, Oztoprak C, Isikman SO, Sencan I, Yaglidere O, et al. Lensfree microscopy on a cellphone. Lab Chip 2010;10(14):1787–92.

105. Ngom B, Guo Y, Wang X, Bi D. Development and application of lateral flow test strip technology for detection of infectious agents and chemical contaminants: A review. Anal. Bioanal. Chem. 2010;397(3):1113–35.

106. Fu E, Kauffman P, Lutz B, Yager P. Chemical signal amplification in two-dimensional paper networks. Sensors Actuators B Chem 2011;149(1):325–8.

107. Heseltine E, editor. Malaria rapid diagnostic test performance: results of WHO product testing of malaria RDTs: Round 5 (2013). WHO Press; 2014.

108. World malaria report 2014. WHO Press; 2014.

109. Beadle C, Long GW, Weiss WR, McElroy PD, Maret SM, Oloo a J, et al. Diagnosis of malaria by detection of Plasmodium falciparum HRP-2 antigen with a rapid dipstick antigen-capture assay. Lancet 1994;343(8897):564–8.

110. Marquart L, Butterworth A, McCarthy JS, Gatton ML. Modelling the dynamics of Plasmodium falciparum histidine-rich protein 2 in human malaria to better understand malaria rapid diagnostic test performance. Malar J 2012;11(1):74.

111. PATH. Malaria Diagnostics Technology Landscape: Enzyme-Linked Immunosorbent Assays (ELISA) for Histidine-Rich Protein 2. 2014;

112. Diamandis EP, Christopoulos TK. The biotin-(strept)avidin system: principles and applications in biotechnology. Clin Chem 1991;37(5):625–36.

113. Green M. Avidin and streptavidin. Methods Enzymol 1990;184:51–67.

114. Noedl H, Yingyuen K, Laoboonchai A, Fukuda M, Sirichaisinthop J, Miller RS. Sensitivity and Specificity of an Antigen Detection Elisa for Malaria diagnosis. Am J Trop Med Hyg 2006;75(6):1205–8.

115. BD Microtainer Contact-Activated Lancet [Internet]. 2006 [cited 2015 Jul 10];Available from: http://www.bd.com/vacutainer/pdfs/vs7573.pdf

116. Clifford GM, Smith JS, Plummer M, Muñoz N, Franceschi S. Human papillomavirus types in invasive cervical cancer worldwide: a meta-analysis. Br J Cancer 2003;88(1):63–73.

117. Saslow D, Castle PE, Cox JT, Davey DD, Einstein MH, Ferris DG, et al. American Cancer Society Guideline for human papillomavirus (HPV) vaccine use to prevent cervical cancer and its precursors. CA Cancer J Clin 2007;57(1):7–28.

118. Centers for Disease Control Vaccine Price List as of February 1, 2016 [Internet]. 2016;Available from: http://www.cdc.gov/vaccines/programs/vfc/awardees/vaccine-management/price-list/

119. Kreimer AR, Rodriguez AC, Hildesheim A, Herrero R, Porras C, Schiffman M, et al. Proof-of-principle evaluation of the efficacy of fewer than three doses of a bivalent HPV16/18 vaccine. J Natl Cancer Inst 2011;103(19):1444–51.

120. Lazcano-Ponce E, Stanley M, Muñoz N, Torres L, Cruz-Valdez A, Salmerón J, et al. Overcoming barriers to HPV vaccination: Non-inferiority of antibody response to human papillomavirus 16/18 vaccine in adolescents vaccinated with a two-dose vs. a three-dose schedule at 21 months. Vaccine 2014;32(6):725–32.

121. Laprise JF, Drolet M, Boily MC, Jit M, Sauvageau C, Franco EL, et al. Comparing the cost-effectiveness of two- and three-dose schedules of human papillomavirus vaccination: A transmission-dynamic modelling study. Vaccine 2014;32:5845–53.

122. Rotich JK, Hannan TJ, Smith FE, Bii J, Odero WW, Vu N, et al. Installing and Implementing a Computer-based Patient Record System in Sub-Saharan Africa: The Mosoriot Medical Record System. J Am Med Inform Assoc 2003;10(4):295–303.

123. Rolnick SJ, Parker ED, Nordin JD, Hedblom BD, Wei F, Kerby T, et al. Self-report compared to electronic medical record across eight adult vaccines : Do results vary by demographic factors ? Vaccine 2013;31(37):3928–35.

124. Villa LL, Ault K a., Giuliano AR, Costa RLR, Petta C a., Andrade RP, et al. Immunologic responses following administration of a vaccine targeting human papillomavirus Types 6, 11, 16, and 18. Vaccine 2006;24(27-28):5571–83.

125. Leder C, Kleinschmidt JA, Wiethe C, Müller M. Enhancement of Capsid Gene Expression : Preparing the Human Papillomavirus Type 16 Major Structural Gene L1 for DNA Vaccination Purposes Enhancement of Capsid Gene Expression : Preparing the Human Papillomavirus Type 16 Major Structural Gene L1 for DNA Va. J Virol 2001;75(19):9201–9.

126. Buck CB, Pastrana D V, Lowy DR, Schiller JT. Efficient intracellular assembly of papillomaviral vectors. J Virol 2004;78(2):751–7.

127. Buck CB, Thompson CD, Pang Y-YS, Lowy DR, Schiller JT. Maturation of papillomavirus capsids. J Virol 2005;79(5):2839–46.

128. Buck CB, Thompson CD. Production of Papillomavirus-Based Gene Transfer Vectors. In: Current Protocols in Cell Biology. John Wiley & Sons, Inc.; 2007.

129. Production of Papillomaviral Vectors (Pseudoviruses) [Internet]. 2015 [cited

2015 May 13];Available from: http://home.ccr.cancer.gov/LCO/pseudovirusproduction.htm

130. Grant BD, Smith CA, Karvonen K, Richards-Kortum R. Highly Sensitive Two-Dimensional Paper Network Incorporating Biotin–Streptavidin for the Detection of Malaria. Anal Chem 2016;88(5):2553–7.